Exploring and modelling the influence of spectral light composition on soybean (Glycine max (L.) Merr.)

Dissertation to obtain the doctoral degree of Agricultural Sciences (Dr. sc. Agr.)

Faculty of Agricultural Sciences

University of Hohenheim

Institute of Crop Science (340)

AG Cropping Systems and Modelling

submitted by

Tina Heldgaard Hitz

from Vejle in Denmark

2019

This thesis was accepted as a doctoral dissertation in fulfillment of the requirements for the degree “Doctor of Agricultural Sciences” (Dr. sc. agr.) by the Faculty of Agricultural Sciences at the University of Hohenheim.

Date of oral examination: 24 July 2020

Examination Committee
Supervisor and Reviewer: Prof. Dr. agr. Simone Graeff-Hönninger
Examiner: Prof. Dr. sc. agr. Hartmut Stützel
Examiner: Prof. Dr. Tobias Würschum
Head of the examination committee: Prof. Dr. Thilo Streck

Table of contents

List of figures

List of abbreviations and acronyms

B	Blue light
BPFD	Blue photon flux density
CCT	Cryptochrome C-terminus
CRY1-2	Cryptochrome 1-2
cv	Cultivar
FLAVIN-BINDING, KELCH REPEAT, F-BOX 1	FKF1
FR	Far-red light
FSP	Functional-structural plant
FWHM	Full width at half maximum
G	Green light
GroIMP	Growth Grammar-related Interactive Modelling Platform
LED	Light-emitting diode
LOV KELCH PROTEIN 2	LKP2
MAE	Mean absolute error
MAPE	Mean absolute percentage error
MRD	Mean relative deviation
phot1-2	Phototropin1-2
Phy A-E	Phytochrome A-E
PLD	Physical light distribution
PPFD	Photosynthetic photon flux density
R	Red light
R:FR	Red to far-red light ratio
RMSE	Root mean square error
SAR	Shade avoidance response
SLA	Specific leaf area
SPD	Spectral power distribution
UVA	UV-A light
UVB	UV-B light
XL	eXtended L-system
ZEITLUPE	ZTL

1. Introduction

Light drives plants assimilation of carbon through photosynthesis, which represents the primary importance of light in crop production. Additionally, plant physiology and morphology respond to light in multiple ways influencing crop yield and quality. In traditional agriculture, the light intensity and spectrum fluctuate depending on crop management e.g. weed pressure (Green-Tracewicz et al., 2011). In intercropping, the light environment can fluctuate substantial depending on e.g. crop arrangement, intercropped species and duration of the overlapping crop growth (Keating and Carberry, 1993). In indoor farming, the grower can directly influence light intensity and spectrum by choice of the light source used as supplemental or sole lighting. Hereby, an adequate knowledge of how light influence plant physiology and morphology can assist in a choice of management to increase crop yield and quality in both traditional- and indoor farming.

1.1 Light environment and the shade avoidance response

The solar spectrum reaching the surface of the earth is comprised of six ranges important for plant morphology and physiology (Table 1.1). The range of the light transmitted through the atmosphere starts at 290 nm, which is within the range of UV-B light (UVB). Shorter wavelengths of UVB and the UV-C light are absorbed by the atmosphere (Tilbrook et al., 2013). The UVB light range continues until 315 nm and is followed by the UV-A light (UVA) range until 400 nm (Tilbrook et al., 2013). Wavelengths until 700 nm constitute the photosynthetic active part of the spectrum, which is comprised of blue (B), green (G) and red light (R). The range from 700 to 800 nm is the range of the far-red light (FR). The photosynthetic photon flux density (PPFD) of B, G and R vary depending on location, time of day and cloud cover (Smith, 1982). The photosynthetic active part of the spectrum represent the fundamentally important light for plant growth through carbon assimilation, but all wavelength from UVB to FR, are important for the adaption of plant morphology and physiology to the fluctuations of light. The solar spectrum is relatively stable and only twilight changes the solar spectrum considerable with increased ratios of FR and B (Smith, 1982). Whereas, the spectrum actually perceived by the plants often diverge from the solar spectrum due to the surrounding environment (Smith, 1982).

Table 1.1. Term and wavelengths of the six light ranges from UV-B to far-red light.

Term of the range	UV-B	UV-A	Blue	Green	Red	Far-red
Wavelengths (nm)	280-315	315-400	400-500	500-600	600-700	700-800

Many adaptations in plants due to fluctuations in the perceived light are collectively referred to as the shade avoidance response (SAR). The SAR adapts plant morphology and physiology according to signals from the surrounding vegetation with the purpose to decrease shade and increase light interception (Casal, 2012). Shade indicating signals from the surrounding vegetation are not only related to light, but also to e.g. leaf tip touching and volatiles, which can work additive or interactive with light signals (Pierik and de Wit, 2014). The perceived spectrum of the plant is influenced of the surroundings since the reflection, absorption and transmission of vegetation are dependent of the wavelength.

Green leaves absorb most R and B especially by the pigments chlorophyll and carotenoid, whereas G is absorbed less and FR is mainly reflected or transmitted (Kasperbauer, 1987). The

reflection of FR from a surrounding short vegetation will be recognized by the plant as decreased R:FR ratio (R:FR) and is hereby an early warning of the threat of shade (Ballare et al., 1990; Green-Tracewicz et al., 2011). True shade from surrounding taller vegetation further decreases R:FR and also reduces PPFD with an associated reduction of blue photon flux density (BPFD).

Genotypic variation and phenotypic plasticity of SAR provide different ecological advantages for plants (Franklin, 2008; Schmitt, 1997), but an overall differentiation is made between shade tolerant and shade avoiding plants (Valladares and Niinemets, 2008). Increased specific leaf area and chlorophyll a/b ratio are general shade adaptations to increase the efficiency of photosynthesis (Valladares and Niinemets, 2008), while additional morphological adaptations helps shade avoiding plants to escape shade and increase light interception. The main purpose of these adaptations is to position the leaves above the surrounding vegetation, which is accomplished by hyponasty of the leaves and taller plants with longer hypocotyls, internodes and petioles (Franklin, 2008). Great investments in elongation of organs to increase light interception can have negative impact on e.g. reproduction, but SAR is also regulated to avoid a tragedy of the common (Bongers et al., 2018). Other responses to shade can be reduced branching, early flowering (Franklin, 2008) and changed allocation of assimilates e.g. arrested leaf development (Carabelli et al., 2007).
Within a field environment, crops perceive spectral fluctuations depending on weed pressure and cropping practice. An emerging weed reflects FR and a decreased R:FR is perceived by the crop, hereby signaling the threat of future shade. Intercropping within a tall crop decreases both the perceived R:FR and PPFD of the shorter crop, hereby signaling true shade. SAR is considered to be a negative adaptation in a field crop although it increases the fitness of plants in a natural plant community (Franklin, 2008; Schmitt, 1997). In mono-cropping, the response increases the heterogeneity of the crop and results in yield loss, compared to a weed free field that does not induce SAR (Green-Tracewicz et al., 2011). In intercropping the response to true shade of the shorter crop can complicate the harvest due to lodging (Liu et al., 2015). Soybean is an example of a shade avoiding plant that is grown both in mono-cropping and as the shorter crop in intercropping e.g. together with maize (Yang et al., 2018).

1.2 Plant photoreceptors

Signals from a fluctuating light environment are perceived by plant photoreceptors, which can alter gene expression and hormone production (Casal, 2012). This regulation controls SAR and other light dependent processes e.g. germination, de-etiolation, phototropism, stomata and chloroplast movement, circadian rhythm and photoperiodic flowering (Christie, 2007; Li et al., 2011; Yu et al., 2010). The latter was studied already in 1920 by Garner et al. (1920) and together with observations of reversible seed germination under FR (Borthwick et al., 1952), it later led to the detection of the R and FR receptor, phytochrome. The inactive form (Pr) of phytochrome is synthesized in darkness in the cytosol. The Pr is activated by R and transformed into the active form (Pfr), which is translocated to the nucleus (Li et al., 2011). This transformation is reversible either slowly in darkness or faster by absorption of FR and enables phytochrome to recognize the momentary R:FR. The balance between Pr and Pfr favors the active Pfr under high R:FR, which suppresses SAR. The Pr is favored under low R:FR and the suppression of SAR declines (Fraser et al., 2016).
In *Arabidopsis thaliana* (L.) Heynh five phytochromes have been identified, designated Phy A-E, which are responsible for both distinct and overlapping functions. Regarding the morphological responses during SAR, Phy B alone is responsible for considerable suppression

of SAR under high R:FR (Nagatani et al., 1991; Somers et al., 1991), but interactions of Phy B with Phy A, D and E also influence SAR (Franklin and Quail, 2010; Li et al., 2011).
The photoreceptors that perceive B and UVA are phototropins (phot1, phot2), the recent discovered proteins of the Zeitlupe family (ZTL, FKF1 and LKP2) and cryptochromes (CRY1 and CRY2). Phototropins mainly control phototropism, stomatal opening and chloroplast movements (Christie, 2007). The ZTL, FKF1, and LKP2 regulate the circadian rhythm and flowering time (Zoltowski and Imaizumi, 2014). The UVB is perceived by the photoreceptor UVR8, which mainly controls the protection against UVB by regulating DNA repair, sunscreen pigments, antioxidants and hypocotyl length (Tilbrook et al., 2013).
The CRYs are the most important of the B and UV perceiving photoreceptors, in the context of SAR. They were discovered later than the phytochromes and the mechanisms behind their activation and regulation of gene expression are not as well understood. The CRY1 protein is stable at high light intensity, whereas CRY2 is unstable, and rapidly degrades under high and continuous B (Lin et al., 1998; Yu et al., 2010). The CRYs are flavoproteins functioning as a dimer of monomers with two major domains the N-terminal Photolyase Homologous Region (PHR) domain and the cryptochrome C-terminus (CCT) domain. The B is sensed by the primary CRY chromophore, flavin adenine dinucleotide (FAD) binding to the PHR domain, which is believed to trigger a conformational change in the CCT domain (Christie et al., 2015). These nuclear conformational modifications and interactions with signaling proteins regulate gene expression, which induce morphological adaptations (Yu et al., 2010).

Several examples reveal co-actions between photoreceptors to fine-tune the response to the perceived light environment, but these interactions are not well understood. For instance, ZTL, FKF1, and LKP2 and CRYs can interact to control related responses e.g. the circadian rhythm and flowering time (Yu et al., 2010) and although controlling distinct responses, phototropin and cryptochrome can interact both synergetic and antagonistic (Kang et al., 2008). Direct interactions have been found between phyA/B and CRY1 and phyB and CRY2 and indirectly they can co-act through interactions with common transcription factors (Wang et al., 2018).
The different absorption spectra of the photoreceptors enable the plant to perceive and react to spectral fluctuations from the UVB to FR. Especially important for SAR is the absorption of phytochrome and cryptochrome. The absorption peaks of phytochrome are at 660 nm for Pr and 730 nm for Pfr, but it also weakly absorbs B (Purple lines; Fig. 1.1) (Li et al., 2011). Dark adapted cryptochrome has two broad absorption peaks at 350-380 within UVA and at 420-490 nm within B (Fig. 1.1) (Banerjee et al., 2007).

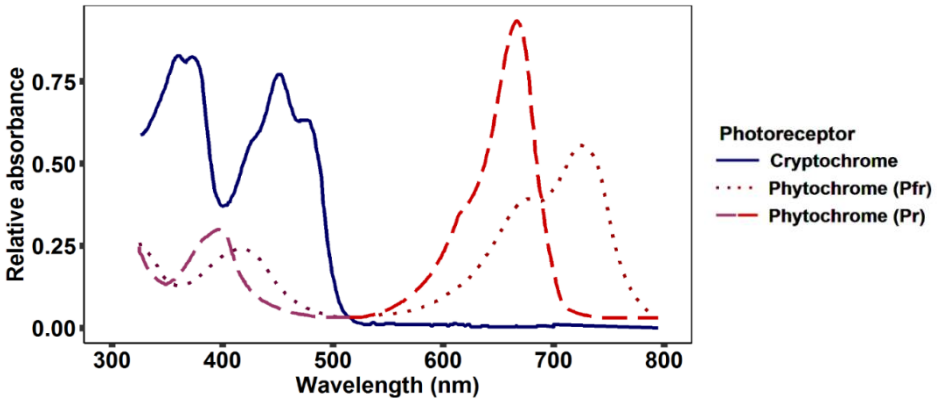

Fig. 1.1. Relative absorption spectra of phytochrome (Pfr: dotted line; Pr: dashed line) (modified from Li et al., 2011) and cryptochrome (solid line) (modified from Banerjee et al., 2007).

1.3 LEDs and indoor plant production

Artificial lighting for crop production has been used for several decades as additional lighting in greenhouses and in recent decades as sole light source for large-scale indoor farming (Kalantari et al., 2018). Traditional light sources for crop production are fluorescent, high-pressure sodium, metal halide and incandescent lamps (Bula et al., 1991), but with a decreased price and increased efficiency of LED lighting, it gained increasing interest as a light source (Morrow, 2008). The first LEDs were produced in the 1960s and were low intensity LEDs emitting only R (Yeh and Chung, 2009). During the following decades, LEDs emitting yellow, G and orange light were developed and the intensity increased, but it was not until 1993 that B LEDs were introduced (Yeh and Chung, 2009). Since then LED technology has further improved leading to an efficient and flexible light source with several advantages compared to traditional lighting. The LEDs have a small size, low energy consumption, long life time and low heat emittance and the spectra can be designed according to the intended application (Massa et al., 2008). The spectra of traditional light sources are general not optimized for plant growth as it is possible with LEDs (Bula et al., 1991) and the increased spectral flexibility allows for easy adjustments e.g. at different developmental stages or for regulating the circadian rhythm.
The first application of LEDs for horticultural lighting over 20 years ago combined R LEDs with B from other light sources to achieve a normal plant growth (Bula et al., 1991). With today's possibility to design a LED spectrum within the entire range relevant for plant physiology and morphology the question arose how to optimize this spectrum. The goal is no longer only to achieve a normal growth, but to optimize the spectrum according to the crop species and purpose of the production (Massa et al., 2008). The main purpose of the LED light source is to supply the plant with light for photosynthesis to produce biomass. The photosynthetic pigments are mainly the R absorbing chlorophyll and the B absorbing carotenoid. R is considered the most effective light source due to more effective transfer between chlorophylls than from carotenoid to chlorophyll and due to a better balance between photosystem I and II (Hogewoning et al., 2012). Recent work of Schlau-Cohen and coworkers showed that carotenoid is more important for photosynthesis than believed so far (Collini, 2019) and even G could be an effective light source for photosynthesis (Lanoue et al., 2018). The FR can also influence the photosynthetic rate due to enhancing effects of some wavelengths on other wavelengths (Emerson et al., 1957; Zhen and van Iersel, 2017).
Apart from increasing carbon assimilation, LED lighting can be optimized regarding several other aspects e.g. the control of flowering time through phytochrome in the production of ornamentals or higher crop quality using B LEDs to increase the content of secondary compounds (Taulavuori et al., 2013). In a speed breeding system, the main purpose is to collect one seed of the plant as fast as possible (Watson et al., 2018) and great emphasis can be put on optimizing the spectra to save space. This can be achieved by producing short plants allowing for more layers of plants as long as the spectra do not delay the time of seed set. In this context SAR is of particular interest due to its impact on plant height.

1.4 Functional-structural plant modelling

The three dimensional representations of plants started in the 1960s, with the most important work performed by Lindenmayer and his successors (Vos et al., 2010), who developed the L-language (Lindenmayer, 1968a, 1968b). During the following decades other platforms were developed for the purpose of functional-structural plant (FSP) modelling e.g. L-studio (Prusinkiewicz, 2007) and GREENLAB (Yan et al., 2004). In the present thesis, the open-source Growth Grammar-related Interactive Modelling Platform (GroIMP) (Kniemeyer et al., 2007) was chosen. This java based platform can execute programs written in the eXtended L-system (XL) language implementing relational growth grammars (Hemmerling et al., 2008).

GroIMP has been used to construct FSP models of several species e.g. oilseed rape (Tian et al., 2017), barley (Buck-Sorlin et al., 2008), wheat (Evers et al., 2015) and *Arabidopsis thaliana* (L.) Heynh (Bongers et al., 2018). For facilitating the development of FSP models for other crops, Henke et al. (2016) developed a generic plant model in GroIMP.
The specific advantage of GroIMP in the context of the present project studying the effect of specific wavelength is the possibility of spectral ray tracer simulations (GPUFlux model) with a resolution down to one nm (Van Antwerpen, 2011). The GPUFlux model is based on a Monte Carlo ray tracer and simulates the light rays emitted from the light sources placed within the virtual scene. The optical properties (phong shader (Phong, 1975)) of the object within the scene determine the proportion of the ray that is reflected, absorbed or transmitted by collision with light ray. Several light sources can be chosen in GroIMP and for virtual LEDs the integrated lightNode module can be used. This module can be parameterized to simulate both light distribution and spectrum according to the technical specifications of the real LEDs (Henke and Buck-Sorlin, 2017).

Results of most spectral experiments are analyzed based on the applied light treatment, whereas the actual perceived light by the plant is not considered. The micro-light climate perceived by the plant organs can differ from the applied treatment due to e.g. surrounding environment, plant density or adaptations in plant morphology induced by the treatment itself. The FSP modelling represents a method to consider the perceived light by simulating micro-light climate within a virtual three dimensional representations of the experiment.
For instance, Kahlen and Stützel (2011) applied an FSP model of cucumber to collect data of the perceived R:FR of the internode during the simulations of a selected experiment. An R:FR response curve was derived from the simulated date and the curve was integrated in the FSP model, which simulated internode length response to the perceived R:FR. The simulation of the calibrated FSP model was found better than a model only sensitive to PPFD and ignoring the morphology of the plant (Kahlen and Stützel, 2011).
Several other FSP models have been constructed, which simulated the morphological response to R:FR with the purpose of optimizing crop production or increasing knowledge of the underlying mechanisms of plant responses. For instance, Gautier et al. (2000) applied a FSP model of clover to describe the impact of self-shading. Two recent studies aimed towards increasing the understanding of SAR with an FSP model of *Arabidopsis thaliana* (L.) Heynh (Bongers et al., 2018) and explored the role of biomass allocation between leaves and petioles to capture light in a dense stand (Yoshinaka et al., 2018).
The final FSP model can simulate the response to a wide variety of environmental combinations exceeding an experimentally feasible extent. Models responding to the perceived light environment can be extended e.g. by implementing available data and knowledge on yield, physiological processes and underlying mechanisms. For instance, Kahlen and Chen (2015) combined light and temperature response in their FSP model of cucumber and Buck-Sorlin et al. (2008) combined the response of light with signal transduction of gibberellic acid. These earlier studies focused on the spectral change of R:FR under shade, whereas no earlier studies were developed with the purpose of simulating the morphological response to BPFD.

1.5 Outline and objectives

This dissertation was performed as a part of the project MoLED-Plant, with the objective to develop a speed breeding system for soybean under LED lighting. The project was funded by the German Federal Ministry for Economic Affairs and Energy according to a decision of the German Federal Parliament within the Central Innovation Program for SMEs (ZF4279901CR6) and was a cooperation between the State Plant Breeding Institute, Institute of Crop Science at the University of Hohenheim and the LED-lighting company COMPLED Solutions GmbH (Dresden, Germany). Soybean was chosen for the project, because an increased production of this crop within Europe is desired to decrease the dependence of the high amounts of soybean currently imported (European commission, 2018). The development of soybean cultivars with a higher cold tolerance is an important factor to increase the European production by expanding the area, where soybean can be grown (Jähne et al., 2019). Speed breeding is a method to accelerate this breeding process by growing several generations per season in growth chambers. For instance, six generations of several cereals and peas can be grown per year instead of 2-3 under normal greenhouse conditions (Watson et al., 2018).

To collect data for determining the best spectrum for a speed breeding system for soybean, LED growth chambers delivered from the project partner COMPLED Solutions GmbH were used. The chambers were designed to have a high degree of spectral flexibility as the intensity of light peaks could be regulated independently. This enabled studies of a wide variety of spectral light compositions. The requirements for the final spectrum were to promote short and stable plants across all cultivars without a delay of flowering.
The major aims of this thesis were: (i) to study the effect of different spectral light compositions on soybean morphology and (ii) to develop an FSP model with an integrated response to the spectrum. The experimental and simulated results should increase the scientific knowledge of the effects of wavelengths on soybean morphology in general and assist in optimizing the speed breeding system for soybean.

The main objectives pursued within the thesis were:

- Construct a three dimensional model of an LED chamber to simulate micro-light climate.
- Develop an FSP model of soybean and derive a BPFD response curve from simulations.
- Apply the FSP model with the integrated response curve for spectral optimization.
- Explore the influence of BPFD under constant PPFD.
- Disentangle the influence of R:FR and PPFD on SAR.

Within LED climate chambers at the University of Hohenheim, various measurements and experiments were conducted for pursuing the above-mentioned objectives (Fig. 1.2). Detailed light measurements were performed with a spectrometer (Ocean Optics Germany GmbH, Ostfildern, Germany) in numerous locations and sensor orientations to evaluate the light simulations of the LED chamber model. For the development of the FSP model of soybean, frequent measurements of plant morphology were performed during BPFD experiments. The data comprised dimensions and biomass of each individual organ on all phytomers and was used to derive growth response functions.

Light treatments to explore the influence of BPFD and disentangle the effect of R:FR and PPFD were set by adjusting the light of the chambers until spectrometer measurements showed the desired spectral intensity. In the BPFD experiments, six levels of BPFD were applied. To disentangle R:FR and PPFD two experiments were performed consisting of nine treatments in total. The technical approaches and experimental designs are described in details in Chapter I-IV of this thesis.

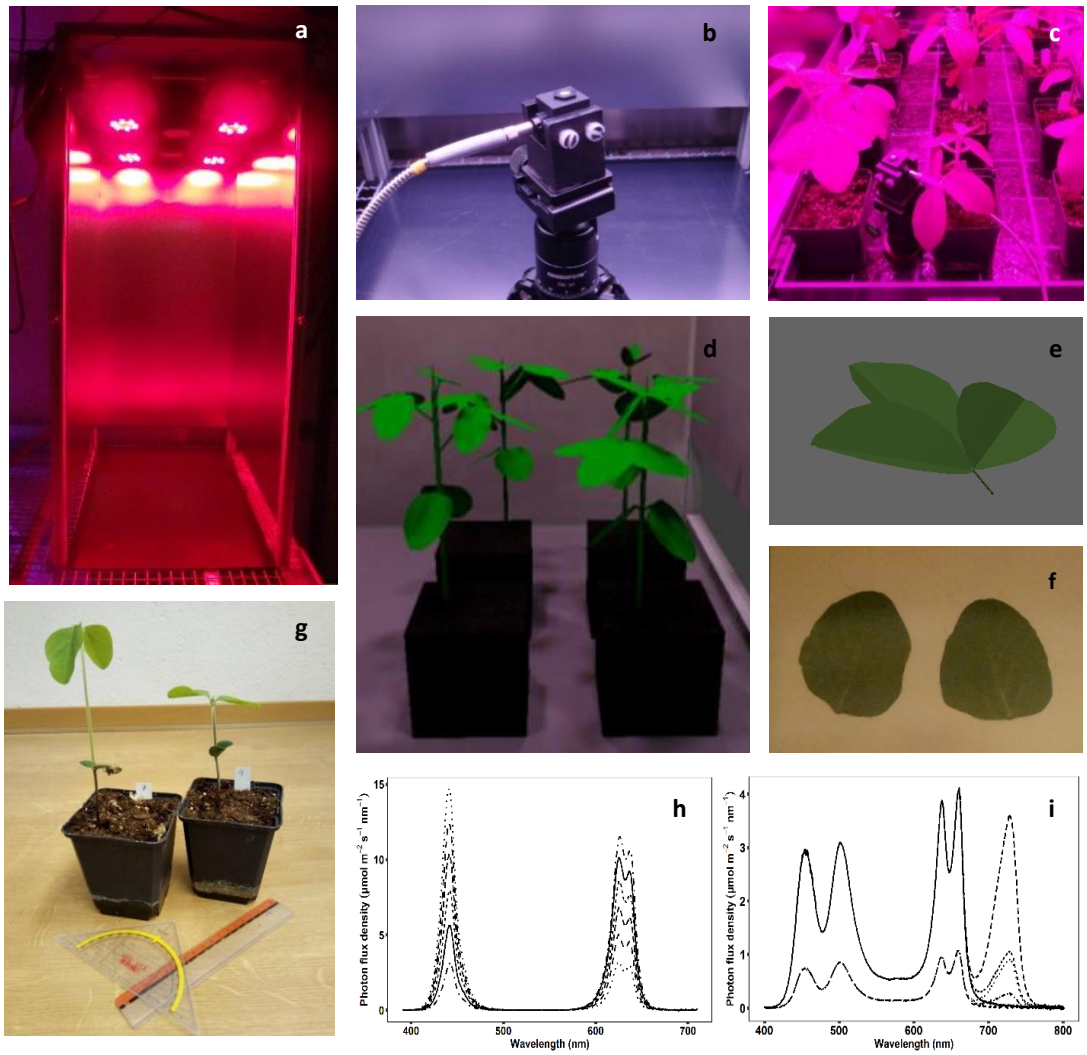

Fig 1.2. LED chamber with red and blue LEDs turned on (a), spectrometer for light measurements in an empty chamber (b) and below a soybean canopy (c), reconstructed static soybean plants (d) and dynamic soybean leaf (e), picture used for measurements of leaf area (f), experimental plants grown under different red to far-red ratio (g) and spectra from experiments on blue photon flux density (h) and red to far-red ratio combined with photosynthetic photon flux density (i).

The results of the experiments and the associated modelling are presented in four papers within Chapter I-IV. Three of the papers have been published by peer reviewed journals and an additional paper has been published as a peer reviewed contribution to the 6th International Symposium on Plant Growth Modeling, Simulation, Visualization and Applications (PMA) in Hefei, China.

Chapter I presents the development and the properties of the three dimensional LED chamber model. Simulations were evaluated by comparisons of simulated and measured light spectra for several positions and sensor orientations within the chamber to assure a high accuracy of the micro-light climatic simulations. The results were discussed in the context of FSP modelling and chamber design.

In **Chapter II**, a static soybean model was integrated into the chamber model by reconstructing soybean plants grown within the LED chamber. Spectral light simulations within the canopy were evaluated for several positions on two dates. The model was applied to evaluate experimental designs by simulating the light heterogeneity under an increase in plant density.

Chapter III presents the response of soybean to BPFD under constant PPFD together with the dynamic FSP model of soybean. The model was calibrated according to the morphological measurements performed during the experiments, and a response curve of internode elongation to the perceived BPFD was derived from simulations. The response curve was integrated into the model and it was applied for spectral optimization to achieve a short plant within an alternative chamber design.

The results of the experiments performed to disentangle the influence of R:FR and PPFD are presented in **Chapter IV.** The influence on morphology and biomass of different organs in three soybean cultivars are discussed in the context of SAR and the aspects for breeding and crop management.

2. Publications and results

Four scientific papers are presented in Chapter I-IV in this cumulative thesis. The papers are all published in peer reviewed international journals or conference proceedings.
For citation of the papers, please use the references as given below.

Chapter I
Hitz, T., Henke, M., Graeff-Hönninger, S., Munz, S., 2019. Three-dimensional simulation of light spectrum and intensity within an LED growth chamber. Comput. Electron. Agric. 156, 540–548. https://doi.org/10.1016/J.COMPAG.2018.11.043

Chapter II
Hitz, T., Henke, M., Graeff-Honninger, S., Munz, S., 2018. Simulating light spectrum within a soybean canopy in an LED growth chamber, in: 2018 6th International Symposium on Plant Growth Modeling, Simulation, Visualization and Applications (PMA). IEEE, pp. 120–125. https://doi.org/10.1109/PMA.2018.8611598

Chapter III
Hitz, T., Graeff-Hönninger, S., Munz, S., 2020. Modelling of Soybean (Glycine max (L.) Merr.) Response to Blue Light Intensity in Controlled Environments. Plants 9, 1757. https://doi.org/10.3390/plants9121757

Chapter IV
Hitz, T., Hartung, J., Graeff-Hönninger, S., Munz, S., 2019. Morphological Response of Soybean (*Glycine max* (L.) Merr.) Cultivars to Light Intensity and Red to Far-Red Ratio. Agronomy 9, 428. https://doi.org/10.3390/agronomy9080428

3. Chapter I: Three-dimensional simulation of light spectrum and intensity within an LED growth chamber

Hitz, T., Henke, M., Graeff-Hönninger, S., Munz, S., 2019. Three-dimensional simulation of light spectrum and intensity within an LED growth chamber. Comput. Electron. Agric. 156, 540–548. https://doi.org/10.1016/J.COMPAG.2018.11.043

An important prerequisite for FSP modelling of plants under LED light was a virtual scene assuring good simulations of the light microclimate perceived by virtual plant organs. No previous publication was found on simulating LED light for this purpose. Chapter I filled this gap in literature by presenting the development of a virtual LED chamber. The chamber model was combined with the point light source and the Monte Carlo ray tracer integrated in GroIMP. A virtual sensor was constructed to compare measurements and simulations at exact locations within the chamber. Technical information on the real LEDs was used to define the parameters of the point light source to achieve a detailed simulation of both the light distribution and the light spectra from different LED types. Easy adjustment of the dimensions of the chamber and LED placement was integrated in the model for adaptions to other scenarios.

Measurements for an evaluation of the model were performed to assure a high accuracy of three desired properties of the model: (i) simulation of different LED types and different wavelengths, evaluated with individual measurements of B, G, R and FR, and (ii) simulation of the light perceived by leaves with varying orientations, evaluated with measurements performed in different elevation and azimuth angles, and (iii) simulation of light heterogeneity to assess new chamber designs, evaluated with horizontal and vertical measurements representing the entire space of the chamber.

Computers and Electronics in Agriculture 156 (2019) 540–548

Contents lists available at ScienceDirect

Computers and Electronics in Agriculture

journal homepage: www.elsevier.com/locate/compag

Original papers

Three-dimensional simulation of light spectrum and intensity within an LED growth chamber

Tina Hitz[a,*], Michael Henke[b], Simone Graeff-Hönninger[a], Sebastian Munz[a]

[a] Institute of Crop Science, University of Hohenheim, Stuttgart, Germany
[b] Leibniz Institute of Plant Genetics and Crop Plant Research (IPK), OT Gatersleben, 06466 Stadt Seeland, Germany

ARTICLE INFO

Keywords:
LED lighting
Spectral ray tracer
Light simulation
GroIMP
Micro-light climate

ABSTRACT

An increased knowledge of different light spectrum on plant structure and physiology is required for improving horticulture production and energy efficiency. This implies a high number of experimental repetitions under uniform and reproducible light conditions. The objective of this study was to create a virtual LED chamber to be used for functional structural plant modelling and for exploring the optimal chamber design regarding light conditions. The spectral light simulations were evaluated in six heights and seven directions with measurements performed in a real LED chamber. The accuracy of the simulations compared to measurements were high with R^2 between 0.901 and 0.965 with data from different heights and R^2 between 0.959 and 0.997 with data from different directions. The mean absolute percentage errors between measured and simulated light intensity in different directions were 12.7%, 2.8%, 8.9% and 30.6% for light in the blue, green, red and far-red wavelength ranges, respectively. MAPE from data in different heights were within the same range and showed consistent tendencies between colors. The model was capable of evaluating the light intensity in different directions and uniformity at different heights. Thus the chosen GPUFlux model in GroIMP can be used to simulate micro-light climate within an LED growth chamber for functional structural plant modelling and to assist in optimizing chamber design and LED placement for uniform and reproducible light conditions.

1. Introduction

Compared to conventional light sources used in climate chambers, light-emitting diodes (LEDs) have the advantage that they can emit a particular light spectrum (Morrow, 2008). Based on the chosen combination of LEDs, a nearly arbitrary qualitative light spectrum can be designed. Increased use of LED light in horticulture has considerably increased the opportunities to adapt the light spectrum to achieve desired structural or physiological properties in a horticultural crop (Berkovich et al., 2017). Exploiting this opportunity requires an increased knowledge on the effect of different wavelengths on plant growth (Olle and Viršile, 2013). This effect can differ between species and genotypes (Gitz et al., 2005; Cope and Bugbee, 2013), which implies the need for a high number of time- and space-consuming experiments to identify the optimal light spectrum and intensity.

Modelling can play a crucial role in exploring the optimal light spectrum and intensity and the corresponding plant architecture for optimizing production and improving energy efficiency. Functional structural plant models (FSPM) are a well-established tool, which can link plant structure and physiological processes in response to the environment (Vos et al., 2010). An FSPM simulating the plant response to light with different wavelengths can assist in identifying an optimal spectrum by reducing the number of experimental treatments to a feasible extent. The majority of previous work on FSPM responding to light has focused on photosynthesis from the intensity of photosynthetic active radiation (PAR) (e.g., Henke et al., 2016; Burgess et al., 2017). The FSPM studies that have incorporated the light spectrum in light simulations, have linked the red to far-red ratio with plant structure to optimize crop management (Chelle et al., 2007a; Evers et al., 2007; Buck-Sorlin et al., 2008), explore phenotypic plasticity (Bongers et al., 2018) or for process understanding (Gautier et al., 2000). For simulating the effects of LED lighting on plant growth, however, precise simulations of both light intensity and spectrum are necessary. Furthermore, there are only a few studies about light intensity in controlled environments, such as greenhouses (Buck-Sorlin et al., 2011; Visser et al., 2014) and climate chambers (Tian et al., 2017).

The simulation of the spectral micro-light climate within an LED growth chamber would be an initial step to create an FSPM responding

* Corresponding author.
E-mail addresses: tina.hitz@uni-hohenheim.de (T. Hitz), henke@ipk-gatersleben.de (M. Henke), simone.graeff@uni-hohenheim.de (S. Graeff-Hönninger), s.munz@uni-hohenheim.de (S. Munz).

https://doi.org/10.1016/j.compag.2018.11.043
Received 7 June 2018; Received in revised form 27 November 2018; Accepted 30 November 2018

to both intensity and spectrum emitted by an LED light source. Herein the micro-light climate corresponds to the physical environment actually perceived by each individual aerial organ of a plant. Previous work on three-dimensional modelling of light within growth chambers is very rare and does not include LEDs as light sources, hence no spectral considerations have been made. For instance, Chelle et al. (2007b) simulated the micro-light climate with a photon tracing model (SEC2) in a chamber with discharge lamps, which was evaluated for light intensity in two horizontal layers. A spectral ray tracer (Van Antwerpen, 2011) implemented in the Growth Grammar-related Interactive Modeling Platform (GroIMP) (Kniemeyer et al., 2007) provides the possibility to simulate the whole light spectrum of arbitrary light sources (Henke and Buck-Sorlin, 2017). However, the model has never been applied within a growth chamber and in general, no evaluations with light measurements have been performed.

It is important to ensure a uniform intensity and spectrum received by all plants within the growth chamber, which is an essential condition for chamber experiments that investigate specific gene expressions. The light micro-climate in climate chambers can vary substantially (Measures et al., 1973; Boonen et al., 2002) and this variation differs between chambers due to great differences in geometry, materials, lighting and control systems (Delepoulle et al., 2009). LED modules are a combination of several LEDs arranged in a defined pattern. These LEDs can differ in their physical light distribution (PLD), hereby creating differences in the behavior and uniformity of light from different LEDs. Delepoulle et al. (2009) incorporated a genetic algorithm in a simulations framework to compute irradiance on virtual plants (SEC2), to investigate the possibilities to improve the placement of light sources within a chamber by optimizing the uniformity of light.

Here, we present and evaluate a three-dimensional model to simulate an accurate micro-light climate (intensity and spectrum) in different directions inside a growth chamber equipped with LEDs. Important aspects of chamber design, like dimensions and placement of LEDs and optical properties are examined. Further, the LED lighting system can be adjusted in number and types of LEDs used.

2. Materials and methods

2.1. Chamber dimensions and materials

CompLED (Compled Solutions GmbH, Dresden, Germany) designed the LED growth chamber with the dimensions: 1.1 m high, 0.5 m wide and 0.7 m deep. To regulate major environmental factors (e.g., temperature, humidity) it was placed inside a larger climate chamber at the University of Hohenheim (Germany). Openings at the top and bottom of the LED growth chamber were designed to enable ventilation and assure homogeneous temperature conditions. In the top, four identical complex LED modules were placed, with a distance of 15.5 cm from the front/back and 11.5 cm from the nearest side. Each of the four modules (Sunsim VIS_v1.1; Compled Solutions GmbH, Dresden, Germany) comprised 10 different LED types (OSRAM GmbH, Munich, Germany) (Fig. 4), which could be turned on by four different channels. Each channel controlled several LED types emitting either blue, green/white, red, or red and far-red light. To describe the physical light distribution, the full width at half maximum (FWHM) was given from CompLED for each LED type. The FWHM is the angle where 50% of the light intensity is reached on both sides of the light source. Most LEDs had an FWHM of 80°, apart from one green and the far-red LED type with an FWHM of 120° and 90°, respectively (Table 1, Fig. 5).

2.2. Measurements of spectral light intensity

Quantitative measurements of the light spectrum ($\mu mol\, m^{-2} s^{-1} nm^{-1}$) were acquired with a FLAME-S-XR1-ES spectrometer (Ocean Optics Germany GmbH, Ostfildern, Germany) equipped with a collimating lens (74-UV-MP) and a right angle reflector with cosine corrector (74-90-UV-CC3) measuring in the range from 200 to 1025 nm with a resolution of around 2 nm. The spectrometer was attached to a tripod and placed within the LED growth chamber for measurements at different positions and sensor directions (Fig. 1). The measurements of the spectrometer for the photosynthetically active radiation (PAR, 400–700 nm) was checked at 60 cm distance from the LED modules in the elevation angles of 90°, 67.5°, 45°, 22.5° and 0° (Fig. 2, right) with a quantum sensor (LI-190 SL; LI-COR, Lincoln, NE, USA).

The spectrometer was set to take an average of 25 measurements and the integration time of each measurement was regulated automatically. For each measurement position, the intensity of light was summed up and stored in five different ranges of wavelengths: 400–700 nm (PAR), 400–500 nm (blue light), 500–600 nm (green light), 600–700 nm (red light), and 700–800 nm (far-red light).

Measurements were performed in six distances (15, 30, 45, 60, 75 and 90 cm) from the LED modules at nine positions with the sensor pointing upwards. The points were located in one corner of the LED growth chamber (Fig. 3, right), which due to the symmetric chamber design were considered representative for the entire chamber. For an evaluation of the light simulations in different directions, measurements were performed at four positions, namely in the center of the chamber and directly below an LED module, each at 30 and 60 cm distance from the LED modules (Fig. 2, left). The two distances represented different horizontal uniformity of light, with low uniformity at 30 cm distance and high uniformity at 60 cm. At each of the four positions, the direction of the sensor was adjusted to point in five elevation angles and three azimuth angles between 0 and 90° (Fig. 2, right). At the elevation angle of 90° the sensor was pointed upwards and

Table 1
Composition of the four light channels in the chamber. Peak wavelength and full width at half maximum (FWHM) of the single LED types and the number of each LED type within each of the four LED modules.

Channel	Peak wavelength (nm)	FWHM (°)	LEDs/module (No)
Blue	465	80	4
	445	80	2
Green	521	80	3
	518	120	3
	503	80	3
	550	80	3
Red	635	80	5
	625	80	5
Red/far-red	659	80	6
	725	90	5

Fig. 1. Spectrometer attached to a tripod and placed within the LED growth chamber. Before measurements, the front wall was closed.

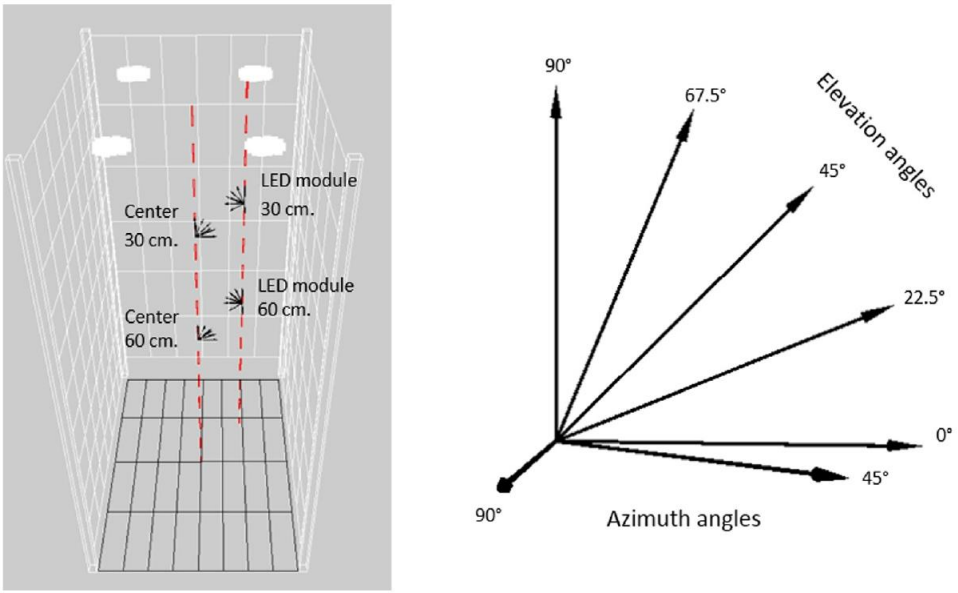

Fig. 2. Visualization of the measurement positions under an LED module and in the center, each at 30 and 60 cm distance (left) and the elevation and azimuth angles of the sensor (right).

from there moved downwards to 67.5°, 45°, 22.5° and 0° (Fig. 2, right). The azimuth angle of 0° was identical to the elevation angle of 0° and from here the sensor was moved counter clockwise to the angles of 45 and 90°. To account for inexact placement of the spectrometer, measurements in all measurement points were repeated on three occasions and a mean was calculated and used.

For evaluating the capability of the model in determining the optimal spatial placement of the four LED modules, the nine measurement points (Fig. 3, right) at 45 cm from the LED modules were used together with identical measurements under two alternative module placements. In alternative one (A1), the modules were evenly distributed with a distance of 17.5 cm to the front/back and 12.5 cm to the nearest side. In alternative two (A2), the modules were placed at a distance of 22.5 cm to the front/back and 11.5 cm to the nearest side (Fig. 3, left). The alternatives were considered realistic possibilities for a chamber design, as A1 was the intuitive way to place the four modules and A2 an alternative to the present placement to still have space for two additional LED modules to be placed in the chamber.

2.3. Modelling in GroIMP

A three-dimensional model of the LED chamber that can be adjusted in its dimensions including the placement of LED modules (Fig. 4, left) was constructed in GroIMP.

For spectral light simulations, it is necessary to describe the light, the light sources and the optical properties of the objects. The incorporated light models in GroIMP for these purposes are validated and well described (Henke and Buck-Sorlin, 2017). The spectral light

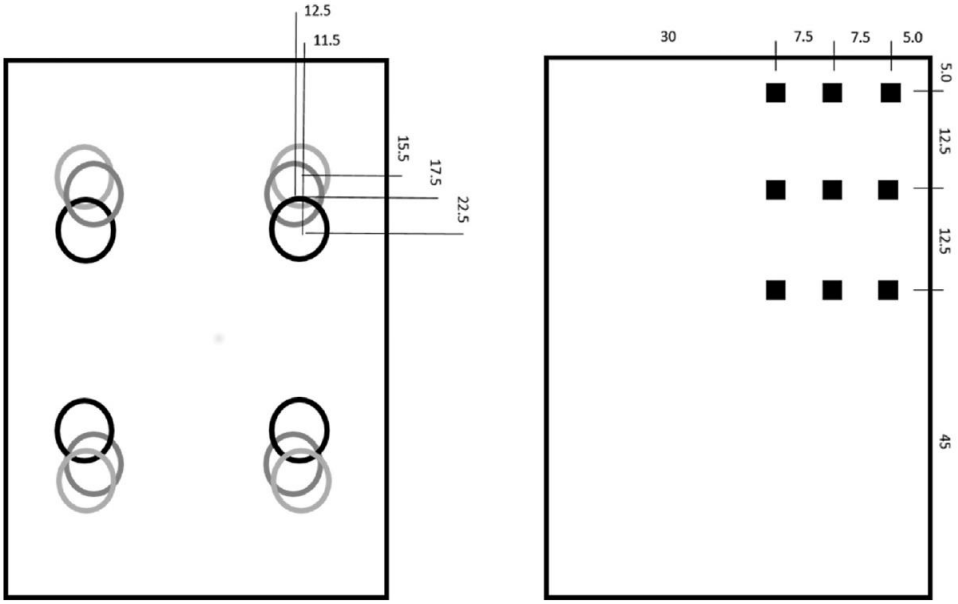

Fig. 3. The three placements of the LED modules (light gray = present, dark gray = A1, black = A2) (left) and the horizontal measurement points located at 45 cm distance from the LED modules at nine positions located in one corner of the LED growth chamber (right). All measurements are given in cm.

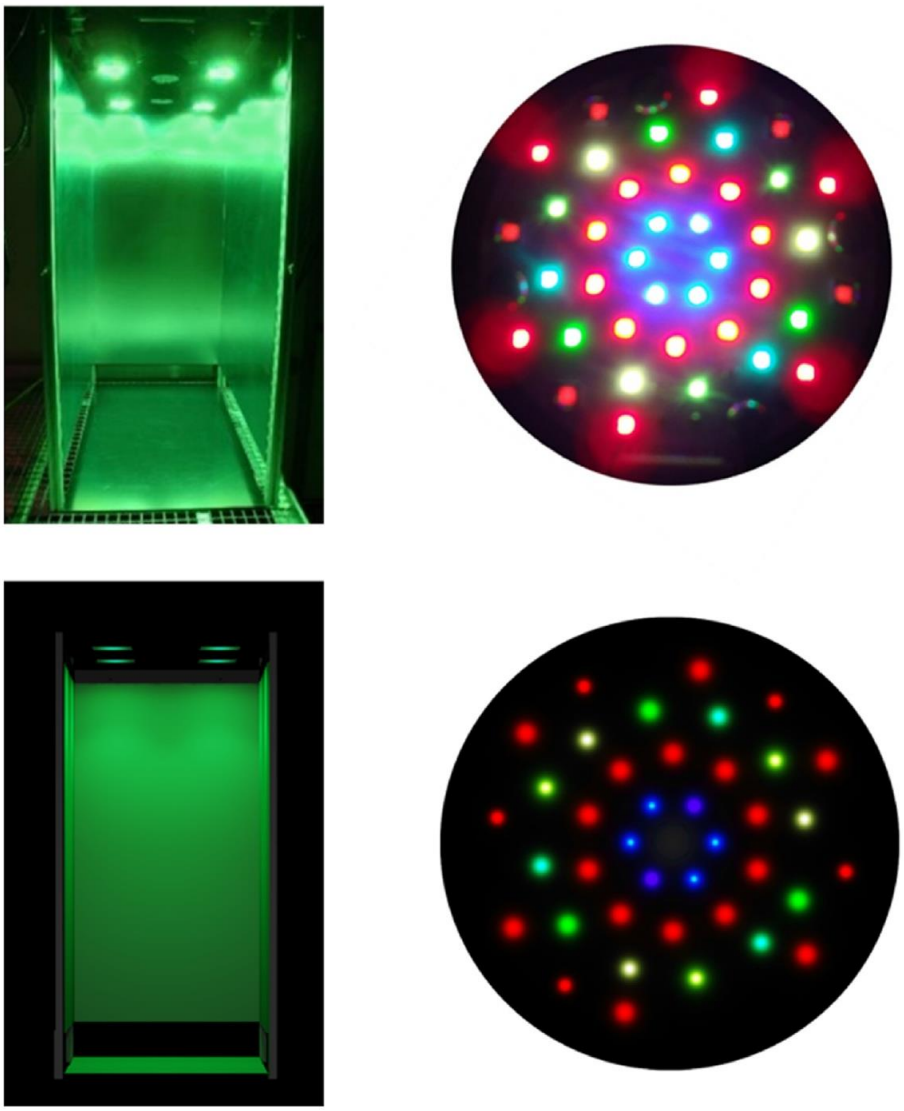

Fig. 4. The LED growth chamber exemplarily with the green channel turned on (top, left) and the reconstructed LED growth chamber in GroIMP (bottom, left) and LED placement within the module (top, right) and the reconstruction in GroIMP (bottom, right). (For interpretation of the references to color in this figure legend, the reader is referred to the web version of this article.)

distribution was simulated with the GPUFlux model (Van Antwerpen, 2011), one of the light models implemented in GroIMP. The GPUFlux model is based on a spectral Monte-Carlo ray tracer, which can be parametrized with the numbers of light rays emitted by the light sources, the spectral ranges to be simulated, the number of reflections and the cut-off power until a light ray is not traced further (Henke and Buck-Sorlin, 2017). For light simulations with the GPUFlux model a user-defined number of light rays are emitted by all light sources according to their individual settings (e.g., power). The light source is defined by the user using two parameters: (1) a physical light distribution (PLD), (2) and a spectral power distribution (SPD) describing the emitted light intensity into different directions and the emitted spectrum (Henke and Buck-Sorlin, 2017). When a light ray hits an object within the scene, its further path is determined by the optical properties of the objects. These were defined by a Phong shader describing direct and diffuse absorption, reflection, transmission, shininess, and specular reflection of light by an object (Phong, 1975). For spectral ray tracing, the SPD and the shader can be defined down to 1 nm buckets within the spectrum to determine distribution and path of different colors of light independently (Henke and Buck-Sorlin, 2017).

In the presented chamber model the light sources were a reconstruction of the LED modules with an exact placement of the individual LEDs within the modules based on the manufacturers' information (Compled Solutions GmbH, Dresden, Germany) (Fig. 4, right). Both the PLD (Fig. 5) and the SPD of the individual LEDs were given as model inputs according to manufacturers' information (OSRAM and CompLED).

For the comparison of measured and simulated light intensity and spectrum, a virtual light sensor was constructed by a parallelogram of the same area (19.36 mm^2) as the spectrometer. The sensor placement could be adjusted in position and direction and the optical properties of the virtual sensor were set to total absorbance of the entire spectrum.

The distribution of the light spectrum within the chamber model is directly affected by the optical properties of the objects within the scene, which for an empty chamber only comprises the sidewalls. It was not possible to measure these properties, instead they were set with a calibration. This calibration was based on measurements in the center of the LED growth chamber at six different distances from the LED modules (15, 30, 45, 60, 75 and 90 cm) to capture the light reduction towards the bottom of the chamber. A provisional light intensity setting

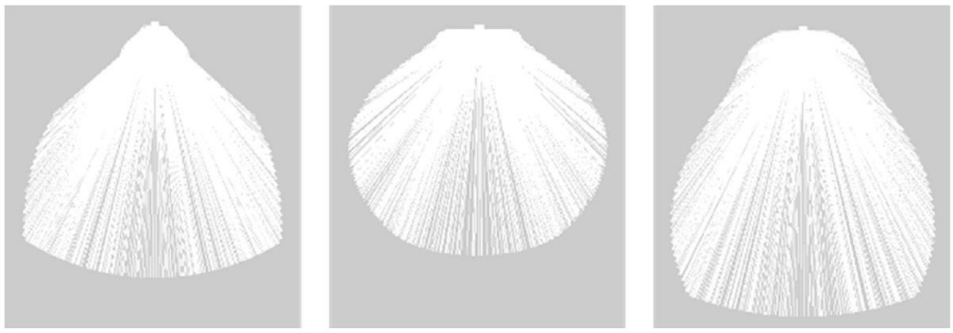

Fig. 5. Visualization in GroIMP of the three different physical light distributions: FWHM90 (left), FWHM120 (center), and FWHM80 (right).

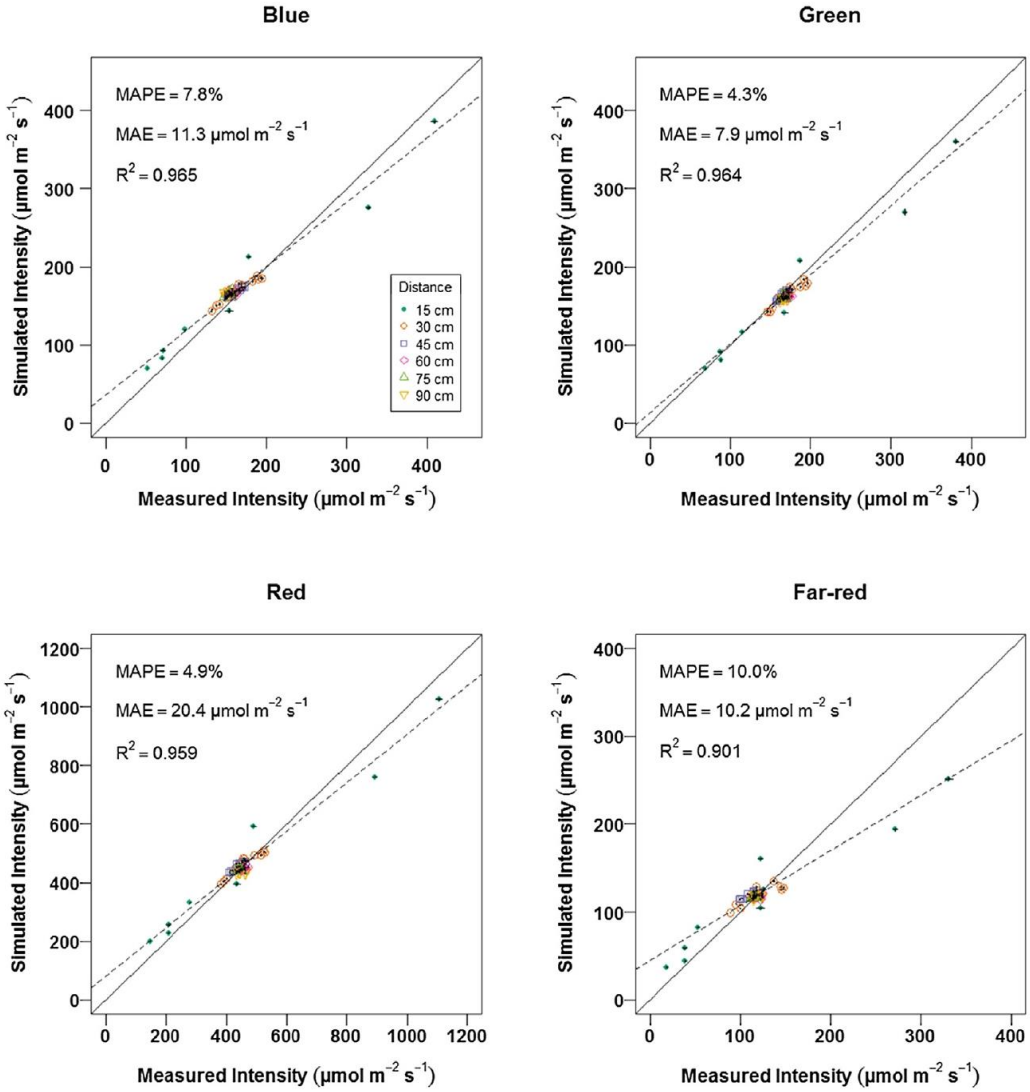

Fig. 6. Linear regression of data from different heights for the four light ranges: blue, green, red and far-red. Error bars represent the standard error of the mean (n = 3). (For interpretation of the references to color in this figure legend, the reader is referred to the web version of this article.)

of the virtual LEDs was made enabling a relative comparison of simulations and measurements in the six distances and hereby the adjustment of the optical properties. To capture the change in intensity towards the bottom of the chamber as measured, the properties of the walls were set to a mirror-like surface with a specular reflection and total shininess for all colors and an absorption of 0.02 for blue, green and far-red, and 0.04 for red. Finally, the power of the virtual LED lights was adjusted by fitting the simulation to the intensity measured at each channel in 60 cm distance from the LED modules.

2.4. Light simulations and statistical indices for model evaluation

In the simulations, the chamber dimensions and the placement of the LED modules were set according to the construction plots of the

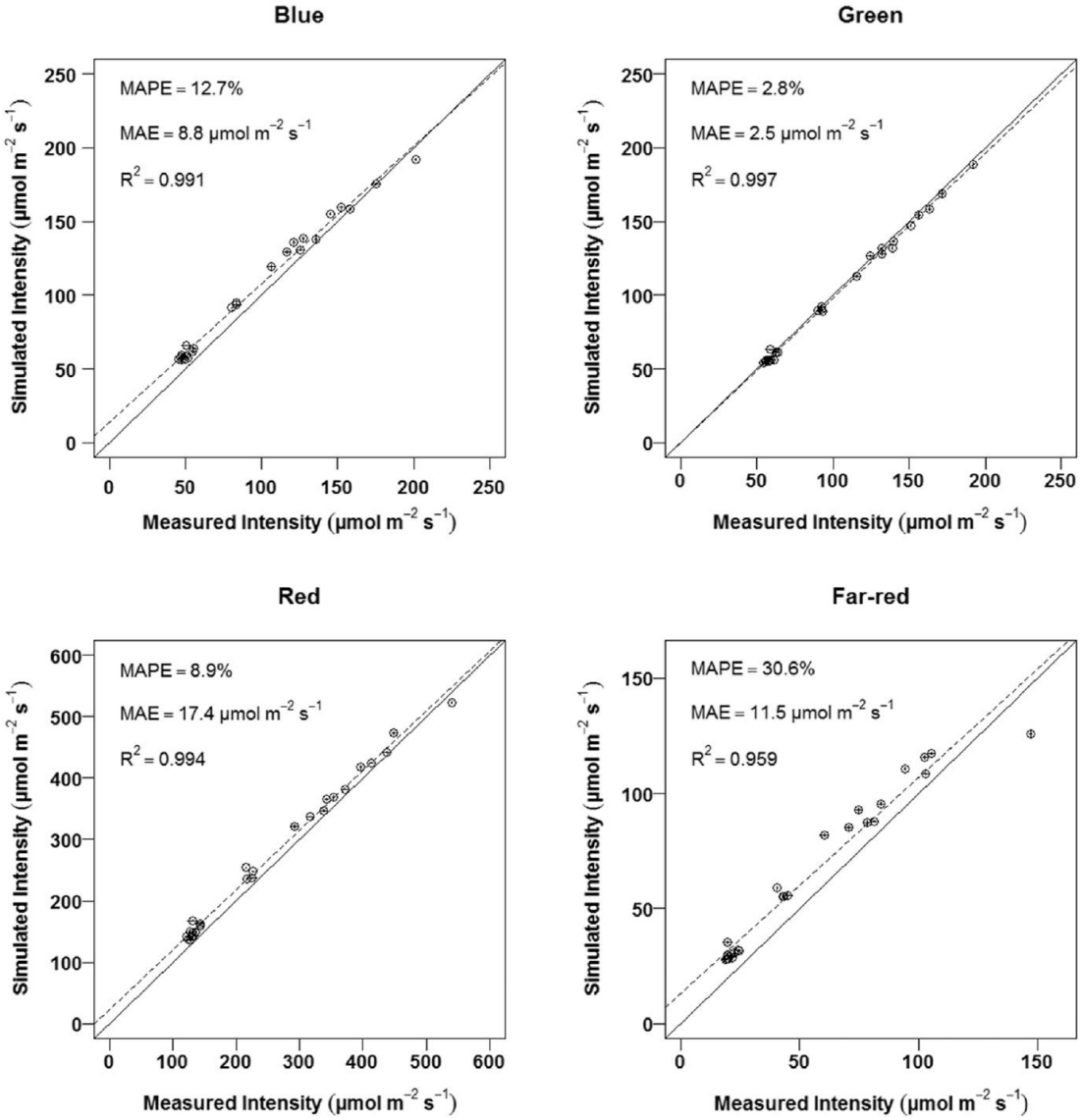

Fig. 7. Linear regression of data from different directions for the four light ranges: blue, green, red and far-red (point of power setting is excluded). Error bars represent the standard error of the mean (n = 3).

climate chamber. To guaranty high accuracy reproducibility of the simulated light scenario, the number of simulated rays was set to 500 million and a reflection depth of 50. The random seed, determining the randomness of emitted rays was changed with each run of the GPUFlux light model and the simulation was repeated three times. The model was set to move the sensor through the LED growth chamber to all measurement positions each time running the light simulation, and saving the result of the absorbed light in the five wavelength ranges identical to the measurements.

The model was evaluated based on the statistical indices mean absolute percentage error (MAPE) (de Myttenaere et al., 2016) (Eq. (1)), mean absolute error (MAE) (de Myttenaere et al., 2016) (Eq. (2)) and R^2:

$$MAPE = \frac{100}{n}\sum_{i=1}^{n}\left|\frac{O_i - S_i}{O_i}\right| \quad (1)$$

$$MAE = \frac{100}{n}\sum_{i=1}^{n}|O_i - S_i| \quad (2)$$

where O are the observed values and S the simulated values. For evaluation of the optimal placement of the LED modules for achieving a uniform light climate, the placements of the modules in the model were changed according to A1 and A2. Sensors in the nine horizontal measurement points were all presented during three runs, and the data for each sensor was saved. For a comparison of the different placement, the Mean Relative Deviation (MRD) was computed to give a relative measure of the deviation of the light level in the nine points from the average of the nine points (Ciolkosz et al., 2001) (Eq. (3)):

$$MRD = \frac{1}{N}\frac{\sum|E_i - E_M|}{E_M} \quad (3)$$

where N is the number of data points, E_i is PAR of point i and E_M is the mean PAR of all points.

Table 2
Mean measured intensity (μmol $m^{-2} s^{-1}$), mean absolute percentage error (MAPE, %) and mean absolute error (MAE, μmol $m^{-2} s^{-1}$) of simulations at different distances from the LED module, positions within the chamber, elevation and azimuth angles. Statistics for each point include the respective distances, positions, elevation and azimuth angles.

Points[a]	Mean measured intensity (μmol $m^{-2} s^{-1}$)	MAPE (%)	MAE (μmol $m^{-2} s^{-1}$)
All data	494.4	9.0	35.3
Distance (cm)			
30	511.7	10.1	41.1
60	475.9	7.9	29.0
Position			
Center	476.5	10.6	40.3
LED module	513.7	7.3	29.9
Elevation angles (°)			
90	890.4	3.2	29.8
67.5	796.1	5.0	38.3
45	647.9	5.7	35.3
22.5	440.2	9.9	43.5
0	262.9	11.9	31.0
Azimuth angles (°)			
0	262.9	11.9	31.0
45	263.9	10.8	28.3
90	258.7	15.3	39.3

[a] Point of power setting is excluded.

3. Results and discussion

3.1. General accuracy

The simulated light intensity for the four light ranges showed a high accuracy both in the dataset from different heights and the dataset from different directions. The R^2 were between 0.901 and 0.965 and MAPE between 4.3% and 10.0% for data from the nine points in different heights (Fig. 6). For data from the different directions in four positions the R^2 were between 0.959 and 0.997 and MAPE were between 2.8% and 30.6% (Fig. 7). Comparing light colors, the MAPE of the far-red light was in both datasets considerably higher than for the three other light ranges. The green light had the lowest MAPE.

In the different heights, the data from 15 cm distance had the lowest uniformity within the nine points and they had the highest spread from the 1:1 line, whereas the points in distances with an increased uniformity of light were close to the 1:1 line.

In the different directions (Fig. 7), the regression lines for blue, red and far-red light were located above the 1:1 line showing that the simulated light intensity was mainly overestimated. On the contrary, the simulated intensity of the green light showed a slight underestimation.

The comparison of measurements and simulations for all light ranges at different positions and directions showed that the simulations were slightly more accurate in 60 cm than in 30 cm distance and more accurate below the LED module than in the center of the chamber (Table 2). The MAPE continuously increased for the elevation angles from 90 to 0° by 2.6% to 11.9% and the azimuth angles were in general less accurate with a MAPE between 10.8% and 15.3% (Table 2).

The results showed that the model is capable of simulating changing micro-light climates regarding both spectra and light intensity within all evaluated positions and directions within the chamber. The lower accuracy of the far-red light could be caused by inaccuracies of the measurements. Although the field of view of the spectrometer is 180°, its accuracy is reduced when the light hits from a very low angle. The light distribution of the far-red LEDs might have hit the spectrometer from these angles to a higher extent than the other LEDs due to the different physical distribution of the far red light. This theory is supported by the fact that the simulations in general, and in far-red in particular, were less accurate when the sensor was pointing in a direction away from the LED module (15 cm distance and azimuth angles) and more light hit the sensor from a low angle. For improving simulations for different colors and directions, more complex characteristics of the virtual sensor, to resemble the spectrometers cosine-correction of light intensity coming from different angles, should be explored. There are very few studies that used virtual sensors to measure irradiation (Buck-Sorlin et al., 2011; Tian et al., 2017), however without any specific adaptations for the sensor used for their measurements. Further, the simulations indicated that the calibration of the optical properties of the sidewalls worked quite well and this low-cost method can be used if no technical equipment, e.g., an integrating sphere, is available. Nevertheless, using direct measurements of the optical properties should be used to further explore the accuracy of this calibration method.

3.2. Application of the model in plant growth simulations

Due to the general overestimation of light intensity, an additional adjustment of the power was done to achieve a better response to different elevation angles, which is an important aspect, considering that light interception depends on leaf angle in plant growth simulations. The power of each channel was slightly adjusted to fit the simulated intensity to the sum of the measurements at the five elevation angles in the two positions (center and below the module) at 60 cm distance

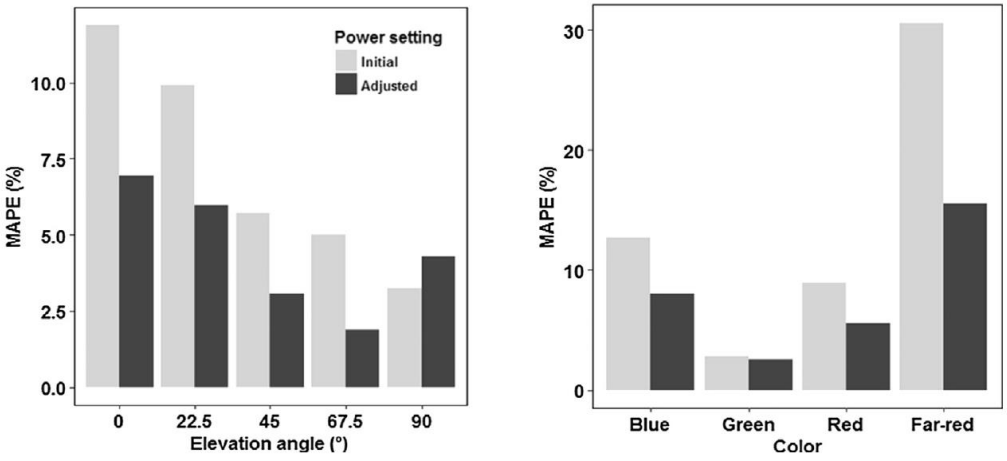

Fig. 8. Mean absolute percentage error (MAPE, %) for the entire spectrum at the five elevation angles for both positions in 60 cm distance (left) and MAPE for the four light colors across positions and directions (right).

Table 3
Measured and simulated Mean Relative Deviation (MRD) of the nine points for the three placements of the LED modules.

Module placement	All light		Blue		Green		Red		Far-red	
	Meas.	Sim.	Meas.	Sim.	Meas.	Sim.	Meas.	Sim.	Meas.	Sim.
Present	0.04	0.02	0.04	0.03	0.03	0.01	0.04	0.03	0.06	0.02
A1	0.01	0.01	0.02	0.02	0.01	0.01	0.01	0.01	0.03	0.02
A2	0.08	0.06	0.08	0.06	0.06	0.05	0.08	0.07	0.10	0.05

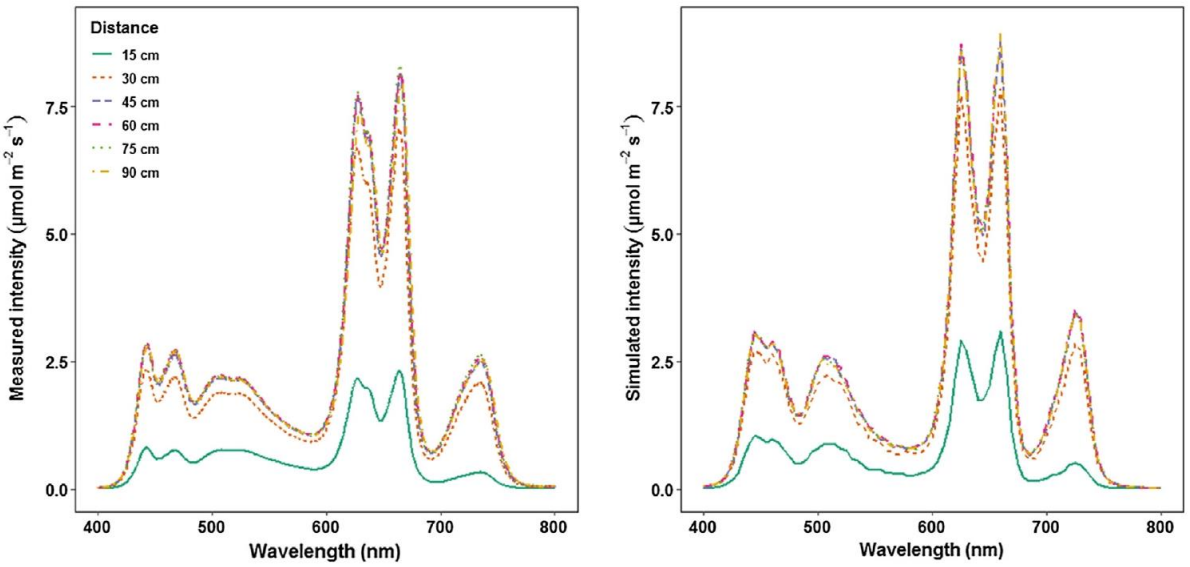

Fig. 9. The measured (left) and simulated (right) spectrum at the distances 15, 30, 45, 60, 75, and 90 cm from the LED modules in the center of the chamber.

Table 4
The ratios between red and the other three light colors at the distances 15, 30, 45, and 60 cm from the LEDs in the center of the chamber.

Distance (cm)	Red light:blue light		Red light:green light		Red light:far-red light	
	Measured	Simulated	Measured	Simulated	Measured	Simulated
15	2.7	2.7	2.1	2.7	9.2	8.1
30	2.9	2.8	2.7	2.8	4.5	4.0
45	2.8	2.7	2.7	2.8	4.3	3.8
60	2.8	2.8	2.7	2.8	4.2	3.7

(where the light from the modules is uniformly mixed and plants should be grown). The necessary adjustments were done by multiplying blue light by 0.92710, green light by 1.02865, red light by 0.96060, and far-red light by 0.85760.

Comparing the entire spectrum before and after adjustment in the five elevation angles at 60 cm distance, the adjustment decreased MAPE in all angles except 90° and resulted in MAPEs all below 8% (Fig. 8, left). The decrease in MAPE were present in all colors, when comparing the colors across all positions and directions and resulted in MAPEs below 20% for all colors (Fig. 8, right). The improvement in the far-red range was especially high because the overestimation under the initial power setting was higher than in the other color ranges.

With an alternative power setting the general overestimations of light intensity were considerably reduced and the overall accuracy of the model further improved. At the present state of the model, we suggest setting the power according to a light measurement at the mean leaf angle of the plant for an optimal simulation of light intensity on leaf- and canopy-level. However, the accuracy of the spectrometer when not pointing directly towards the light source should be considered. A model by Chelle et al. (2007a,b) also proved to capture tendencies of micro-light climate variability within a growth chamber concerning light intensity, but to our knowledge, no measures of accuracy were presented. In addition, the model presented in our study adds the possibility to simulate light spectra, which is an essential feature to explore the spectral possibilities of LED lighting. The possibility to simulate accurate micro-light climate is an important step to reproduce the environmental condition, which is for instance essential for plant breeders to investigate gene/QTL expressions.

3.3. Application of the model in chamber design

The different placements of the LED modules were compared to determine which one would give the most uniform light distribution at 45 cm distance. The smaller the MRD, the more uniform were the light across the nine points. Within all color ranges, it could be concluded from both measurements and simulations, that A1 had the most uniform light distribution and A2 had the least uniform light distribution (Table 3).

A module placement with less uniform light in 45 cm distance would imply that experiments could only be conducted with plants of shorter canopy height, considerably limiting species and cultivar selection as well as the duration of the growing period. The distance until

maximum light intensity from the four modules was evaluated to determine the effect of the three module placements until uniform light for plant growth experiments. The maximum light intensity was found at a position located in the center or close to the sidewall away from the direct light below the modules. With the present module placement, measurements and simulations of light intensity (PAR) were made in 5 cm intervals from 15 to 60 cm distance in the center of the LED growth chamber. The measured and simulated distance until maximum light intensity were 60 and 55 cm, while simulations determined the distance to be 45 cm for A1 and 65 cm for A2 (data not shown). With only a slightly underestimated simulated distance by 5 cm, we consider the model to deliver useful guidelines in the context of chamber design to determine the distance to light uniformity and the change of that distance if the module placement is changed.

Another aspect of light uniformity is the distance at which the single LED module emits a uniform light spectrum. In this study, this was investigated with the different physical light distribution of the far-red LEDs (FWHM90) and the blue and red LEDs (FWHM80). The effect of the different distributions could be observed in the center of the chamber in both measurements (Fig. 9, left) and simulations (Fig. 9, right) of the light spectrum in different distances from the LEDs.

The spectra showed a higher increase of the far-red peak than the other peaks between the 15 and 30 cm distance. This resulted in a lower ratio of far-red light in the center of the chamber close to the LEDs than at longer distances, meaning that the modules did not emit a uniform spectrum at small distances. The measured and simulated ratios between red light and the three other colors ranges were calculated for 15, 30, 45, and 60 cm distances (Table 4). A comparison showed in both datasets the tendency of a considerably higher red to far-red ratio at 15 cm distance than other distances, contrary to the other ratios, which were in the same range at all distances.

The well simulated ratios of light ranges at different distances to the LED modules, are important as a changing ratio (e.g., red:far-red ratio) strongly influences plant growth and development.

4. Conclusion

In this study, we presented a three-dimensional model of a LED chamber, which includes important aspects of both micro-light climate simulations and LED chamber design for spectral experiments. The results showed that the model is capable of simulating micro-light climate regarding both light intensity and spectra in different directions and positions within a growth chamber with high accuracy. Having the importance of light quality to growth, nutrition content, growth dynamics and overall biomass production in mind, the developed model will be a powerful tool, offering scientists several new possibilities to simulate plant growth under controlled environmental conditions. The model was also capable of determining the optimal placement of LED modules and gave good guidelines for points of uniform light intensity and spectrum. This makes the model a useful tool to design LED chambers with a high uniformity of light intensity and spectrum, important for reproducible experimental conditions to explore the effects of light spectrum on plant structure and physiology. Further development will focus on complex characteristics of the virtual sensor, using direct measurements of optical properties of the side walls and algorithms for easier setting of LED power and calibration of optical properties.

Declarations of interest

None.

Acknowledgements

This research was funded by the German Federal Ministry for Economic Affairs and Energy according to a decision of the German Federal Parliament within the Central Innovation Program for SMEs (ZF4279901CR6).

Proofreader: Cameron Anderson

References

Berkovich, Y.A., Konovalova, I.O., Smolyanina, S.O., Erokhin, A.N., Avercheva, O.V., Bassarskaya, E.M., Kochetova, G.V., Zhigalova, T.V., Yakovleva, O.S., Tarakanov, I.G., 2017. LED crop illumination inside space greenhouses. Reach – Rev. Hum. Sp. Explor. 6, 11–24. https://doi.org/10.1016/j.reach.2017.06.001.

Bongers, F.J., Pierik, R., Anten, N.P.R., Evers, J.B., 2018. Subtle variation in shade avoidance responses may have profound consequences for plant competitiveness. Ann. Bot. 121, 863–873. https://doi.org/10.1093/aob/mcx151.

Boonen, C., Samson, R., Janssens, K., Pien, H., Lemeur, R., Berckmans, D., 2002. Scaling the spatial distribution of photosynthesis from leaf to canopy in a plant growth chamber. Ecol. Modell. 156, 201–212. https://doi.org/10.1016/S0304-3800(02)00171-0.

Buck-Sorlin, G., de Visser, P.H., Henke, M., Sarlikioti, V., van der Heijden, G.W., Marcelis, L.F., Vos, J., 2011. Towards a functional–structural plant model of cut-rose: simulation of light environment, light absorption, photosynthesis and interference with the plant structure. Ann. Bot. 108, 1121–1134. https://doi.org/10.1093/aob/mcr190.

Buck-Sorlin, G., Hemmerling, R., Kniemeyer, O., Burema, B., Kurth, W., 2008. A rule-based model of barley morphogenesis, with special respect to shading and gibberellic acid signal transduction. Ann. Bot. 101, 1109–1123. https://doi.org/10.1093/aob/mcm172.

Burgess, A.J., Retkute, R., Pound, M.P., Mayes, S., Murchie, E.H., 2017. Image-based 3D canopy reconstruction to determine potential productivity in complex multi-species crop systems. Ann. Bot. 119, 517–532. https://doi.org/10.1093/aob/mcw242.

Chelle, M., Evers, J.B., Combes, D., Varlet-Grancher, C., Vos, J., Andrieu, B., 2007a. Simulation of the three-dimensional distribution of the red:far-red ratio within crop canopies. New Phytol. 176, 223–234. https://doi.org/10.1111/j.1469-8137.2007.02161.x.

Chelle, M., Renaud, C., Delepoulle, S., Combes, D., 2007b. Modeling light phylloclimate. Functional-Structural Plant Models. Abstracts of papers and posters (p. 57, 4 p.). Presented at 5. International Workshop, Napier, NZL. (2007-11-04 – 2007-11-09).

Ciolkosz, D.E., Both, A.J., Albright, L.D., 2001. Selection and placement of greenhouse luminaires for uniformity. Appl. Eng. Agric. 17 (6), 875–882. https://doi.org/10.13031/2013.6842.

Cope, K.R., Bugbee, B., 2013. Spectral effects of three types of white light-emitting diodes on plant growth and development: absolute versus relative amounts of blue light. HortScience 48, 504–509.

de Myttenaere, A., Golden, B., Le Grand, B., Rossi, F., 2016. Mean absolute percentage error for regression models. Neurocomputing, Adv. Artif. Neural Netw. Mach. Learn. Comput. Intell. 192, 38–48. https://doi.org/10.1016/j.neucom.2015.12.114.

Delepoulle, S., Renaud, C., Chelle, M., 2009. Improving light position in a growth chamber through the use of a genetic algorithm. In: Artificial Intelligence Techniques for Computer Graphics, Studies in Computational Intelligence. Springer, Berlin, Heidelberg, pp. 67–82. https://doi.org/10.1007/978-3-540-85128-8_5.

Evers, J.B., Vos, J., Chelle, M., Andrieu, B., Fournier, C., Struik, P.C., 2007. Simulating the effects of localized red:far-red ratio on tillering in spring wheat (*Triticum aestivum*) using a three-dimensional virtual plant model. New Phytol. 176, 325–336. https://doi.org/10.1111/j.1469-8137.2007.02168.x.

Gautier, H., Měch, R., Prusinkiewicz, P., Varlet-Grancher, C., 2000. 3D architectural modelling of aerial photomorphogenesis in white clover (*Trifolium repens* L.) using L-systems. Ann. Bot. 85, 359–370. https://doi.org/10.1006/anbo.1999.1069.

Gitz, D.C., Liu-Gitz, L., Britz, S.J., Sullivan, J.H., 2005. Ultraviolet-B effects on stomatal density, water-use efficiency, and stable carbon isotope discrimination in four glasshouse-grown soybean (*Glycine max*) cultivars. Environ. Exp. Bot. 53, 343–355. https://doi.org/10.1016/j.envexpbot.2004.04.005.

Henke, M., Buck-Sorlin, G.H., 2017. Using a full spectral raytracer for calculating light microclimate in functional-structural plant modelling. Comput. Inform. 36, 1492–1522. https://doi.org/10.4149/cai_2017_6_1492.

Henke, M., Kurth, W., Buck-Sorlin, G.H., 2016. FSPM-P: towards a general functional-structural plant model for robust and comprehensive model development. Front. Comput. Sci. 10, 1103–1117. https://doi.org/10.1007/s11704-015-4472-8.

Kniemeyer, O., Buck-Sorlin, G., Kurth, W., 2007. GroIMP as a platform for functional-structural modelling of plants. In: Functional–Structural Plant Modelling in Crop Production. Springer, Dordrecht, the Netherlands, pp. 43–52.

Measures, M., Weinberger, P., Baer, H., 1973. Variability of plant growth within controlled-environment chambers as related to temperature and light distribution. Can. J. Plant Sci. 53, 215–220. https://doi.org/10.4141/cjps73-038.

Morrow, R.C., 2008. LED lighting in horticulture. HortScience 43, 1947–1950.

Olle, M., Viršile, A., 2013. The effects of light-emitting diode lighting on greenhouse plant growth and quality. Agric. Food Sci. 22, 223–234. https://doi.org/10.23986/afsci.7897.

Phong, B.T., 1975. Illumination for computer generated pictures. Commun. ACM 18, 311–317. https://doi.org/10.1145/360825.360839.

Tian, T., Wu, L., Henke, M., Ali, B., Zhou, W., Buck-Sorlin, G., 2017. Modeling allometric relationships in leaves of young rapeseed (*Brassica napus* L.) grown at different temperature treatments. Front. Plant Sci. 8, 313. https://doi.org/10.3389/fpls.2017.00313.

Van Antwerpen, D.G., 2011. Unbiased Physically based Rendering on the GPU. (PhD thesis). TU Delft, available on: https://repository.tudelft.nl/islandora/object/uuid:4a5be464-dc52-4bd0-9ede-faefdaff8be6?collection=education.

Visser, D., Bram, P.H., van der Heijden, G., Buck-Sorlin, G., 2014. Optimizing illumination in the greenhouse using a 3D model of tomato and a ray tracer. Front. Plant Sci. 5. https://doi.org/10.3389/fpls.2014.00048.

Vos, J., Evers, J.B., Buck-Sorlin, G.H., Andrieu, B., Chelle, M., de Visser, P.H.B., 2010. Functional-structural plant modelling: a new versatile tool in crop science. J. Exp. Bot. 61, 2101–2115. https://doi.org/10.1093/jxb/erp345.

4. Chapter II: Simulating light spectrum within a soybean canopy in an LED growth chamber

Hitz, T., Henke, M., Graeff-Honninger, S., Munz, S., 2018. Simulating light spectrum within a soybean canopy in an LED growth chamber, in: 2018 6th International Symposium on Plant Growth Modeling, Simulation, Visualization and Applications (PMA). IEEE, pp. 120–125. https://doi.org/10.1109/PMA.2018.8611598

In Chapter I, the LED chamber model was constructed and fulfilled the desired properties. High accuracy of simulations with multiple sensor orientations *was important for the future use of the chamber model for FSP modelling with various leaf orientations. In Chapter II, a static plant model was integrated in the chamber model and measurements and simulations below the soybean canopy were compared.*
The measurements consisted of light measurements at nine points in the chamber and detailed measurements of plant architecture for a virtual reconstruction of the scene. The light measurements were compared with simulations using the virtual sensor from Chapter I. The comparison further substantiated that the model assured good light simulations for FSP modelling and represents an intermediate step between the empty chamber and the integration of a dynamic FSP model of soybean. The model was applied to evaluate alternative experimental scenarios by simulating an increased plant density in the chamber and the influence on light interception and heterogeneity was discussed.

2018 6th International Symposium on Plant Growth Modeling, Simulation, Visualization and Applications (PMA)

Simulating light spectrum within a soybean canopy in an LED growth chamber

Tina Hitz[1]
1. Department of Agronomy, Institute of Crop Science,
University of Hohenheim
Stuttgart, Germany
tina.hitz@uni-hohenheim.de

Michael Henke
Leibniz Institute of Plant Genetics and Crop Plant Research
(IPK), OT Gatersleben
06466 Stadt Seeland, Germany

Simone Graeff-Hönninger
Department of Agronomy, Institute of Crop Science,
University of Hohenheim
Stuttgart, Germany

Sebastian Munz
Department of Agronomy, Institute of Crop Science,
University of Hohenheim
Stuttgart, Germany

***Abstract*—Knowledge on the effect of light spectra on different crops is important in the exploration of possibilities to regulate crop growth and quality with LED lighting. Functional structural plant modelling can be an important tool to cope with the large number of experimental treatments necessary to identify the effect of specific wavelengths and the interaction with other environmental factors. Therefore, the objectives were to create a virtual environment that can simulate light intensity and spectrum within a soybean canopy grown within an LED growth chamber. Measurements were made at two dates, on two plant sets and at two placements. Simulated light intensities were accurate with a R^2 between 0.798 and 0.956; mean absolute percentage errors between 5.85 and 35.14 % and simulated change in light spectrum below the canopy changed similar to the measurements. The chosen GPUFlux model in GroIMP can be used for functional structural plant modelling in response to light spectra and intensity and to explore an optimal experimental design within an LED chamber.**

Keywords—functional-structural plant model, LED lighting, spectral ray tracer, virtual sensor, light simulation, GroIMP, micro-light climate.

I. INTRODUCTION

With an increased use of light-emitting diode (LED) lighting in horticulture, growers have the chance to design specific light spectra to achieve a desired growth or quality of a crop [1]. Changing ratios of red to far-red wavelength ranges [2] and red to blue ranges [3] induce changes in, e.g. stem elongation, leaf area and dry weight of the plant. To take advantage of these possibilities an increased knowledge of spectral effects on plant growth is necessary [4]. However, this implies many treatments in an experimental setup since effects on plant growth can change with other light treatments as photoperiod, light intensity, impulse or continuous lighting [1] and plant species and cultivar [3, 5].

Functional structural plant models (FSPMs) taking light spectra and -intensity into account can simulate the effects of different light scenarios on plant growth and herby be an important tool to reduce the large number of treatments necessary to increase knowledge of spectral effect on plant growth. In the Growth Grammar-related Interactive Modeling Platform (GroIMP) [6] a spectral ray tracer [7] is implemented to perform spectral simulations. With the possibility to simulate the complete light spectrum of arbitrary light sources (e.g., LEDs, or high-pressure sodium lamps, or a diffuse sky with direct sun light) [8] an experimental setup for LED experiments can be reconstructed [9]. Earlier studies in GroIMP with spectral plant response have focused only on the red to far-red response in an open environment [10,11] and studies under controlled conditions (climate chamber [12], greenhouse [13, 14]) have focused on light intensity.

Therefore, our objective were to: (i) simulate light spectrum within a soybean canopy grown in an LED chamber, and (ii) evaluate the model in the context of an ideal experimental setup in LED chambers and future FSPM within the virtual LED growth chamber.

II. MATERIALS AND METHODS

A. Plants

Soybean (*Glycine max* (L.) Merr.) were sown in pots (9.5*9.0*9.0 cm) and grown for 21 days at two different light treatments (red:blue light ratios of 1.5 in plant set one and 2.6 in plant set two) in a LED growth chamber, with adjustable light intensity and spectrum, produced by CompLED (Sunsim VIS_v1.1; Compled Solutions GmbH,

978-1-5386-7816-9/18/$31.00 ©2018 IEEE

Dresden, Germany). The measures of the chamber were 1.1 m high, 0.5 m wide and 0.7 m deep and it was placed inside a climate chamber with an average temperature of 27.2 °C and relative humidity between 50-100 %. In each treatment, a set of four plants was grown. Just prior to the light measurements, the architecture of the plants was assessed manually comprising length and width of internodes, petioles and leaves, angle and azimuth direction of petioles and angle of the leaves measured in length from base to tip and in width from side to side. The two plant sets and measurement dates differed in average height and estimated leaf area (0.754 + 0.655*Length*Width [15]) (Table I).

TABLE I. MEAN HEIGHT AND ESTIMATED LEAF AREA (± STANDARD DEVIATION) OF THE TWO PLANTS SETS ON THE TWO MEASUREMENTS DATES.

	Plant set one		Plant set two	
	1st date	2nd date	1st date	2nd date
Height	19.8 ± 0.7	22.3 ± 0.42	22.2 ± 1.0	24.9 ± 3.5
Leaf area	129.5 ± 21.9	180.2 ± 34.5	160.3 ± 32.0	220.8 ± 41.2

B. *Light measurements*

During the light measurements, a broad spectrum (400-800 nm) (Fig. 4) with a light intensity of 700 µmol m^{-2} s^{-1} was turned on. Quantitative measurements of the light spectrum (µmol m^{-2} s^{-1} nm^{-1}) were acquired with a FLAME-S-XR1-ES spectrometer (Ocean Optics Germany GmbH, Ostfildern, Germany) equipped with a collimating lens (74-UV-MP) and a right-angle reflector with cosine corrector (74-90-UV-CC3) measuring in the range from 200-1025 nm with a resolution of around 2 nm. The spectrometer took an average of 25 measurements and automatically regulated the integration time to the optimum for each measurement (1.799 E^{-2} - 2.107 E^{-1} sec.). For each measurement, the intensity of light was summed up and stored in four ranges of wavelengths: 400-500 nm (blue light), 500-600 nm (green light), 600-700 nm (red light), and 700-800 nm (far-red light). To place the spectrometer within the chamber while the front of the chamber was closed it was attached to a tripod, with the sensor pointing upwards. The measurements were performed at a height of 16 cm (93 cm distance to the LEDs), 18 and 21 days after sowing and in an empty chamber. At this distance from the LEDs the light from the individual LEDs and the LED modules is uniformly mixed [9]. The pots were placed with a distance between pots of 5.5 cm at two placements within the chamber. The first placement (front) was in the right corner towards the front of the chamber and in the second placement (center) each pot was moved 15 cm to the back of the chamber (Fig. 1). Light intensity and spectrum were measured within both plant sets in nine points at each placement of the four pots and in the same points in an empty chamber. The distance between the points was 3.5 cm/7.5 cm (Fig. 1). The distance from the side to the nearest points was 14 cm and the distance from the front was 14.5 cm in placement front and 29.5 cm in placement center. In some cases, the point were directly under a leaf resulting in low light intensities compared to the rest of the points, which created a gap in the dataset with no measured values.

This research was funded by the German Federal Ministry for Economic Affairs and Energy within the Central Innovation Programme for SMEs (ZF4279901CR6).

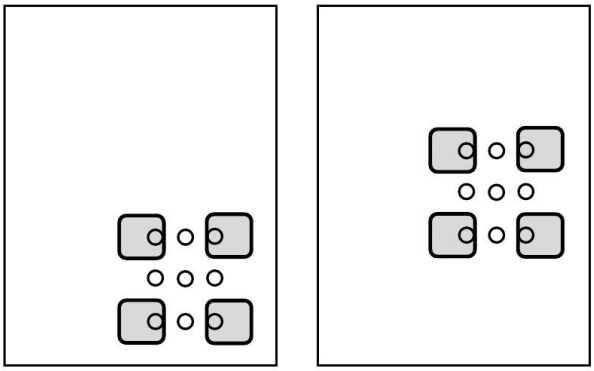

Fig. 1. Pot (square) position front (left) and center (right) and the nine measurement points (circle).

C. *Light simulations*

A 3D model of a LED growth chamber was constructed identical to the experimental chamber [9] according to measurements and manufacturers' information (Compled Solutions GmbH, Dresden, Germany). The four LED modules were comprised of nine different LED types and reconstructed with the position, spectrum and half width angle (80-120°) of the individual LEDs. Virtual soybean plants were constructed (Fig. 2) based on the described architectural measurements. Internodes and petioles were simple cylinder objects, while the leaves were reconstructed with a triangulation to achieve a more realistic shape. For the comparison of measured and simulated light intensity and spectrum, a virtual light sensor was constructed using a parallelogram object with the same area as the sensor of the spectrometer (19.36 mm^2) [9].

Fig. 2. Plant set one (left) and reconstruction in GroIMP (right).

The spectral light distribution was simulated in a five nm interval between 400 to 800 nm with the spectral Monte-Carlo ray tracer GPUFlux [7] integrated in GroIMP [8] and already evaluated in different directions for spectral simulations in an empty virtual LED growth chamber [9]. The light source and the optical properties of the objects were defined in a five nm interval for spectral light simulations. The spectra of the virtual LEDs were set for

each LED type according to manufacture information. A measurement of light intensity in the center of the chamber in 16 cm height was used to set the power of the virtual LEDs and for a final adjustment of the spectrum peaks to fit the measured spectrum (Fig. 4). The power was adjusted until the simulated intensity within the four wavelength ranges was the same as the measured.

The optical properties of the objects were defined by a Phong-type shader that describes direct and diffuse absorption, reflection, transmission, shininess, and specular reflection of light [16]. The optical properties of the leaves were set according to measurements from a typical soybean leaf [17] and the properties of the substrate as an organic-affected soil [18]. The optical properties of the chamber side were adjusted to give a decrease in light intensity towards the bottom of the chamber according to measurements in different heights [9]. The number of rays and reflections in the light simulations were set to 500 million rays and 50 reflections to guarantee accuracy and reproducibility of the simulated light scenario [8]. One run of the simulation with these setting took three minutes. To assure that the complexity of the scene was not too high for these settings they were tested by simulation with an increased number of rays and/or reflections, which was found not to change the simulations (data not shown).

For an evaluation of the effect from plant number (density) on light microclimate within the chamber, simulations were performed with one plant placed with different densities in the chamber. No measurements were made for this evaluation. The densities for the simulations were 2, 6, 12, 20, 30 and 42 plants in the chamber placed from one column and two rows to six columns and seven rows (Fig. 3). During the run of the model, the absorbed light of the unifoliate leaves of each plant was recorded.

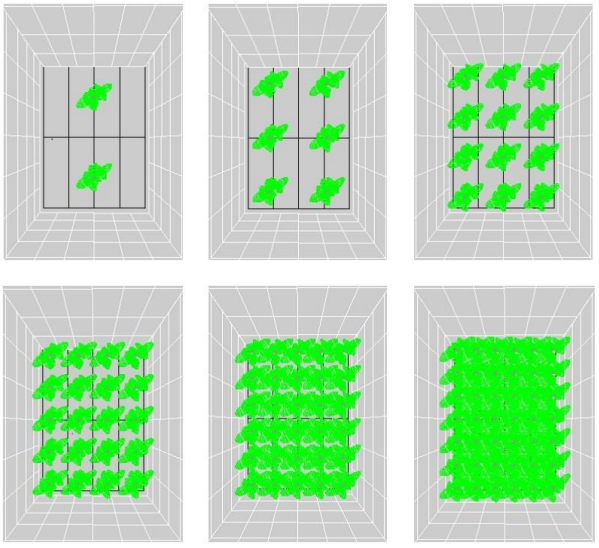

Fig. 3. Illustration of the six plant densities (2, 6, 12, 20, 30 and 42) in a simplified wireframe top-view.

D. Statistical indices

The simulations were evaluated based on the statistical indices mean absolute percentage error (MAPE) [19] (1), mean absolute error (MAE) [19] (2) and R^2.

$$MAPE = \frac{100}{n}\sum_{i=1}^{n}\left|\frac{O_i - S_i}{O_i}\right| \quad (1)$$

$$MAE = \frac{100}{n}\sum_{i=1}^{n}|O_i - S_i| \quad (2)$$

$$O = Observed\ values$$
$$S = Simulated\ values$$

III. Results and Discussion

The measured and simulated spectrum in the point of power setting had a high similarity (Fig. 4), and the light simulations across the nine points in the empty chamber were highly accurate with a MAPE between measurements and simulations of 1.12 and 0.96 % in pot placement one and two, respectively. The standard error of the measurements in the nine points were 3.29 µmol m^{-2} s^{-1}, which substantiates the assumption of uniform light at this distance from the LEDs.

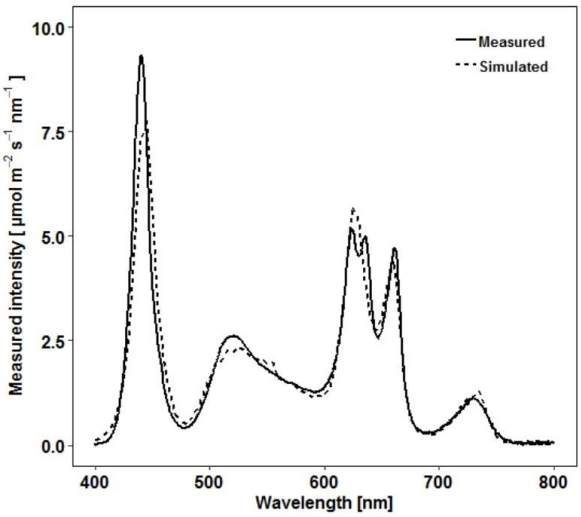

Fig. 4. Measured and simulated spectrum in the center of the chamber in 16 cm height.

Linear regressions for the simulations within the soybean canopy at the two pot placements resulted in R^2 values between 0.798 and 0.956 and MAPE between 5.85 and 35.14 % in plant set one. In plant set two, the R^2 values were between 0.955 and 0.854, and MAPE between 6.12 and 9.35 % (Fig. 5). A similar accuracy was found at both

placements, and in both plant sets, but with a common tendency of lower accuracy at the second measurement date compared to the first date (Table II). The height and leaf area of plant set two were higher than plant set one at both dates, which indicates no general decrease in accuracy with increased height or leaf area. The tendency of decreased accuracy at the second measurement date could be due to the more complex scenes that were reconstructed at the second date, due to one more internode of each plant.

Interesting for spectral simulations is how the ratios between wavelengths change through the canopy. The average ratios between the recorded wavelength ranges in the nine points in an empty chamber and within the two plant sets showed the same tendency in measurements and simulations (Table III). The simulation captured both the slight increase in red to blue ratio and slight decrease in the red to green ratio as well as the clear decrease in red to far-red ratios through the canopy.

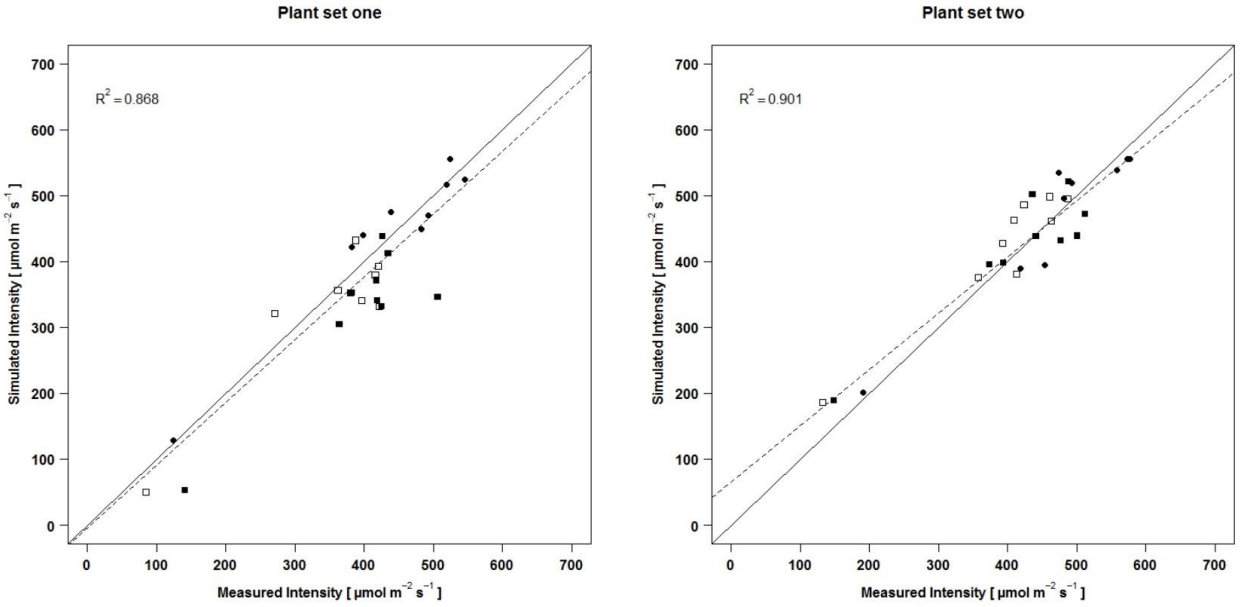

Fig. 5. Linear regression of the two plant sets at first (circle) and second (square) measurement dates at pot placement front (open symbols) and pot placement center (filled symbols).

TABLE II. MEAN MEASURED INTENSITY AND R^2, MEAN ABSOLUTE PERCENTAGE ERROR (MAPE), AND MEAN ABSOLUTE ERROR (MAE) BETWEEN MEASURED AND SIMULATED LIGHT INTENSITY IN THE TWO PLANT SETS AT THE TWO PLACEMENTS AND THE TWO MEASUREMENT DATES.

Plant set	Measurement	Pot Placement	Mean measured intensity (µmol m^{-2} s^{-1})	R^2	MAPE (%)	MAE (µmol m^{-2} s^{-1})
One	1st	Front	460.56	0.956	6.39	28.8
		Center	433.92	0.946	5.85	26.0
	2nd	Front	348.63	0.838	18.27	41.5
		Center	390.68	0.798	35.14	65.7
Two	1st	Front	492.07	0.955	6.12	29.4
		Center	468.95	0.946	6.40	28.8
	2nd	Front	418.95	0.854	9.01	34.9
		Center	392.95	0.917	9.35	33.5

TABLE III. AVERAGE MEASURED AND SIMULATED RATIOS OF RED TO BLUE, GREEN AND FAR-RED RANGES AT THE NINE MEASUREMENT POINTS IN THE EMPTY CHAMBER AND BELOW THE CANOPY OF TWO PLANT SETS.

Data	Red:blue ratio		Red:green ratio		Red:far-red ratio	
	Measured	*Simulated*	*Measured*	*Simulated*	*Measured*	*Simulated*
Empty Chamber	1.20	1.18	1.41	1.38	6.19	5.85
Plant set one	1.32	1.26	1.35	1.31	5.10	4.67
Plant set two	1.28	1.23	1.37	1.33	5.32	4.84

The results of the simulations with different plant densities showed that with 42 plants in the chamber the mean light intensity absorbed in the lower canopy decreased to below half of what is absorbed with two plants in the chamber (Fig. 6). Simultaneously, the standard deviation of the mean absorption increased then the number of plants increased. That indicates a decreased homogeneity of the received light treatments by the plants although placed below the same light. Plotting the absorption of the unifoliate leaves of the individual plants with the placement of the plant in the chamber show that the higher standard deviation at a higher plant density is due to an increasing effect from the sidewalls. With 42 plants in the chamber, a clear effect was present in the border rows (Fig 7; right), but not with 12 plants (Fig 7; right).

In additional simulations (data not shown), it was determined that the lower increase in absorption in row one and seven compared with column one and six were due to the direction of the unifoliate leaves.

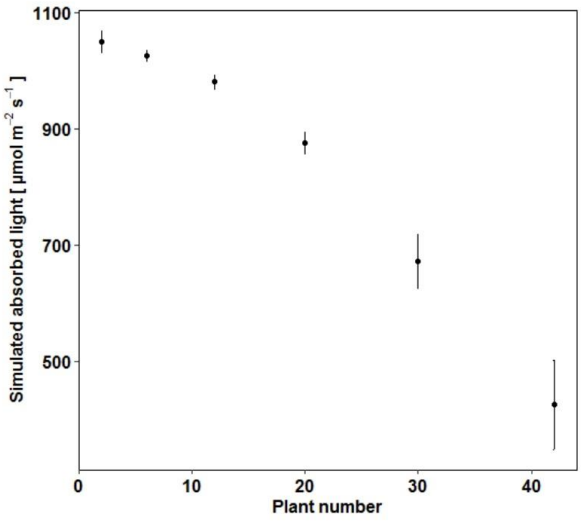

Fig. 6. Mean simulated absorbed light (error bars = standard deviation) of the unifoliate leaves of all plants plotted against plant number in the chamber.

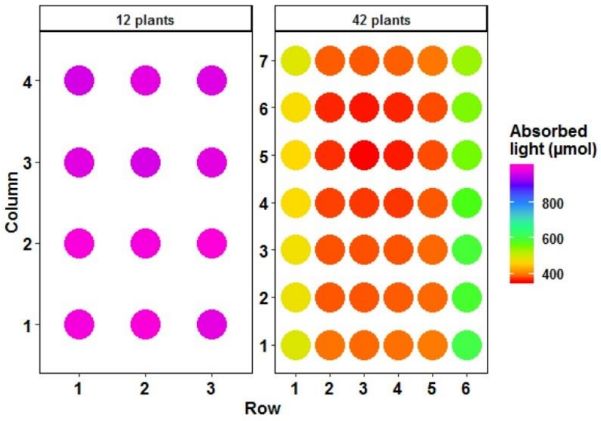

Fig. 7. Absorption in the first true leaves of the individual plants at a density of 12 and 42 plants.

IV. CONCLUSION

The results showed that the chosen model captured differences in spectral light intensity within a plant canopy very well. This allows simulating realistic light scenarios for light distributions and light quality to explore the effect of light treatments on plant growth. The model can as well be a useful tool in the design of an experimental setup to choose the optimal plant density and can be further extended for choosing pot placements and experimental design.

REFERENCES

[1] Y. A. Berkovich et al., "LED crop illumination inside space greenhouses," Reach - Rev. Hum. Sp. Explor., vol. 6, pp. 11–24, Jun. 2017.

[2] W. J. Corré, "Growth and morphogenesis of sun and shade plants II. The influence of light quality," Acta Bot. Neerl., vol. 32, no. 3, pp. 185–202, May 1983.

[3] K. R. Cope and B. Bugbee, "Spectral Effects of Three Types of White Light-emitting Diodes on Plant Growth and Development: Absolute

versus Relative Amounts of Blue Light," HortScience, vol. 48, no. 4, pp. 504–509, Jan. 2013.

[4] M. Olle and A. Viršile, "The effects of light-emitting diode lighting on greenhouse plant growth and quality," Agric. Food Sci., vol. 22, no. 2, pp. 223–234, Jun. 2013.

[5] D. C. Gitz, L. Liu-Gitz, S. J. Britz, and J. H. Sullivan, "Ultraviolet-B effects on stomatal density, water-use efficiency, and stable carbon isotope discrimination in four glasshouse-grown soybean (Glyicine max) cultivars," Environ. Exp. Bot., vol. 53, no. 3, pp. 343–355, Jun. 2005.

[6] O. Kniemeyer, G. Buck-Sorlin, and W. Kurth, "GroIMP as a platform for functional-structural modelling of plants," in *Functional–structural plant modelling in crop production*, 22nd ed., Dordrecht, the Netherlands: Springer, 2007, pp. 43–52.

[7] D. G. Van Antwerpen, "Unbiased physically based rendering on the GPU.," Dissertation for the Master Degree, Delft University of Technology, 2011.

[8] M. Henke and G. H. Buck-Sorlin, "Using a full spectral raytracer for calculating light microclimate in functional-structural plant modelling," Comput. Informatics, vol. 36, no. 6, 2017.

[9] T. Hitz, M. Henke, S. Graeff-Hönninger, and S. Munz, "Three-dimensional simulation of light spectrum and intensity within an LED growth chamber," unpublished.

[10] G. Buck-Sorlin, R. Hemmerling, O. Kniemeyer, B. Burema, and W. Kurth, "A rule-based model of barley morphogenesis, with special respect to shading and gibberellic acid signal transduction.," *Ann. Bot.*, vol. 101, no. 8, pp. 1109–23, May 2008.

[11] F. J. Bongers, R. Pierik, N. P. R. Anten, and J. B. Evers, "Subtle variation in shade avoidance responses may have profound consequences for plant competitiveness," *Ann. Bot.*, vol. 121, no. 5, pp. 863–873, Apr. 2018.

[12] T. Tian, L. Wu, M. Henke, B. Ali, W. Zhou, and G. Buck-Sorlin, "Modeling Allometric Relationships in Leaves of Young Rapeseed (Brassica napus L.) Grown at Different Temperature Treatments," Front. Plant Sci., vol. 8, p. 313, 2017.

[13] G. Buck-Sorlin et al., "Towards a functional–structural plant model of cut-rose: simulation of light environment, light absorption, photosynthesis and interference with the plant structure," Ann. Bot., vol. 108, no. 6, pp. 1121–1134, 2011.

[14] D. Visser, P. H. Bram, G. van der Heijden, and G. Buck-Sorlin, "Optimizing illumination in the greenhouse using a 3D model of tomato and a ray tracer," Front. Plant Sci., vol. 5, 2014.

[15] E. Bakhshandeh, B. Kamkar, and J. T. Tsialtas, "Application of linear models for estimation of leaf area in soybean [Glycine max (L.) Merr]," Photosynthetica, vol. 49, no. 3, pp. 405–416, Sep. 2011.

[16] B. T. Phong, "Illumination for Computer Generated Pictures," Commun. ACM, vol. 18, no. 6, pp. 311–317, Jun. 1975.

[17] M. J. Kasperbauer, "Far-Red Light Reflection from Green Leaves and Effects on Phytochrome-Mediated Assimilate Partitioning under Field Conditions.," Plant Physiol., vol. 85, no. 2, pp. 350–4, Oct. 1987.

[18] E. R. Stoner and M. F. Baumgardner, "Characteristic Variations in Reflectance of Surface Soils1," Soil Sci. Soc. Am. J., vol. 45, no. 6, p. 1161, 1981.

[19] A. de Myttenaere, B. Golden, B. Le Grand, and F. Rossi, "Mean Absolute Percentage Error for regression models," Neurocomputing, vol. 192, pp. 38–48, Jun. 2016.

5. Chapter III: Modelling of Soybean (Glycine max (L.) Merr.) Response to Blue Light Intensity in Controlled Environments

Hitz, T., Graeff-Hönninger, S., Munz, S., 2020. Modelling of Soybean (Glycine max (L.) Merr.) Response to Blue Light Intensity in Controlled Environments. Plants 9, 1757. https://doi.org/10.3390/plants9121757.

Previous chapters evaluated the chamber model to assure correct simulation of micro-light climate. The model was applied in scenarios representing alternative chamber design in Chapter I and alternative experimental setups with a static plant model in Chapter II.

In Chapter III, the dynamic FSP model of soybean was introduced in the chamber model. Earlier FSP models responding to the perceived spectrum integrated the response to R:FR, whereas Chapter III integrated the influence of BPFD. The BPFD was chosen to fill this gap and due to promising results of preliminary experiments in context of the speed breeding system. To calibrate the model, experiments with six levels of BPFD were performed to collect data on the morphological responses. Chapter III also presents the results of soybean response to BPFD regarding elongation, biomass and photosynthesis.

First, the calibrated model was used to simulate the actual perceived BPFD by the internodes during the experiments to fit a response curve of internode elongation to the perceived BPFD. Second, the response curve was integrated in the model to simulate internode elongation in response to the perceived BPFD. Finally, simulations were made to evaluate the optimum BPFD in an alternative chamber design for a reduction of energy consumption.

plants

MDPI

Article

Modelling of Soybean (*Glycine max* (L.) Merr.) Response to Blue Light Intensity in Controlled Environments

Tina Hitz, Simone Graeff-Hönninger and Sebastian Munz *

Institute of Crop Science, Cropping Systems and Modelling, University of Hohenheim, 70599 Stuttgart, Germany; tina.hitz@uni-hohenheim.de (T.H.); graeff@uni-hohenheim.de (S.G.-H.)

* Correspondence: s.munz@uni-hohenheim.de; Tel.: +49-711-22359

Received: 29 October 2020; Accepted: 9 December 2020; Published: 11 December 2020

Abstract: Low photosynthetic photon flux density (PPFD) under shade is associated with low blue photon flux density (BPFD), which independent from PPFD can induce shade responses, e.g., elongation growth. In this study, the response of soybean to six levels of BPFD under constant PPFD from LED lighting was investigated with regard to morphology, biomass and photosynthesis to increase the knowledge for optimizing the intensity of BPFD for a speed breeding system. The results showed that low BPFD increased plant height, leaf area and biomass and decreased leaf mass ratio. Photosynthetic rate and internode diameter were not influenced. A functional structural plant model of soybean was calibrated with the experimental data. A response function for internode length to the perceived BPFD by the internodes was derived from simulations and integrated into the model. With the aim to optimize lighting for a speed breeding system, simulations with alternative lighting scenarios indicated that decreasing BPFD during the growth period and using different chamber material with a higher reflectance could reduce energy consumption by 7% compared to the experimental setup, while inducing short soybean plants.

Keywords: photomorphogenesis; blue photon flux density; functional structural plant modelling; indoor farming; LED lighting

1. Introduction

In horticulture and indoor farming, LEDs have several advantages e.g., they save energy, emit less heat and have a long lifetime [1,2]. A spectrum can be designed depending on the response of the specific crop and the production aim. However, to fully exploit the spectral flexibility of LED lighting an increased knowledge of the spectral effects on plant morphology and growth is required [3]. Energy consumption can also be considered during spectral optimization as this can vary between spectra depending on the LED types [4]. A higher energy consumption of red than of blue LEDs has been reported [4,5], but theoretically the energy consumption of blue LEDs is higher than of red LEDs due to the higher energy level per photon of shorter than of longer wavelengths [6].

The advantages of LED lighting can be used in speed breeding, a breeding system developed particularly for growth chambers. The aim of a speed breeding system is to grow many generations per year to shorten the time for developing new cultivars. For instance, in a speed breeding system for several cereals, pea and chickpea six generations can be grown per year [7]. For a more efficient use of space, plants can be grown in a multi-layer system. For these systems, short plants are desirable to increase the number of layers of plants and hereby the possibility to include more genotypes at the same time. Therefore, a spectrum for speed breeding should not delay seed setting (many generations) and induce a shorter plant height to cultivate in more layers (many genotypes). These requirements

deviate from other indoor plant productions aiming to increase resource use efficiency considering other properties, such as yield and nutritional value [5]. Recently, a speed breeding protocol for soybean was developed using LED lighting. Red and blue light was found not to influence flowering time and was recommended to induce short compact plants. However, only two ratios of red and blue light (1:1 and 2:1) were studied [8].

The spectral light environment is perceived by the plant photoreceptors, which in a natural environment induce morphological changes such as those that express shade adaptations [9]. Shaded plants experience a reduced red to far-red ratio perceived by phytochrome [10] and a reduced photosynthetic photon flux density (PPFD). The latter is associated with a reduced blue photon flux density (BPFD) perceived by cryptochrome [11]. Typical shade responses of soybean are elongated internodes and petioles, increased specific leaf area (SLA) and decreased biomass and internode diameter [12–14]. Under LED lighting, BPFD can be reduced by lowering the ratio of blue light in the spectrum without a simultaneous reduction of PPFD. By reducing BPFD, some morphological shade responses, e.g., increased height, can be triggered also under constant PPFD [15,16]. For soybean, earlier studies found an increased plant height with decreasing BPFD [17–19] showing that high BPFD can be applied to induce short soybean plants, but these studies used a broad spectrum and included only one treatment [17] with a blue light ratio over 30%. None of these studies derived a response function to BPFD for soybean height under LED lighting with narrow peaks and none focused on blue light ratios between 15–78%. Earlier studies in other species than soybean also explored relatively low BPFD ratios (<50%) with the aim of avoiding extreme elongation under sole red LED lighting [15] or explored an intermediate BPFD to maximize biomass [20]. The aim in the present study was to reduce plant height to its minimum under a high BPFD.

Beside the influences on plant growth through the perceptions of photoreceptors, the light spectra can also influence the photosynthetic rate. Whereby, carbon assimilation can differ depending on the spectrum even under a constant PPFD. Photosynthetic pigments of plants absorb light mainly within the range of wavelength from 400 to 700 nm. The photosynthetic most effective part is considered to be the light within the red range (600–700 nm) due to a better balance of excitation between photosystem I and II and due to a more effective transfer between the red light absorbing chlorophylls than from the blue light absorbing carotenoids to chlorophyll [21]. Despite this, several studies measuring photosynthesis on plants grown under different light spectra found similar rates of photosynthesis under spectra with different ratios of light within the blue range (400–500 nm) [22–24].

The optimization of light spectrum for a specific crop and production system is very time-consuming given the many aspects that have to be considered, e.g., light quality, intensity and day length. Also, the transfer of knowledge between studies and into practice can be impaired by variability in several factors, e.g., plant density, type of light source and dimensions of the climate chambers. In this context, functional structural plant (FSP) modeling can assist as a tool for optimization of crop production and understanding of plant responses to its environment. An FSP model simulates plant growth and development, while considering its architectural appearance, by responding to the experienced environment on the individual organ level [25,26]. Hereby, responses can be related to the actually perceived spectrum of individual organs. The perceived spectral light environment can differ from the environment above the canopy and between phytomers due to self-shading and light reflection, as other studies found focusing on PPFD [27–29] or the red to far red ratio [30–34].

Earlier FSP models using artificial light sources for indoor plant production addressed the light regime for greenhouse production [35–37], while only one study used an FSP model with LEDs being the only light source [38]. An FSP model within an LED chamber can be a tool to reduce the amount of necessary experiments for spectral optimization and assist in the understanding of the plant response to the indoor environment and in the transfer of knowledge between studies and into practice.

The aim of this study was to find an optimal BPFD inducing short soybean plants under a narrow peaked red and blue LED spectrum, also considering energy consumption. We hypothesize that an optimum BPFD for minimum plant height, not influencing flowering time, could be determined with a

combination of experiments and FSP modelling. The objectives were to (i) examine the influence of different levels of BPFD under constant PPFD on soybean biomass, photosynthesis and morphology and (ii) calibrate an FSP model of soybean and integrate a response function to BPFD for internode length and (iii) to find by simulation the minimum BPFD to reduce plant height and energy consumption.

2. Results

2.1. Experimental Data—Plant Scale

Biomass and leaf area per plant showed similar differences among the six light treatments with a BPFD of 60, 110, 160, 210, 260 and 310 µmol m^{-2} s^{-1} (B60–B310). The treatments B110–B160 resulted in the highest values and B210–B310 in the lowest values, whereas plant height consistently decreased with increasing BPFD (Figure 1).

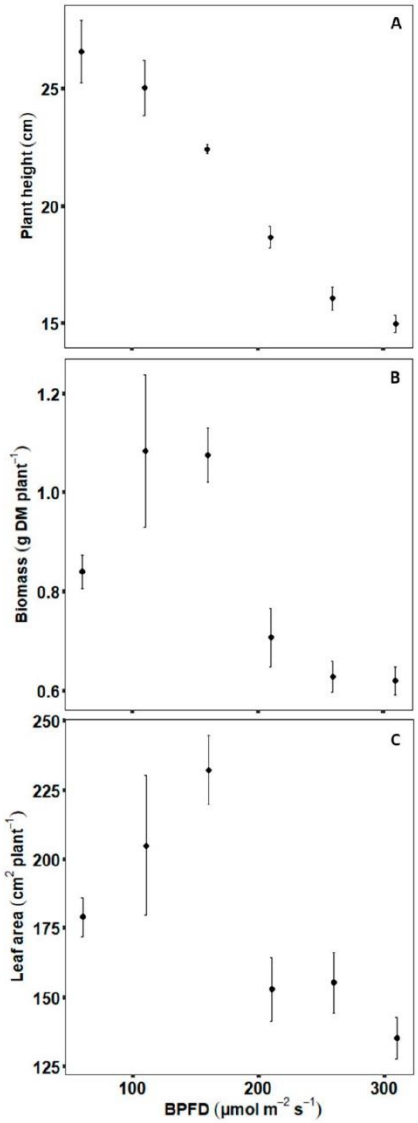

Figure 1. Final plant height (**A**), biomass (**B**) and leaf area (**C**) under different blue photosynthetic flux densities (BPFD). Error bars indicate standard error of the mean (n = 8).

Plant height responded rapidly after beginning of the experiment and the differences between treatments became more pronounced over time with differences between the highest and lowest values of 34%, 46%, and 34% on day 9 and 77% 75% and 72% on day 23 for plant height, biomass, and leaf area, respectively (Supplementary Materials, Figure S1).

2.2. Experimental Data—Phytomer Scale

2.2.1. Biomass

At the third phytomer, significant differences between treatments were found for biomass of internodes and leaf laminas. An increase in BPFD decreased the biomass of internodes and leaf laminas with the minimum of 0.022 and 0.078 g under B260 and the maximum of 0.046 and 0.136 g under B160. The same tendency was found for biomass of the second internode and the petiole, with the latter being less expressed with no significant differences between treatments. The leaf mass ratio (LMR) differed significantly between BPFD levels with a minimum value of 0.64 under B160 increasing to 0.69 under B60 and 0.71 under B310. The internode mass ratio of the stalk (IMRS) decreased from 0.72 under B260 to 0.63 under B60 (Table 1).

Table 1. Least square means of the final measurement of organ biomass, leaf mass ratio (LMR) and internode mass ratio of the stalk (IMRS) at phytomer scale under different blue photosynthetic flux densities (BPFD). Letters indicate significant differences between treatments ($p < 0.05$).

Phytomer Level	Organ/Ratio	Treatment					
		B60	B110	B160	B210	B260	B310
Second	Internode (g)	0.082 ^{a}	0.082 ^{a}	0.076 ^{a,b}	0.058 ^{b,c}	0.047 ^{c}	0.049 ^{c}
Third	Internode (g)	0.041 ^{a}	0.044 ^{a}	0.046 ^{a}	0.030 ^{b}	0.022 ^{b}	0.023 ^{b}
	Petiole (g)	0.016 ^{a}	0.018 ^{a}	0.018 ^{a}	0.015 ^{a}	0.013 ^{a}	0.013 ^{a}
	Leaf lamina (g)	0.127 ^{a}	0.136 ^{a,b}	0.116 ^{a,c}	0.100 ^{a,c}	0.078 ^{c}	0.081 ^{b,c}
	LMR	0.69 ^{a,b}	0.68 ^{b,c}	0.64 ^{c}	0.67 ^{b,c}	0.71 ^{a}	0.71 ^{a}
	IMRS	0.72 ^{a}	0.72 ^{a}	0.71 ^{a}	0.68 ^{a,b}	0.62 ^{b}	0.63 ^{b}

2.2.2. Leaf Morphology and Physiology

At the third phytomer, the SLA significantly increased from 303 under B110 to 346 cm^2 g^{-1} under B310. No significant differences were observed for carbon assimilation, but there was a slight reduction with increased BPFD from 28.81 µmol CO_2 m^{-2} s^{-1} under B110 to the minimum assimilation of 26.53 µmol CO_2 m^{-2} s^{-1} under B310. SPAD values did not differ significantly between treatments and showed no tendency (Table 2).

Table 2. Least square means of the final measurement of specific leaf area (SLA), carbon assimilation (A) and SPAD at phytomer scale under different blue photosynthetic flux densities (BPFD). Letters indicate significant differences between treatments ($p < 0.05$).

Phytomer Level	Measurement	Treatment					
		B60	B110	B160	B210	B260	B310
Third	SLA (cm^2 g^{-1})	324.35 ^{a,b}	303.04 ^{b}	327.68 ^{a,b}	327.02 ^{a,b}	341.41 ^{a,b}	346.38 ^{a}
	SPAD value	26.51 ^{a}	30.08 ^{a}	31.65 ^{a}	28.81 ^{a}	30.37 ^{a}	30.92 ^{a}
Youngest fully developed	A (µmol CO_2 m^{-2} s^{-1})	27.49 ^{a}	28.81 ^{a}	27.78 ^{a}	27.03 ^{a}	26.79 ^{a}	26.53 ^{a}

2.2.3. Elongation

The internode responded more to a decrease in BPFD at the third than the second phytomer with a length of 2.14 cm under B310 and 3.81 cm under B60, corresponding to a 78% increase (Figure 2; Table 3). Whereas, the second internode increased from 4.33 to 6.86 cm, corresponding to 59%. The response of the petiole was smaller with a length increase from 4.46 cm under B310 to 5.61 cm under B160,

corresponding to a 26% increase. The tendency differed from that of the internodes with a maximum length under B160 and an insignificant decrease until B60. Increasing BPFD from B160 also decreased the length of the petiole, but with no significant differences from B210 to B310. Length of the leaf lamina did not respond significantly but had a tendency to decrease from B160 to B310, similarly to the petiole. The internode elongation was not accompanied by a reduced internode diameter, which showed no significant differences with a slight tendency of responding similar to the petiole.

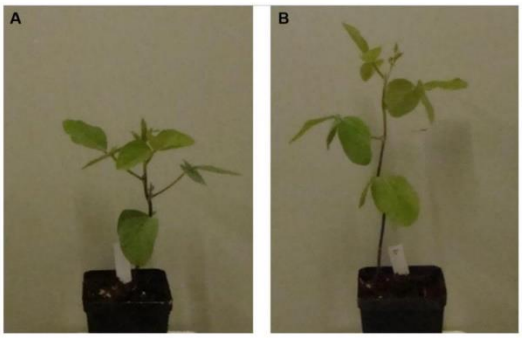

Figure 2. Soybean grown under B310 (**A**) and B60 (**B**).

Table 3. Least square means of the final measurement for lengths of internodes, petioles and leaves and diameter of internodes at phytomer scale under different blue photosynthetic flux densities (BPFD). Lower case letters indicate significant differences between treatments ($p < 0.05$).

Phytomer Level	Organ	Treatment					
		B60	B110	B160	B210	B260	B310
Second	Internode (cm)	6.86 ^{a}	5.86 ^{b}	5.39 ^{b}	4.70 ^{c}	4.26 ^{c}	4.33 ^{c}
Third	Internode (cm)	3.81 ^{a}	3.41 ^{a,b}	3.28 ^{a,b}	2.75 ^{b,c}	2.28 ^{c}	2.14 ^{c}
	Petiole (cm)	5.11 ^{a,b}	5.08 ^{a,b}	5.61 ^{a}	4.80 ^{b,c}	4.72 ^{b,c}	4.46 ^{c}
	Leaf lamina (cm)	5.25 ^{a}	5.07 ^{a}	5.27 ^{a}	4.58 ^{a}	4.49 ^{a}	4.48 ^{a}
	Internode diameter (mm)	3.09 ^{a}	3.29 ^{a}	3.52 ^{a}	3.41 ^{a}	3.46 ^{a}	3.28 ^{a}

2.2.4. Growth Dynamics

Growth of the individual organs was fitted to the beta-function and parameters for the third phytomer showed significant differences for internode and petiole, but not for the leaf lamina. The absolute differences of the parameters for all three organs were relatively small and did not show any tendency to change with decreased BPFD (Table 4).

Table 4. Least square means of estimated parameters of the beta-function. Time of elongation (te) and time of maximum elongation (tm) for internode, petiole and leaf at the third phytomer under different blue photosynthetic flux densities (BPFD). Letters indicate significant differences between treatments ($p < 0.05$).

Organ of Third Phytomer	Parameter	Treatment					
		B60	B110	B160	B210	B260	B310
Internode	te	13.96 ^{b}	14.39 ^{a,b}	14.21 ^{b}	14.41 ^{a,b}	14.67 ^{a}	14.36 ^{a,b}
	tm	5.23 ^{a}	6.86 ^{a}	6.60 ^{a}	6.33 ^{a}	6.60 ^{a}	6.13 ^{a}
Petiole	te	15.76 ^{c}	16.03 ^{b,c}	15.85 ^{c}	16.47 ^{a,b}	16.39 ^{a,c}	16.68 ^{a}
	tm	9.79 ^{b}	10.25 ^{a,b}	10.18 ^{a,b}	10.25 ^{a,b}	10.74 ^{a}	10.70 ^{a}
Leaf lamina	te	13.94 ^{a}	14.12 ^{a}	14.04 ^{a}	14.11 ^{a}	14.19 ^{a}	13.89 ^{a}
	tm	5.19 ^{a}	5.04 ^{a}	4.57 ^{a}	4.55 ^{a}	5.50 ^{a}	4.95 ^{a}

2.2.5. Energy Consumption

The highest energy consumption was measured under a high BPFD (Table 5). The consumption increased from 94.4 W under B60 to 107.2 W under B310 corresponding to an increase of 14% under B310.

Table 5. Measured energy consumption (Watt) of the LED chambers under different blue photosynthetic flux densities (BPFD).

Treatment	Energy Consumption (W)
B60	94.4
B110	95.1
B160	96.4
B210	97.6
B260	101.7
B310	107.2

2.3. Modelling

Simulations based on the found parameters of the beta-function resulted in simulated length of internodes, petioles and leaf laminas following the measurements well (exemplified by the treatments B60 and B310 in Supplementary Materials, Figure S2).

2.3.1. Blue Light Response Function of Internodes

Based on the simulated $BPFD_{per}$, the relative elongation response of the second and third internode were closer to each other compared to using the emitted BPFD (Figure 3). Especially at high BPFD levels, the response of the two internodes was close, implying a common response function to $BPFD_{per}$.

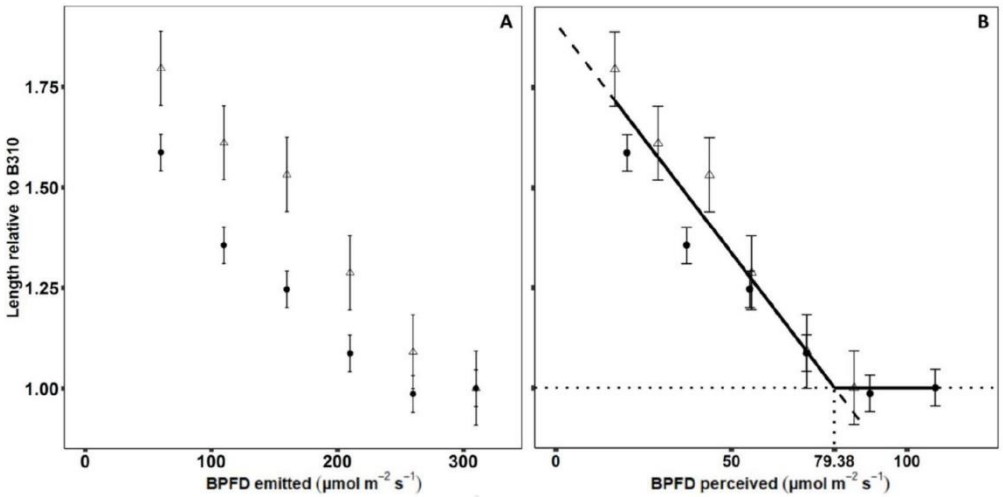

Figure 3. Least square mean of length of second (point) and third (triangle) internode relative to B310 in response to BPFD emitted by the LED modules (**A**) or simulated BPFD perceived by the internode (**B**). Dashed line showing the function fitted to relative internode lengths higher than one and dotted lines showing the interception of the function with 1. Black line showing the final response function to BPFD. Error bars indicate standard error of the LS-mean (n = 8).

Due to the relatively small differences between the parameters t_e and t_m of the beta-function and no clear tendencies in their response to BPFD, only differences in the final length of the internode (L_{max}) were considered in the response function. Internodes with a relative length to B310 below one were considered to have no elongation response to $BPFD_{per}$ and a common function for final internode

length was fitted to the $BPFD_{per}$ of the internodes under treatments with a relative length to B310 higher than one (Figure 3B).

The common function for the relative length of the second and third internode was:

$$L_{rel} = -0.01 * BPFD_{per} + 1.91, \quad (1)$$

The interception of this function with one was at 79.38 µmol m^{-2} s^{-1} $BPFD_{per}$, which was hereby the minimum amount of BPFD that an internode should perceive to express no elongation response to $BPFD_{per}$.

This resulted in the BPFD response function:

$$Internode\ length = L_{min}\left(1 + (79.38 - BPFD_{per}\right) * 0.01),\ 79.38 - BPFD_{per} > 0, \quad (2)$$

where L_{min} is the final internode length with no elongation response to $BPFD_{per}$ and $BPFD_{per}$ is the BPFD perceived by the internode. The black line in Figure 3B shows the response function in the range from the minimum (16.78 µmol m^{-2} s^{-1}) to maximum (108.13 µmol m^{-2} s^{-1}) perceived light during the simulations.

2.3.2. Evaluation and Light Optimization

During the simulations based on the found response function, L_{min} and the growth parameters t_e and t_m were set according to the treatment B310 (baseline scenario). The simulated height until the third internode fitted well with the measurement at the last day, which was also used for parameterization of the model. This shows that the response function was well integrated in the model. Comparing to earlier measurement days which were not used for parameterization of the model, the simulations had a tendency of underestimating the height under low BPFD levels (B60–B110). Importantly for the alternative scenarios the simulated height until third internode fitted well under the higher BPFD levels (B160–B310) (Figure 4).

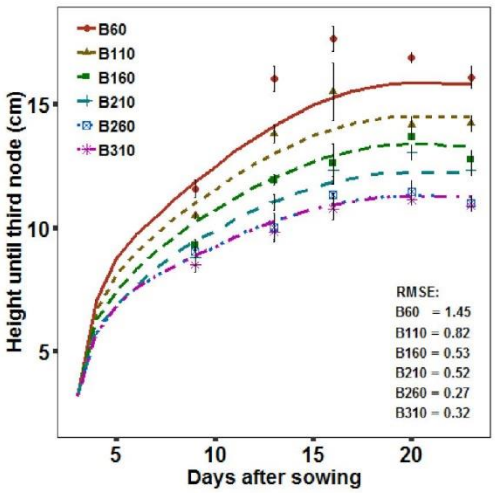

Figure 4. Simulated (line) and measured (points) plant height until the third node and root mean square error (RMSE) between simulations and measurements. Error bars indicate standard error of the mean (day 9–20: $n = 4$, day 23: $n = 8$).

The simulations from the first scenario with a reflective surface of pots, soil and bottom resulted in an increase of perceived BPFD. The total height until the third node decreased under all treatments (Figure 5A) compared with the experimental chamber design (Figure 4). In the experimental design, the minimum height was reached between B260 and B310, while in the alternative scenario it was

reached between B210 and B260. The simulated length of the second and third internode (Figure 5B,C) showed that the shorter height was a result of an increase in the perceived BPFD of the second internode, where the minimum length was already reached between B160 and B210 (Figure 5B).

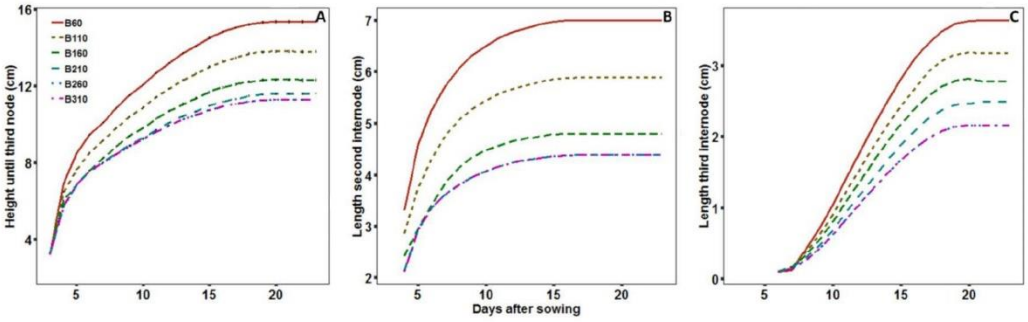

Figure 5. Simulated height until the third node (**A**) and length of second (**B**) and third (**C**) internode with a reflective surface of pots, soil and bottom.

The optimization indicated by the first scenario was applied in the second scenario by optimizing BPFD during the growth period. When the third internode started to develop the treatment changed from B210 to B260 and hereby increased BPFD. The results of the second scenario showed that increasing BPFD on day nine resulted in the minimum length of both internodes and the minimum height of 11.28 cm until the third node. The reduction in the average BPFD emitted by the LED modules resulted in a reduction of energy consumption from 107.2 W in the experimental scenario to 101.7 W in the first and 100.1 W (−7%) in the second scenario (Table 6).

Table 6. Average energy consumption during 23 days of growth for the three simulated scenarios to reach the minimum plant height.

Scenario	Light Spectra	Average Energy Consumption (W)
Experimental	B310	107.2
First scenario	B260	101.7
Second scenario	B210/B260	100.1

3. Discussion

3.1. Biomass and Photosynthesis

During the experiments, data on photosynthesis and biomass was collected. This data shows the response of carbon assimilation and translocation to BPFD, which is of minor importance in a speed breeding system, but of interest for improving yield in indoor farming.

No significant influence on carbon assimilation per leaf area was observed with increased BPFD, which is in agreement with earlier studies, although red light is considered to be the most effective for photosynthesis [21,39]. An increased maximum assimilation with increased BPFD in cucumber was associated with an increased leaf thickness [16,22]. Similar, the tendency of decreased assimilation in this study was associated with thinner leaves under high BPFD. In ice plant He et al. [23] found no change in saturated assimilation between BPFD ratios of 10 and 100%. Although an increasing BPFD ratio from 0 to 20% increased photosynthesis in lettuce, it dropped again at 30% [24]. In this study, the lowest BPFD ratio was 15% under the B60 treatment and an effect below this ratio cannot be excluded.

The decrease in biomass at high BPFD found in this study was most probably related to similar differences in leaf area, which decreased light interception and consequently carbon assimilation per plant. Another reason could be an increased root biomass, but earlier studies found no change

in the biomass ratio of soybean under BPFD ratios of 10 and 25% [19]. In addition, an influence of BPFD on the assimilation over time could reduce biomass. For instance, the photosynthetic rate of tomato decreased more in the afternoon under monochromatic red and blue light than under a broader spectra [40].

Increased LMR under high BPFD confirming earlier results [18,19] indicated a reduced carbon export from the leaves. In tomato, light spectra also influenced the ratio of carbon export from the leaves, but not in agreement with this study as export increases under monochromatic blue and orange light at intermediate PPFD [40]. This can be caused by different responses comparing monochromatic spectra with broader spectra exploring ratios between wavelengths. A decreased fraction of the carbon translocated from the leaves to the stem (internode and petiole) was located in the internodes (low IMRS) under increased BPFD. These results of biomass proportion between organs showed, that an elongation response to reduced BPFD increased the translocation of carbon from the leaves to the stem, but with a higher priority of internodes than petioles. Extensions of the FSP model could assist in the exploration of carbon assimilation and translocation between organs following a similar approach as Bongers et al. [33] combining response functions to light environment with increased carbon demand of specific organs.

3.2. Response to BPFD Under Shade

Low BPFD in Nature is associated with low PPFD and low red to far-red ratio under shade, which trigger morphological responses, e.g., by interactions of the photoreceptors cryptochrome and phytochrome, to increase light interception [41]. The performed experiments represented unnatural spectra that do not occur in nature and hereby show the response of soybean to BPFD without interactions with PPFD and red to far-red ratio.

The elongation response of internode and petiole to low BPFD was in accordance with a shade avoidance response of soybean to low PPFD [12,42] and show that low BPFD can trigger the response also under high PPFD and in the absence of far-red light. The stronger response of internodes than of petioles supports earlier indications of internode elongation being the main shade avoidance response to low PPFD (associated with low BPFD), whereas petiole elongation responded strongly to low red to far-red ratio [12]. The slight decrease in SLA under low BPFD in this study is not in accordance with earlier studies in soybean, which found no response to BPFD in SLA under high PPFD [18,19]. This could be an effect of the lower maximum BPFD ratios applied in earlier studies. Cucumber under low BPFD responded with an increased SLA, which indicates differences between species or an effect of the lower light intensity (100 µmol m^{-2} s^{-1}) applied in these studies [16,22]. Decreased SLA and unchanged internode diameter under low BPFD differ from the soybean response to low PPFD resulting in increased SLA [12,18,19] and decreased internode diameter [12,42]. This indicated that SLA and internode diameter are not regulated by the perception of low BPFD associated with low PPFD, but instead supports earlier studies indicating that SLA is regulated e.g., by sugar signaling [43–45].

3.3. BPFD Response Function

A linear function described well the response to BPFD and was applied for the simulations. Kahlen and Stützel [46] also applied a linear response to PPFD and red to far-red ratio for modeling the response of cucumber to light environment. Other studies found a non-linear response function to BPFD for stem length of soybean [17–19]. This can be due to lower BPFD levels in these studies (BPFD levels < 5%) based on which a non-linear function could be fitted [19]. A continuation of the function in the present study below a BPFD ratio of 15% could evolve non-linear, but in the context of speed breeding this low BPFD levels are not important as this would result in tall plants. For the speed breeding system, it was important to determine the point of a saturated response to BPFD to reach short plants and reduce the BPFD to reduce energy consumption. A saturated response to emitted BPFD was reached under treatments between 210 and 310 µmol m^{-2} s^{-1} in the experimental setup. Two earlier studies on soybean found a saturated response already under 30–50 µmol m^{-2} s^{-1}

BPFD [17,18], whereas one study also found an effect from higher BPFD (130 µmol m^{-2} s^{-1}) [19], indicating interactions with other factors resulting in these discrepancies. One aspect could be the light spectrum, as earlier studies used broader spectra containing green and far-red light [17–19] and additionally included UV-A light in the BPFD [19]. Green light can influence cryptochrome antagonistic to blue light and especially under high PPFD [47]. The addition of green light to a red and blue spectrum increased plant height of soybean under a PPFD of 200 µmol m^{-2} s^{-1} but had no influence under 500 µmol m^{-2} s^{-1} [48]. Far-red light can lead to an increase in plant height by reducing the red to far-red ratio perceived by phytochrome as shown for soybean by adding far-red light to a broad light spectrum [12]. In addition, a broader spectrum within the blue range can influence the magnitude of the blue light effect on cryptochrome. For hypocotyl elongation of *Arabidopsis thaliana* (L.) Heynh., the action spectrum of cryptochrome to monochromatic light did not change within the range 390–530 nm, but an increased stability of CRY2 protein was observed under monochromatic light compared to a broader blue spectrum [49]. These differences in the reactions under narrow peaks compared to the reactions during the response to high PPFD, here imitated with high BPFD, indicated that a broader spectrum within the blue range could affect the BPFD level necessary to avoid an elongation response.

In the experiments, the elongation response of the third internode to low BPFD was slightly stronger than at the second internode, and a higher BPFD level was necessary to achieve the minimum length of the third internode. Simulations indicated that this was due to self-shading, which was larger at the third than the second internode. Based on the simulated $BPFD_{per}$, a common response function was found for the second and third internode. This emphasizes the importance of knowing the perceived light environment at organ-level, e.g., as in this study by means of simulations with an FSP model, as it enables a better evaluation of the influence from the light microclimate than relating the response directly to the light emitted from the light source [46].

The parameters t_e and t_m of the beta-function were in most cases not significantly different between treatments and no trend was present, which indicated that a common parameter could be used for all levels of BPFD only changing L_{max} according to the $BPFD_{per}$. This was confirmed by the accurate simulations of internode length at all BPFD levels based on t_e and t_m found under B310. Importantly, the small difference in height between B310 and B260 were well simulated, showing that the model was very useful to determine the necessary BPFD to reach the minimum height.

3.4. Optimization of Light Spectrum

The decreased biomass with increased BPFD is in accordance with earlier studies in soybean [19] and other species [5,23]. This results in a decreased efficiency of the applied PPFD in indoor farming producing biomass, but in a speed breeding system there are no apparent advantages of a high biomass. Further consideration for a spectral optimization would be whether the minimum necessary BPFD found here could be reduced through other light microclimatic factors. Light intensity would be an important factor to determine possible interactions between absolute and relative amount of BPFD on morphology and interactions between PPFD and BPFD on photosynthesis. Further studies could also investigate whether the necessary BPFD could be reduced with an increased effect on cryptochrome with a broader blue spectrum or the addition of other wavelengths.

The alternative scenarios showed that the amount of necessary BPFD of the emitted light could be reduced through increased reflection of the bottom and soil and by changing the amount of BPFD during the growth period. Within the used LED modules, the blue LEDs had a higher energy consumption than the red LEDs, as expected from theory [6]. Simulations with BPFD levels optimized for the alternative chamber design showed the potential to decrease energy consumption. Additionally, decreased BPFD can increase water use efficiency by decreasing stomatal conductance [5]. The simulations showed a high potential for light optimization in indoor crop production and speed breeding as the model can be adjusted to the dimensions, LED types and placements and reflective properties for a system-specific recommendation for the light spectrum. Further development of the model could include response functions to more wavelengths and light intensities and make the model sink-source driven [33].

4. Materials and Methods

4.1. Experimental Setup

Soybean plants were grown inside three LED chambers (Compled Solutions GmbH, Dresden, Germany) with the dimensions: 1.1 m high, 0.5 m wide and 0.7 m deep inside a larger climate chamber at the University of Hohenheim (Germany). The LED chambers had openings at the top and bottom enabling ventilation to keep a constant temperature around 27 °C. Seeds of the soybean (*Glycine max* (L.) Merr.) cultivar Merlin (Saatbau Linz eG, Leonding, Austria) were inoculated (Soya BeanInoculant, Legume Technology Ltd., Nottinghamshire, UK) and sown in a mixture of peat substrate (Substrat 5 + Perlite; Klasmann-Deilmann GmbH, Geeste, Germany). The initial three plants per pot were thinned to one plant according to homogenous development on day nine by the start of the plant measurements. Twelve pots (9.5 × 9.0 × 9.0 cm) were distributed evenly within each chamber (0.35 m^2) resulting in a plant density of around 34 plants m^{-2}. The twelve pots were placed in a common tray and irrigated regularly to avoid water limitations. The experiment consisted of four runs within three LED growth chambers to achieve two repetitions for each of the six light treatments.

4.2. Light Treatments

Within each chamber, four LED modules (Sunsim VIS_v3; Compled Solutions GmbH, Dresden, Germany) were placed which allowed to adjust light intensity for the different wavelength ranges. The applied light treatments were comprised only of red and blue light, with one peak in the blue range at 440 nm and two peaks in the red range at 620 and 640 nm (Figure 6). The day length was set to 10 h and all treatments had a PPFD of 400 µmol m^{-2} s^{-1} to test the influence of different levels of BPFD independent from changes in PPFD. The spectrum of the six light treatments had a BPFD of 60, 110, 160, 210, 260 and 310 µmol m^{-2} s^{-1} (B60–B310) (Figure 6), while the remaining PPFD was delivered by the red LEDs. The light spectrum did not include any far-red light to exclude differences in phytochrome-mediated responses between the light treatments. Setting of the spectral intensity of the treatments was performed at 80 cm distance from the LED modules according to the measurements from a FLAME-S-XR1-ES spectrometer (Ocean Optics Germany GmbH, Ostfildern, Germany). The spectrometer measured in the range from 200–1025 nm with a resolution of around 2 nm and was equipped with a collimating lens (74-UV-MP) and a right-angle reflector with cosine corrector (74-90-UV-CC3). The photon flux density was recorded for 400–700 nm (PPFD), 400–500 nm (BPFD) and 600–700 nm (red light).

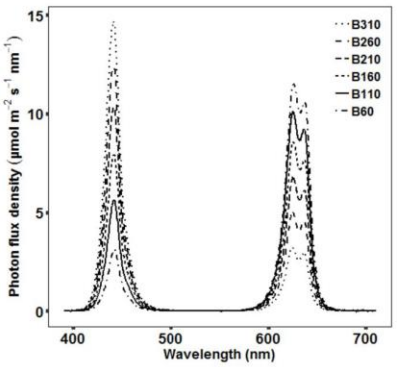

Figure 6. The measured spectrum of the six treatments with a BPFD of 60, 110, 160, 210, 260 and 310 µmol m^{-2} s^{-1}.

Energy consumption of the treatments was measured with a volt-ohm meter (Voltcraft, Energy Check 3000, Conrad Electronic SE, Wernberg-Köblitz, Germany). The measurements were reasonable as compared to the estimated energy consumption given by the software of the LED chambers.

4.3. Plant Measurements

Biomass and leaf area were measured on five dates during each run. For the first four measurements (on day 9, 13, 16 and 20), two plants were randomly selected, and the remaining four plants were used for the final measurement on day 23. On each of the five dates, total plant height (from soil to apical bud), and leaf area and biomass of each phytomer of the two/four plants were determined. Leaf area was estimated with ImageJ [50] from pictures of the leaves and dry mass was measured separately for internodes, petioles and leaf laminas after drying for at least 48 h at 60 °C until constant weight.

On day 23—when start of flowering was observed under all treatments—additional measurements of the photosynthetic rate and SPAD values were performed on the remaining four plants. The SPAD, which is representative for chlorophyll content, was measured using a SPAD meter (SPAD 502 Plus, Konica Minolta, Inc., Tokyo, Japan) and the photosynthetic rate was measured on the youngest fully developed leaf on each of the four plants per light treatment with a LCpro-SD portable system (ADC BioScientific Ltd., Hoddesdon, UK). Measurements were performed under ambient conditions within the chambers (clear glass cover to measure under the applied light treatments). Values were recorded when a steady photosynthetic rate was reached (after around 20 min).

LMR was calculated from leaf biomass/above ground biomass and IMRS was calculated from internode biomass/biomass of stalk (internode plus petiole).

Morphological measurements were performed at seven dates (day 9, 11, 13, 16, 18, 20, and 23) on the four plants within each chamber used for the final measurements. These measurements were used for calibration of the FSP model of soybean and for statistical analysis of the influence of BPFD on growth dynamics. They comprised length and diameter of internodes and petioles, length and width of leaflets, angle between internodes and petioles and angles of the leaf lamina. The latter comprising the lamina inclination measured from the base to the tip of the lamina, and the rotation angle around the midrib. To describe the unfolding of the leaf lamina, the angle between the midrib and each of the two halves of the leaf lamina was determined. Diameters were measured with a caliper, length and width with a ruler and angles with a protractor.

4.4. Statistical Design and Analysis

Measurements of growth dynamics of internodes, petioles and leaflets of each phytomer were used to fit the beta-function (Equation (3)) [51]:

$$\begin{aligned} L(t) = L_{max}\left(1 + \frac{t_e - t}{t_e - t_m}\right)\left(\frac{t}{t_e}\right)^{\frac{t_e}{t_e - t_m}} \quad 0 \le t_m < t_e \\ L(t > t_e) = L_{max} \end{aligned} \tag{3}$$

where $L(t)$ is the size at day t, L_{max} is the final size, t_e is the day when the final size is reached and t_m is the day on which the growth rate peaks. The parameters L_{max}, t_e and t_m were estimated with the nls-function in the R-package stats [52].

To determine the plants used for the destructive measurements during each experiment, randomizations were performed within two blocks (plant location). The first block comprised the first and last row and the second block the two center rows (Figure 7).

The six light treatments of the experiment were performed with two replicates. Given three LED chambers, three out of the six light treatments could be tested in the same run, i.e., each replicate comprised two runs, resulting in four runs in total (Supplementary Materials, S1). For the arrangement of treatments within the LED chambers over time and space, an α-design with two replicates and a block (time) size of two was used. The effect of BPFD on biomass, morphology, leaf physiology and parameters of the beta-function was tested. The second and mostly third phytomer (hypocotyl counted as first phytomer) were chosen for specific analysis, because they comprised the most comprehensive

measurements from beginning to end of growth. According to the experimental design, the following mixed model was used to analyze the data in the SAS® software (SAS Institute, Inc., Cary, NC, USA):

$$y_{iklmn} = \mu + b_k + i_{kl} + p_{klm} + r_{klmn} + \tau_i + e_{iklmn} \quad (4)$$

where μ is the intercept, b_k is the fixed effect of the k^{th} complete replicate, i_{kl} is the random effect of the l^{th} incomplete block (time) within the k^{th} replicate, p_{klm} is the random effect of the m^{th} chamber within the l^{th} run, r_{klmn} is the random effect of the n^{th} block (plant location) within the m^{th} chamber of the l^{th} run and the k^{th} replicate, τ_i is the main effect of the i^{th} light treatment, and e_{iklmn} is the error effect of observation y_{iklmn} with homogeneous variance. Residuals were checked graphically for normal distribution and homogeneous variance. After finding significant effects via F-test, a multiple t-test to compare least square means was used to create a letter display [53]. Note that least square means are presented in the results section as data was not balanced, because only three out of six light treatments were tested within each run. Least square means are based on model (Equation (4)) to adjust for block effects.

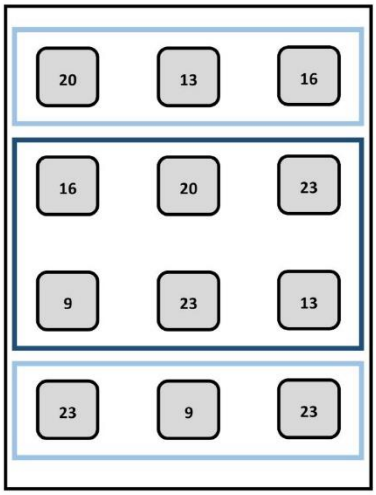

Figure 7. Illustration of the randomization for the plants used for the destructive measurements within the first (light blue square) and second (dark blue square) block (plant location). The numbers exemplarily show the day of the destructive measurements the plants were used for.

4.5. FSP Model

An existing 3D model of the LED growth chamber [54] in the modelling platform GroIMP [55] was used. The virtual LED chamber can be adjusted in its dimensions and the placement of the LED modules and proved to simulate the spectral light distribution with a high accuracy [54]. The single LED types are defined by their spectral and physical light distribution and total emitted power. Then, individual LEDs can be placed according to their position within the LED module. The simulations of the spectral light distribution were performed with the integrated spectral Monte-Carlo ray tracer GPUFlux [56] set to a spectral resolution of 5 nm within the 400–800 nm range. The optical properties (reflection, absorption and transmittance) of the sidewalls were zero transmission and an absorption of 0.02 within the 400–600 and 700–800 range and 0.04 within the 600–700 range.

The optical properties of the chamber were not changed from the setting in the original model [54] as the side wall material was the same. The optical properties of the soybean leaf and the substrate were set in a 5 nm resolution according to measurements from a typical soybean leaf ([57], Supplementary Materials, Figure S3) and peat [58]. The adjustments of the original model of the virtual LED chamber were location and intensity of the individual LEDs and the location of the LED modules. The intensity of the virtual LEDs were parameterized to emit the same intensity of red and blue light at 80 cm distance

as in the experimental treatments (Supplementary Materials, Figure S4) using virtual sensors [54]. The virtual LEDs were set to emit 25 million rays with a maximum of 50 reflections, ensuring that all rays were absorbed by an object or reflected outside of the virtual chamber before reaching the maximum number of reflections.

Within the virtual LED chamber, an FSP model of soybean was constructed based on the generic model FSPM-P [27]. Internodes and petioles of the virtual plants were constructed as simple cylinder objects, while the shape of the leaf lamina was triangulated, based on a picture of a soybean leaflet and was composed of 42 triangles (Supplementary Materials, Figure S5).

Each leaflet was constructed from two half leaflets enabling unfolding of the leaflet from the midrib according to measurements (Supplementary Materials, Figure S5A,B). Simultaneously with the unfolding of the two leaflet halves, the leaflet moved from a vertical position with the leaflet tip pointing upwards towards a final inclination according to the measurements from leaflet base to tip and rotation around the midrib according to measurements from one side of the leaflet to the other (Supplementary Materials, Table S2; Figure S5C). The leaflet unfolded with 0.7°/hour.

The virtual plants grew according to the found growth parameters of the beta-function to simulate the plant structure according to the experimental observations. Additional inputs taken from the experiment were final organ length, petiole angles and length to diameter ratio of internodes for each treatment and ratio between length of side leaflets and center leaflet of the trifoliate leaf, leaflet length to leaflet area ratio and length to diameter ratio of petioles as an average of all treatments (Supplementary Materials, Table S2).

According to the experimental design, twelve virtual plants were simulated at the beginning, and then during the simulation two of them were randomly chosen within the two blocks to be taken out of the virtual scene on day 9, 13, 16, and 20, respectively.

4.6. Response Function

The response function was derived and integrated following four steps: (1) fit beta-function for all treatments, (2) run FSP model to obtain perceived BPFD of internodes for each treatment, (3) derive response function across all treatments for internode length in dependence of simulated perceived BPFD and (4) integrate the derived response function into the model for all treatments.

Based on the experimental observations, the parameters for the beta-function were derived for each light treatment. Based on these parameters, the FSP model of soybean dynamically simulated the plant architecture over time under each of the six light treatments.

At this stage, the growth of the internodes stopped at a final length according to the measurements. During the simulations, BPFD perceived by the internodes was recorded for each hour. The simulated perceived BPFD was used to fit a response function to the internode length observed under the different BPFD treatments:

$$Internode\ length = L_{min}\left(1 + \left(BPFD_{min} - BPFD_{per}\right)a\right)\ \ BPFD_{min} - BPFD_{per} > 0 \quad (5)$$

where L_{min} is the minimum possible length of the internode, $BPFD_{min}$ is the lowest BPFD giving L_{min}, $BPFD_{per}$ is the average perceived BPFD of the internode during the first four days of growth and a is the slope of the response to $BPFD_{per}$. The first four days of growth were used due to a very rapid growth inhibiting effect of blue light [59] and according to the results of Kahlen and Stützel [46] who found four successive days starting one week before reaching maximum growth rate to be particularly sensitive to changes in PPFD.

The found BPFD response function was integrated in the FSP model to determine L_{max} of the beta-function and the final internode length. They were hereby simulated in dependence of the perceived BPFD during the simulations and at this stage no longer determined by experimental measurements. Internode two until nine elongated according to the integrated response function, with L_{min}, and t_m set for each internode according to the found parameter values for the treatment

B310 (baseline scenario with shortest internodes). Because the first internode (hypocotyl) grew before thinning and beginning of experimental measurements, its length was set to grow to the final average length of all treatments.

4.7. Model Evaluation and Alternative Scenarios

The light simulations were evaluated in an earlier study by comparing light measurements and simulations within a soybean canopy grown under two treatments identical to this study (B110 and B160) [38]. The integration of the parameters of the beta-function used to calibrate the dynamic model in this study was evaluated by comparing length over time for internodes, petioles and leaf laminas at all phytomer levels under all treatments. Model simulations after integration of the response function to blue light were evaluated by comparing the measured and simulated plant height until the third phytomer (hypocotyl counted as first phytomer). The comparison included the eight plants per chamber selected for the first four dates of destructive measurements, which were not used for the model parameterization.

Then, the model was applied for spectral optimization with the aim of minimizing BPFD emitted by the LED modules to reduce energy consumption, but still reach the minimum internode length. The first alternative scenario was run with a different virtual LED chamber design for evaluating the effect on the perceived BPFD. The chamber design was changed by setting the reflection of the bottom, pots and substrate to the same level as the sidewalls of the chamber. This was chosen for simulating a situation similar to e.g., hydroponics with plants placed in more reflective containers than the substrate and black pots in the experiment. This change in chamber design was expected to increase the perceived BPFD and hereby reduce BPFD emitted by the LEDs that is necessary to induce short plants. Simulations from the first scenario indicated that the spectrum could be optimized according to the developmental stage. The suggested optimization was applied in the second scenario by changing the emitted BPFD during the growth period.

5. Conclusions

The length of internodes and petioles increased under low BPFD, similar to the shade response under low PPFD, whereas the limited response of SLA and internode diameter indicated that the shade responses of these might not be regulated by cryptochrome. Further studies could investigate alternative regulation of these together with extended photosynthetic measurements over time to increase the understanding of carbon assimilation and translocation under different BPFD levels. Several aspects of the exact spectral effects on morphology and physiology should be further investigated, both for narrow peaks independent and the interactions with broader spectra.

Internode length dependent on perceived BPFD was well simulated in the FSP model and the simulations gave an increased insight into the response of the second and third internode based on the perceived BPFD. The model was a useful tool to determine the minimum necessary BPFD within an alternative chamber environment. Modelling with an FSP can be applied for further optimizations of indoor plant production implementing advances in knowledge of spectral effects on plant morphology and physiology.

Supplementary Materials: The following are available online at http://www.mdpi.com/2223-7747/9/12/1757/s1, Figure S1: Plant height (A), biomass (B) and leaf area (C) per plant and under different blue photosynthetic flux densities (BPFD). Error bars indicate standard error of the mean (day 9–20: $n = 4$, day 23: $n = 8$), Figure S2: Simulated (line) and measured (points) length of petioles, internodes and leaf laminas under the treatments B310 and B60, Figure S3: The absorption, reflection and transmission of radiation (%, relative to the incident radiation) from 400–700 nm by a soybean leaf used for the optical properties of the simulated soybean leaves. Data taken from Kasperbauer (1987), Figure S4: The simulated spectra (total PFFD of 400 μmol m^{-2} s^{-1}) of the six treatments with a simulated BPFD of 60, 110, 160, 210, 260 and 310 μmol m^{-2} s^{-1}, Figure S5: Visualizations of the simulated unfolding (A, B) and fully developed (C) trifoliate leaf, Table S1: The spread of the six treatments within three chambers over time, Table S2: Model inputs to determine ratios and angles of organs.

Author Contributions: Conceptualization, T.H. and S.M.; methodology, T.H. and S.M.; software, T.H.; validation, T.H.; formal analysis, T.H.; investigation, T.H.; data curation, T.H.; writing—original draft preparation, T.H.; writing—review and editing, T.H., S.M. and S.G.-H.; visualization, T.H.; supervision, S.M. and S.G.-H.; project administration, T.H., S.M. and S.G.-H.; funding acquisition, S.M. and S.G.-H. All authors have read and agreed to the published version of the manuscript.

Funding: This research was funded by the German Federal Ministry for Economic Affairs and Energy according to a decision of the German Federal Parliament within the Central Innovation Program for SMEs (ZF4279901CR6).

Conflicts of Interest: The authors declare no conflict of interest and the funders had no role in the design of the study; in the collection, analyses, or interpretation of data; in the writing of the manuscript, or in the decision to publish the results.

References

1. Bantis, F.; Smirnakou, S.; Ouzounis, T.; Koukounaras, A.; Ntagkas, N.; Radoglou, K. Current status and recent achievements in the field of horticulture with the use of light-emitting diodes (LEDs). *Sci. Hortic.* **2018**, *235*, 437–451. [CrossRef]
2. Singh, D.; Basu, C.; Meinhardt-Wollweber, M.; Roth, B. LEDs for energy efficient greenhouse lighting. *Renew. Sustain. Energy Rev.* **2015**, *49*, 139–147. [CrossRef]
3. Olle, M.; Viršile, A. The effects of light-emitting diode lighting on greenhouse plant growth and quality. *Agric. Food Sci.* **2013**, *22*, 223–234. [CrossRef]
4. Ahlman, L.; Bånkestad, D.; Wik, T. Using chlorophyll a fluorescence gains to optimize LED light spectrum for short term photosynthesis. *Comput. Electron. Agric.* **2017**, *142*, 224–234. [CrossRef]
5. Pennisi, G.; Blasioli, S.; Cellini, A.; Maia, L.; Crepaldi, A.; Braschi, I.; Spinelli, F.; Nicola, S.; Fernandez, J.A.; Stanghellini, C.; et al. Unraveling the role of red:blue LED lights on resource use efficiency and nutritional properties of indoor grown sweet basil. *Front. Plant Sci.* **2019**, *10*, 305. [CrossRef]
6. Schulze, P.S.C.; Barreira, L.A.; Pereira, H.G.C.; Perales, J.A.; Varela, J.C.S. Light emitting diodes (LEDs) applied to microalgal production. *Trends Biotechnol.* **2014**, *32*, 422–430. [CrossRef]
7. Watson, A.; Ghosh, S.; Williams, M.J.; Cuddy, W.S.; Simmonds, J.; Rey, M.-D.; Asyraf Md Hatta, M.; Hinchliffe, A.; Steed, A.; Reynolds, D.; et al. Speed breeding is a powerful tool to accelerate crop research and breeding. *Nat. Plants* **2018**, *4*, 23–29. [CrossRef]
8. Jähne, F.; Hahn, V.; Würschum, T.; Leiser, W.L. Speed breeding short-day crops by LED-controlled light schemes. *Theor. Appl. Genet.* **2020**, *133*, 2335–2342. [CrossRef]
9. Fraser, D.P.; Hayes, S.; Franklin, K.A. Photoreceptor crosstalk in shade avoidance. *Curr. Opin. Plant Biol.* **2016**, *33*, 1–7. [CrossRef]
10. Li, J.; Li, G.; Wang, H.; Deng, X.W. Phytochrome signaling mechanisms. *Arab. Book* **2011**, *9*, e0148. [CrossRef]
11. Yu, X.; Liu, H.; Klejnot, J.; Lin, C. The cryptochrome blue light receptors. *Arab. Book* **2010**, *8*, e0135. [CrossRef]
12. Hitz, T.; Hartung, J.; Graeff-Hönninger, S.; Munz, S. Morphological response of soybean (Glycine max (L.) Merr.) cultivars to light intensity and red to far-red ratio. *Agronomy* **2019**, *9*, 428. [CrossRef]
13. Yang, F.; Huang, S.; Gao, R.; Liu, W.; Yong, T.; Wang, X.; Wu, X.; Yang, W. Growth of soybean seedlings in relay strip intercropping systems in relation to light quantity and red:far-red ratio. *Field Crop. Res.* **2014**, *155*, 245–253. [CrossRef]
14. Gong, W.Z.; Jiang, C.D.; Wu, Y.S.; Chen, H.H.; Liu, W.Y.; Yang, W.Y. Tolerance vs. avoidance: Two strategies of soybean (Glycine max) seedlings in response to shade in intercropping. *Photosynthetica* **2015**, *53*, 259–268. [CrossRef]
15. Wollaeger, H.M.; Runkle, E.S. Growth and acclimation of impatiens, salvia, petunia, and tomato seedlings to blue and red light. *HortScience* **2015**, *50*, 522–529. [CrossRef]
16. Hernández, R.; Kubota, C. Physiological responses of cucumber seedlings under different blue and red photon flux ratios using LEDs. *Environ. Exp. Bot.* **2016**, *121*, 66–74. [CrossRef]
17. Wheeler, R.M.; Mackowiak, C.L.; Sager, J.C. Soybean stem growth under high-pressure sodium with supplemental blue lighting. *Agron. J.* **1991**, *83*, 903–906. [CrossRef]
18. Cope, K.R.; Bugbee, B. Spectral effects of three types of white light-emitting diodes on plant growth and development: Absolute versus relative amounts of blue light. *HortScience* **2013**, *48*, 504–509. [CrossRef]
19. Dougher, T.A.; Bugbee, B. Differences in the response of wheat, soybean and lettuce to reduced blue radiation. *Photochem. Photobiol.* **2001**, *73*, 199–207. [CrossRef]

20. Naznin, M.; Lefsrud, M.; Gravel, V.; Azad, M. Blue light added with red LEDs enhance growth characteristics, pigments content, and antioxidant capacity in lettuce, spinach, kale, basil, and sweet pepper in a controlled environment. *Plants* **2019**, *8*, 93. [CrossRef]
21. Hogewoning, S.W.; Wientjes, E.; Douwstra, P.; Trouwborst, G.; van Ieperen, W.; Croce, R.; Harbinson, J. Photosynthetic quantum yield dynamics: From photosystems to leaves. *Plant Cell* **2012**, *24*, 1921–1935. [CrossRef]
22. Hogewoning, S.W.; Trouwborst, G.; Maljaars, H.; Poorter, H.; van Ieperen, W.; Harbinson, J. Blue light dose-responses of leaf photosynthesis, morphology, and chemical composition of Cucumis sativus grown under different combinations of red and blue light. *J. Exp. Bot.* **2010**, *61*, 3107–3117. [CrossRef]
23. He, J.; Qin, L.; Chong, E.L.C.; Choong, T.-W.; Lee, S.K. Plant growth and photosynthetic characteristics of mesembryanthemum crystallinum grown aeroponically under different blue- and red-LEDs. *Front. Plant Sci.* **2017**, *8*, 361. [CrossRef]
24. Kang, W.H.; Park, J.S.; Park, K.S.; Son, J.E. Leaf photosynthetic rate, growth, and morphology of lettuce under different fractions of red, blue, and green light from light-emitting diodes (LEDs). *Hortic. Environ. Biotechnol.* **2016**, *57*, 573–579. [CrossRef]
25. Vos, J.; Evers, J.B.; Buck-Sorlin, G.H.; Andrieu, B.; Chelle, M.; de Visser, P.H.B. Functional-structural plant modelling: A new versatile tool in crop science. *J. Exp. Bot.* **2010**, *61*, 2101–2115. [CrossRef]
26. Evers, J.B. *Simulating Crop Growth and Development Using Functional-Structural Plant Modeling*; Springer: Dordrecht, The Netherlands, 2016; pp. 219–236.
27. Henke, M.; Kurth, W.; Buck-Sorlin, G.H. FSPM-P: Towards a general functional-structural plant model for robust and comprehensive model development. *Front. Comput. Sci.* **2016**, *10*, 1103–1117. [CrossRef]
28. Burgess, A.J.; Retkute, R.; Pound, M.P.; Mayes, S.; Murchie, E.H. Image-based 3D canopy reconstruction to determine potential productivity in complex multi-species crop systems. *Ann. Bot.* **2017**, *119*, 517–532. [CrossRef]
29. Evers, J.B.; Bastiaans, L. Quantifying the effect of crop spatial arrangement on weed suppression using functional-structural plant modelling. *J. Plant Res.* **2016**, *129*, 339–351. [CrossRef]
30. Chelle, M.; Evers, J.B.; Combes, D.; Varlet-Grancher, C.; Vos, J.; Andrieu, B. Simulation of the three-dimensional distribution of the red:far-red ratio within crop canopies. *N. Phytol.* **2007**, *176*, 223–234. [CrossRef]
31. Evers, J.B.; Vos, J.; Chelle, M.; Andrieu, B.; Fournier, C.; Struik, P.C. Simulating the effects of localized red:far-red ratio on tillering in spring wheat (Triticum aestivum) using a three-dimensional virtual plant model. *N. Phytol.* **2007**, *176*, 325–336. [CrossRef]
32. Buck-Sorlin, G.; Hemmerling, R.; Kniemeyer, O.; Burema, B.; Kurth, W. A rule-based model of barley morphogenesis, with special respect to shading and gibberellic acid signal transduction. *Ann. Bot.* **2008**, *101*, 1109–1123. [CrossRef] [PubMed]
33. Bongers, F.J.; Pierik, R.; Anten, N.P.R.; Evers, J.B. Subtle variation in shade avoidance responses may have profound consequences for plant competitiveness. *Ann. Bot.* **2018**, *121*, 863–873. [CrossRef] [PubMed]
34. Gautier, H.; Měch, R.; Prusinkiewicz, P.; Varlet-Grancher, C. 3D Architectural Modelling of Aerial Photomorphogenesis in White Clover (*Trifolium repens* L.) using L-systems. *Ann. Bot.* **2000**, *85*, 359–370. [CrossRef]
35. Buck-Sorlin, G.; de Visser, P.H.; Henke, M.; Sarlikioti, V.; van der Heijden, G.W.; Marcelis, L.F.; Vos, J. Towards a functional–structural plant model of cut-rose: Simulation of light environment, light absorption, photosynthesis and interference with the plant structure. *Ann. Bot.* **2011**, *108*, 1121–1134. [CrossRef] [PubMed]
36. Dieleman, J.A.; De Visser, P.H.B.; Meinen, E.; Grit, J.G.; Dueck, T.A. integrating morphological and physiological responses of tomato plants to light quality to the crop level by 3D modeling. *Front. Plant Sci.* **2019**, *10*, 839. [CrossRef]
37. Kalaitzoglou, P.; van Ieperen, W.; Harbinson, J.; van der Meer, M.; Martinakos, S.; Weerheim, K.; Nicole, C.C.S.; Marcelis, L.F.M. Effects of continuous or end-of-day far-red light on tomato plant growth, morphology, light absorption, and fruit production. *Front. Plant Sci.* **2019**, *10*, 322. [CrossRef]
38. Hitz, T.; Henke, M.; Graeff-Honninger, S.; Munz, S. Simulating light spectrum within a soybean canopy in an LED growth chamber. In Proceedings of the 6th International Symposium on Plant Growth Modeling, Simulation, Visualization and Applications (PMA), Hefei, China, 4–8 November 2018; pp. 120–125.

39. McCree, K.J. The action spectrum, absorptance and quantum yield of photosynthesis in crop plants. *Agric. Meteorol.* **1972**, *9*, 191–216. [CrossRef]
40. Lanoue, J.; Leonardos, E.D.; Grodzinski, B. Effects of light quality and intensity on diurnal patterns and rates of photo-assimilate translocation and transpiration in tomato leaves. *Front. Plant Sci.* **2018**, *9*, 756. [CrossRef]
41. Pierik, R.; de Wit, M. Shade avoidance: Phytochrome signaling and other aboveground neighbor detection cues. *J. Exp. Bot.* **2014**, *65*, 2815–2824. [CrossRef]
42. Feng, L.; Raza, M.A.; Li, Z.; Chen, Y.; Khalid, M.H.B.; Du, J.; Liu, W.; Wu, X.; Song, C.; Yu, L.; et al. The influence of light intensity and leaf movement on photosynthesis characteristics and carbon balance of soybean. *Front. Plant Sci.* **2019**, *9*, 1952. [CrossRef]
43. Park, Y.; Runkle, E.S. Far-red radiation and photosynthetic photon flux density independently regulate seedling growth but interactively regulate flowering. *Environ. Exp. Bot.* **2018**, *155*, 206–216. [CrossRef]
44. Kim, G.-T.; Yano, S.; Kozuka, T.; Tsukaya, H. Photomorphogenesis of leaves: Shade-avoidance and differentiation of sun and shade leaves. *Photochem. Photobiol. Sci.* **2005**, *4*, 770. [CrossRef] [PubMed]
45. Weston, E.; Thorogood, K.; Vinti, G.; López-Juez, E. Light quantity controls leaf-cell and chloroplast development in Arabidopsis thaliana wild type and blue-light-perception mutants. *Planta* **2000**, *211*, 807–815. [CrossRef] [PubMed]
46. Kahlen, K.; Stützel, H. Modelling photo-modulated internode elongation in growing glasshouse cucumber canopies. *New Phytol.* **2011**, *190*, 697–708. [CrossRef] [PubMed]
47. Sellaro, R.; Crepy, M.; Trupkin, S.A.; Karayekov, E.; Buchovsky, A.S.; Rossi, C.; Casal, J.J. Cryptochrome as a Sensor of the blue/green ratio of natural radiation in Arabidopsis. *Plant Physiol.* **2010**, *154*, 401–409. [CrossRef]
48. Snowden, M.C.; Cope, K.R.; Bugbee, B. Sensitivity of seven diverse species to blue and green light: interactions with photon flux. *PLoS ONE* **2016**, *11*, e0163121. [CrossRef]
49. Ahmad, M.; Grancher, N.; Heil, M.; Black, R.C.; Giovani, B.; Galland, P.; Lardemer, D. Action spectrum for cryptochrome-dependent hypocotyl growth inhibition in Arabidopsis. *Plant Physiol.* **2002**, *129*, 774–785. [CrossRef]
50. Schneider, C.A.; Rasband, W.S.; Eliceiri, K.W. NIH Image to ImageJ: 25 years of image analysis. *Nat. Methods.* **2012**, *9*, 671–675. [CrossRef]
51. Yin, X.; Goudriaan, J.; Lantinga, E.A.; Vos, J.; Spiertz, H.J. A flexible sigmoid function of determinate growth. *Ann. Bot.* **2003**, *91*, 361–371. [CrossRef]
52. R Core Team. *R: A Language and Environment for Statisticalcomputing*; R Foundation for Statistical Computing: Vienna, Austria, 2019; Available online: https://www.R-project.org/ (accessed on 10 December 2020).
53. Piepho, H.-P. An algorithm for a letter-based representation of all-pairwise comparisons. *J. Comput. Graph. Stat.* **2004**, *13*, 456–466. [CrossRef]
54. Hitz, T.; Henke, M.; Graeff-Hönninger, S.; Munz, S. Three-dimensional simulation of light spectrum and intensity within an LED growth chamber. *Comput. Electron. Agric.* **2019**, *156*, 540–548. [CrossRef]
55. Henke, M.; Buck-Sorlin, G.H. Using a full spectral raytracer for calculating light microclimate in functional-structural plant modelling. *Comput. Inform.* **2018**, *36*, 1492–1522. [CrossRef]
56. Van Antwerpen, D.G. Unbiased Physically Based Rendering on the GPU. Master's Thesis, Delft University of Technology, Delft, The Netherlands, 2011.
57. Kasperbauer, M.J. Far-red light reflection from green leaves and effects on phytochrome-mediated assimilate partitioning under field conditions. *Plant Physiol.* **1987**, *85*, 350–354. [CrossRef] [PubMed]
58. Jacquemoud, S.; Baret, F.; Hanocq, J.F. Modeling spectral and bidirectional soil reflectance. *Remote Sens. Environ.* **1992**, *41*, 123–132. [CrossRef]
59. Parks, B.M.; Folta, K.M.; Spalding, E.P. Photocontrol of stem growth. *Curr. Opin. Plant Biol.* **2001**, *4*, 436–440. [CrossRef]

6. Chapter IV: Morphological Response of Soybean (*Glycine max* (L.) Merr.) Cultivars to Light Intensity and Red to Far-Red Ratio

Hitz, T., Hartung, J., Graeff-Hönninger, S., Munz, S., 2019. Morphological Response of Soybean (*Glycine max* (L.) Merr.) Cultivars to Light Intensity and Red to Far-Red Ratio. Agronomy 9, 428. https://doi.org/10.3390/agronomy9080428

Chapter III focused on the influence of BPFD level on soybean under constant PPFD. This spectral change does not appear in nature, where decreased BPFD is associated with a decrease in PPFD. Chapter IV instead aimed towards an increased understanding of the fundamental morphological response of soybean to the light environment under natural shade, e.g. in cropping systems. The objective was to disentangle the effects of the two shade factors low PPFD and R:FR on the induction of SAR. This is difficult in a natural environment and instead the advantages of LED lighting were utilized by applying treatments with variation of only one factor. The treatments combined different levels of PPFD and R:FR in two experiments to explore both a high PPFD and an R:FR corresponding to shade in intercropping.
Knowledge of the interaction between light environment and cultivars is important for breeding cultivars for specific cropping practices e.g. mono- and intercropping. Studies of these interactions are limited and therefore three different cultivars were tested and analyzed for interactions between cultivar and light.

agronomy

MDPI

Article

Morphological Response of Soybean (*Glycine max* (L.) Merr.) Cultivars to Light Intensity and Red to Far-Red Ratio

Tina Hitz [1,*], Jens Hartung [2], Simone Graeff-Hönninger [1] and Sebastian Munz [1]

[1] Institute of Crop Science, University of Hohenheim, 70599 Stuttgart, Germany
[2] Department of Biostatistics, Institute of Crop Science, University of Hohenheim, 70599 Stuttgart, Germany
* Correspondence: tina.hitz@uni-hohenheim.de

Received: 16 July 2019; Accepted: 2 August 2019; Published: 3 August 2019

check for updates

Abstract: In soybean production, the shade avoidance response can affect yield negatively in both mono- and inter-cropping systems due to increased heterogeneity of the crop and lodging. This is mainly regulated by photoreceptors responding to the ratio between red and far-red light (R:FR) and photosynthetic photon flux density (PPFD). In this study, three soybean cultivars were grown under different R:FR and PPFD in a light emitting diode (LED) climate chamber to disentangle the effect of each on morphology and dry matter. Results showed that plant organs were influenced differently and indicated an interaction with the increase in assimilates at high PPFD. Internode elongation was mainly influenced by low PPFD with an additive effect from low R:FR, whereas petiole elongation responded strongly under low R:FR. Hence, petiole elongation can be seen as the main response to the threat of shade (high PPFD and low R:FR) and both petiole and internode elongation as a response to true shade (low PPFD and low R:FR). Interactions between cultivar and light treatment were found for internode length and diameter and leaf mass ratio, which may be unique properties for specific cropping systems.

Keywords: photomorphogenesis; shade avoidance response; far-red radiation; photosynthetic photon flux density; red to far-red ratio; LED lighting

1. Introduction

Plants competing for light recognize neighboring vegetation through changes in the light quality, which leads to shade avoidance responses (SARs), with the aim to increase light interception and consequently competitiveness. Typical SARs of plant organs are thinner leaves, increased lamina:petiole length and elongation of hypocotyl, internode, petiole, and leaves [1,2]. The change in light quality is a result of different absorption and reflection of different wavelengths in leaves particularly due to the low absorption and high reflection and transmittance of far-red light (FR) (700–800 nm) compared to other wavelengths. A reduction in red to far-red ratio (R:FR) while photosynthetic photon flux density (PPFD) is still high, appears by the threat of future shade from surrounding short vegetation [3,4]. In this situation, FR is reflected from the surrounding vegetation, whereas red light (R) is absorbed and decreases the R:FR perceived by the taller crop. Under shading, both perceived PPFD and R:FR are reduced, due to the high absorption of other wavelengths when compared to FR by the tall vegetation. The light quality is recognized by plant photoreceptors, with phytochrome and cryptochrome being the main regulators of SAR to R:FR and PPFD, respectively [5]. The two forms of phytochrome (Pr and Pfr) regulate the response by a dynamic photo-equilibrium dependent on R:FR. By absorption of FR, Pfr is transformed to the inactive form Pr, which relieves gene suppression, and in turn, induces SARs [6]. Cryptochromes regulate, while interacting with multiple regulating proteins, the response to changed

PPFD by recognizing the change in blue light intensity (400-500 nm) associated with changed PPFD [7]. In *Arabidopsis thaliana* (L.) Heynh, several studies have shown that phytochrome and cryptochrome interact to fine-tune SAR [5,8–10]. Interacting of cryptochrome with Phytochrome Interacting Factors (PIFs) under low blue light enhanced the response of petioles [8] and hypocotyl [10] to low R:FR. Not only photoreceptors regulate the SAR, as increased leaf thickness under high PPFD has been found, independent of a blue light level [11] and cryptochrome mutations [12].

In crop production, the light environment can change with weed pressure or cropping system. Emerging weeds increase R:FR due to the increased reflection of FR while intercropping reduces both PPFD and R:FR perceived by the shorter crop. The SAR of the crop to the given environment can affect yield negatively e.g., SAR to emerging weeds reduced the yield of mono-cropped soybean (*Glycine max* (L.) Merr.), due to increased crop heterogeneity [4]. The intercropped soybean is often the shorter crop grown together with a taller crop like maize and a strong elongation response of soybean to the given light environments, which can lead to lodging [13]. Earlier studies showed that soybean shaded by maize had a reduced stem diameter [13,14], root length, aboveground biomass, total root biomass, and root–shoot ratio [14,15] and an increased seedling height [13,14,16]. Additionally, the shaded soybean has increased chlorophyll content and reduced the photosynthetic capacity and chlorophyll *a*/*b* ratio [16,17]. Plants are considered more shade tolerant if they have a high specific leaf area (SLA), leaf area ratio (LAR), and leaf mass ratio (LMR) [18]. Intercropped soybean leaves had reduced leaf area and mass per area [19] and increased SLA and LAR [16].

From field observations, it is difficult to determine the distinct effect from low PPFD and low R:FR. Studies on the distinct effect of decreased R:FR on soybean found elongated petioles, retarded rates of stem elongation [20], increased internode length only of epicotyl and hypocotyl [4], or increased length of the measured internode with no significant change of total stem length [21]. Regarding the effect of R:FR on leaf area, Green-Tracewicz et al. [4] found a decreased leaf area from the four-leaf stage to seed fill, while Pauch et al. [20] found an increase or insignificant decrease depending on other growth conditions. In addition, the response in LAR and LMR to R:FR depended on growth conditions, but could increase LAR and decrease LMR [20]. Only one study focused on the effect of PPFD and found increased plant height and decreased stem diameter and leaf thickness with decreased PPFD [22]. However, there are no studies on soybeans, which investigated the effect of a change only in PPFD, i.e., without any influence of FR, facilitating the disentanglement of the individual effects of PPFD and R:FR.

Breeding for cultivars with an optimal SAR for a specific cropping system could increase yield and is particularly important to improve productivity in intercropping systems of maize with a shorter crop like soybean [23,24], but can also be important for increasing weed tolerance [25]. For exploiting this potential, genetic variability in SAR has to be examined [16]. Intercropped soybean cultivars differed e.g., in their degree of vining, stem diameter [13], internode elongation [16], dry matter [15], yield [26], and photosynthetic capacity [17]. The underlying molecular mechanisms of the response in soybean are being explored, but are still unclear [25]. A disentanglement of the effects of PPFD and R:FR on morphology could help in understanding these mechanisms and to determine the most important molecular mechanisms for specific cropping systems.

We hypothesized that the morphological response of soybean to a change only in PPFD would differ from the response to a change only in R:FR due to the regulation by different photoreceptors and that the response would vary between cultivars. Therefore, a climate chamber experiment was conducted with different levels of PPFD combined with different ratios of R:FR and with no FR including three morphologically different soybean cultivars to investigate the effect of PPFD and R:FR on morphology of soybean and to assess the variability among cultivars.

2. Materials and Methods

2.1. Experimental Setup

Two experiments were performed in an LED climate chamber (poly klima®S-chamber, Poly klima GmbH, Freising, Germany) at the University of Hohenheim (Germany). The chamber was designed for research applications and had the following dimensions: 0.6 m high, 0.6 m wide, and 0.5 m deep. The chamber consisted of two compartments each with two LED modules comprised of several LED types adjustable in light intensity and spectrum (Figure 1). Each LED type corresponded to a different wavelength and was represented by several individual LEDs arranged across the LED module for homogenous illumination. Each set of LED type, which was called channel, could be turned on and adjusted independently in intensity, which allows for several spectral compositions from the same LED module. The photoperiod was 16 h with 28 °C day temperature, 22 °C night temperature, and a relative humidity of 45%. The three soybean cultivars of maturity group 000, namely Lissabon (I.G. Pflanzenzucht GmbH, Ismaning, Germany), Merlin (SAATBAU LINZ eGen, Leonding, Austria), and Sultana (R.A.G.T. Saaten Deutschland GmbH, Hiddenhausen, Germany) were selected for their known differences in plant height. According to the cultivar descriptions, among the three cultivars, cv. Lissabon is the shortest cultivar and cv. Merlin is the tallest. Additionally, Merlin has a fast youth development and an intermediate tendency for lodging, whereas cvs. Lissabon and Sultana have a low lodging tendency. Within each compartment of the LED chamber, nine soybean plants (three of each cultivar) were grown in pots (9.5 × 9.0 × 9.0 cm) containing peat substrate (Substrat 5+Perlite, Klasmann-Deilmann GmbH) and irrigated from below in a common tray. At the start of the experiment, four seeds were sown in each pot. During germination and early growth, PPFD was 200 µmol m^{-2} s^{-1} with very low photon flux density of far-red light (2 µmol m^{-2} s^{-1}). After one week, seedlings were thinned to one plant per pot, according to homogenous development, and the light treatments were applied. The plants were grown for another 13 days under the light treatments (in a total of 20 days of growth) until the first trifoliate leaf was developed. During the experiment, the shelves with the plants were moved downward to maintain a distance of 10 cm to the LED modules ensuring a constant spectral photon flux density at the top of the canopy.

(**a**) (**b**)

Figure 1. Soybean within the chamber (**a**) and the empty chamber showing the LED modules (**b**).

2.2. Light Treatments

To set the light treatments, quantitative measurements of the light spectrum (µmol m^{-2} s^{-1} nm^{-1}) were acquired with a FLAME-S-XR1-ES spectrometer (Ocean Optics Germany GmbH, Ostfildern, Germany). The spectrometer measured the light spectrum within the range from 200 to 1025 nm with a resolution of around 2 nm. It was equipped with a collimating lens (74-UV-MP) and a right-angle reflector with a cosine corrector (74-90-UV-CC3). The photon flux density was recorded for five ranges: 400–700 nm (photosynthetic active radiation), 400–500 nm (blue light), 500–600 nm (green light), 600–700 nm (R), and 700–800 nm (FR) and the R:FR was calculated. Setting of the light treatments

(Table 1) was done by adjusting the intensities of the channels of the LED modules by comparing them to measurements of the spectrometer. The setting was performed at a 10-cm distance from the LED modules equivalent to the distance to the soybean canopy during the experiments.

Different light treatments were applied in the two experiments. In the first experiment, the light treatments were low and high PPFD of 100 µmol m^{-2} s^{-1} ($PPFD^{100}$) and 400 µmol m^{-2} s^{-1} ($PPFD^{400}$), respectively, in combination with a low or high R:FR or a very high R:FR further referred to as no FR. The low R:FR was 1.5 ($rfr^{1.5}$) and the high ratio was 5 (rfr^{5}) (Table 1). In the second experiment, PPFD was 160 µmol m^{-2} s^{-1} ($PPFD^{160}$). This intensity was chosen because it enabled under the experimental maximum intensity of FR, which is the creation of a lower R:FR ratio of 0.6 ($rfr^{0.6}$). This can be considered comparable to natural shade by vegetation [14]. The R:FR ratios of 1.5 ($rfr^{1.5}$) and 5 (rfr^{5}) were kept for comparison with the first experiment. All light treatments were comprised of a broad spectrum (shown for experiment one in Figure 2) with the same blue to R and blue to green ratios of 1 and 1.5, respectively.

Table 1. Photon flux density (µmol m^{-2} s^{-1}) within the four-color ranges, total photosynthetic photon flux density (PPFD), and the red to far-red ratio (R:FR, rfr) for each treatment within the first and second experiment.

Treatment	PPFD (400–700 nm)	Blue (400–500 nm)	Green (500–600 nm)	Red (600–700 nm)	Far-Red (700–800 nm)	R:FR
First Experiment						
$PPFD^{100}$	100	37.5	25	37.5	1	37.5
$PPFD^{100}$ rfr^{5}	100	37.5	25	37.5	7.5	5
$PPFD^{100}$ $rfr^{1.5}$	100	37.5	25	37.5	25	1.5
$PPFD^{400}$	400	150	100	150	4	37.5
$PPFD^{400}$ rfr^{5}	400	150	100	150	30	5
$PPFD^{400}$ $rfr^{1.5}$	400	150	100	150	100	1.5
Second Experiment						
$PPFD^{160}$ rfr^{5}	160	60	40	60	12	5
$PPFD^{160}$ $rfr^{1.5}$	160	60	40	60	40	1.5
$PPFD^{160}$ $rfr^{0.6}$	160	60	40	60	100	0.6

2.3. Plant Measurements

In both experiments, measurements were performed 20 days after sowing. The morphological measurements comprised length and diameter of the third internode and the petiole of the first trifoliate leaf (located on the third node) and length of rachis bearing the center leaf of the first trifoliate leaf. The third phytomer was chosen because it included the first and fully developed trifoliate leaf. Measurements of leaf area and dry mass were made separately for leaves and stem (internodes and petioles) of the entire above ground plant and were used to calculate the specific leaf area (SLA = leaf area/leaf dry mass), leaf area ratio (LAR = leaf area/total above ground dry mass), and leaf mass ratio (LMR = leaf dry mass/total above ground dry mass). Diameters were measured with a caliper and lengths with a ruler. Leaf area was measured with a leaf area meter (LI-3100 Area Meter, LI-COR, Lincoln, NE, USA) and dry mass was recorded after drying for at least 48 h at 60 °C until it reached a constant weight.

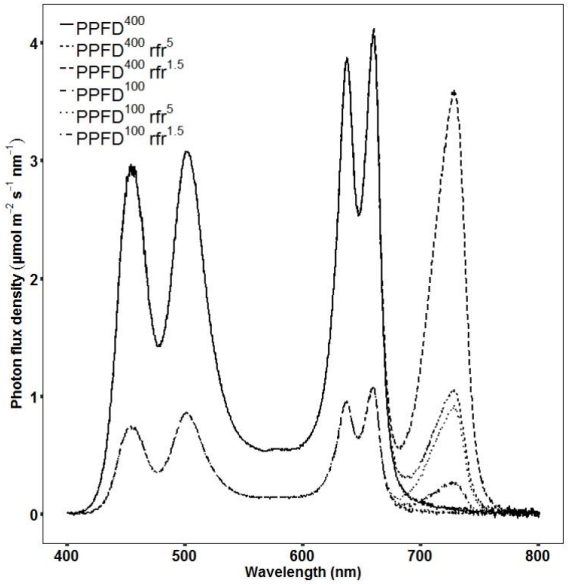

Figure 2. Spectral photon flux density of the six light treatments in the first experiment at high ($PPFD^{400}$) and low ($PPFD^{100}$) photosynthetic photon flux density (PPFD) and high (rfr^{5}) and low ($rfr^{1.5}$) red to far-red ratio (R:FR).

2.4. Statistical Design and Analysis

In both experiments, the effect of light treatments and cultivars on SAR were tested. In the first experiment, six light treatments were tested. In the second experiment, there were three light treatments (Table 1). Both experiments were performed with two replicates within the single chamber with two compartments. This resulted in six runs for the first experiment and three runs for the second experiment. In each run, two out of six or three light treatments, respectively, could be tested. An α-design with two replicates and a block size of two was used in the first experiments. An incomplete non-resolvable block design with two replicates was used in the second experiment. Within a compartment, each cultivar was tested in triplicates. The nine pots were arranged according to a 3 × 3 latin square to block out effects in two dimensions. In total, each treatment was measured on six plants including two runs with three plants each.

To verify the number of replicates to be statistically sufficient, the statistical power for the trait length of the third internode was estimated after performing the first experiment. Error variances were heterogeneous. Therefore, we calculated an average variance using a generalized linear model, by assuming a gamma distribution. The light treatment specific variances varied between 0.07 cm^2 and 3.61 cm^2 and the estimated average was 1.075 cm^2. With this error variance, we calculated the power for 1 to 5 cm and two or three replicates using the approach of Stroup [27]. The power satisfied two replicates, as shown in Table 2.

Table 2. Power for the trait length of the third internode.

Difference in cm	Two Replicates	Three Replicates
1	0.362	0.509
2	0.894	0.977
3	0.998	>0.999
4	>0.999	>0.999
5	>0.999	>0.999

According to the design, the following mixed model was used to analyze the data in the Statistical Analysis System (SAS):

$$y_{ijklmno} = \mu + b_k + i_{kl} + p_{lm} + r_{lmn} + c_{klmo} + \tau_i + \varphi_j + (\tau\varphi)_{ij} + e_{ijklmno}, \quad (1)$$

where μ is the intercept, b_k is the fixed effect of the kth complete replicate, i_{kl} is the random effect of the lth incomplete block (=run) within the kth replicate, p_{klm} is the random effect of the mth compartment within the lth run, and r_{lmn} and c_{lmo} are random row and column effects within the mth compartment of the lth run. τ_i, φ_j, and $(\tau\varphi)_{ij}$ are the main effects of the ith light treatment, the jth cultivar, and their interactions, respectively. $e_{ijklmno}$ is the error effect of observation $y_{ijklmno}$ with either homogeneous variance, PPFD-specific variance, or R:FR-specific and PPFD-specific variance. All three error structures were fitted and the model with the best model fit measured via the Akaike information criterion (AIC) [28] was used. Studentized residuals were checked graphically for normal distribution and homogeneous variances. After finding significant effects via the F-test, a multiple t-test was used to create a letter display [29]. Note that, for the second experiment, b_k was dropped from the model and i_{kl} was replaced by i_l since there are no complete replicates. Further note that ratios of means were calculated from least square means for solely a presentation purpose.

3. Results

All soybean cultivars responded significantly to both factors, PPFD and R:FR, but the quantitative response to each of the two factors differed between plant organs. Cultivars differed significantly in their response of internode length and diameter, petiole length LAR, SLA, and LMR. Regarding the response on plant level, plant height increased under both low PPFD and low R:FR in the first experiment. Furthermore, the experiment had few significant differences that were present. Plant weight decreased under low PPFD and increased under low R:FR (Table 3).

Table 3. The least square means of plant height and weight for the three cultivars in the first (top) and second (bottom) experiment. For each experiment, lower case letters indicate significant differences between treatments for each cultivar, and upper case letters indicate significant differences between cultivars for each treatment ($p < 0.05$).

Treatment	Plant Height (cm)			Plant Weight (g)		
	Lissabon	**Merlin**	**Sultana**	**Lissabon**	**Merlin**	**Sultana**
First experiment						
$PPFD^{400}$	12.31 ^{eA}	11.88 ^{fA}	8.89 ^{eB}	0.71 ^{bA}	0.64 ^{bAB}	0.52 ^{bB}
$PPFD^{400}$ rfr^{5}	13.97 ^{eA}	15.07 ^{eA}	10.48 ^{eB}	0.69 ^{bA}	0.80 ^{abA}	0.61 ^{bA}
$PPFD^{400}$ $rfr^{1.5}$	17.16 ^{dB}	18.65 ^{dA}	16.50 ^{dB}	0.92 ^{aA}	0.98 ^{aA}	0.86 ^{aA}
$PPFD^{100}$	39.74 ^{cA}	29.87 ^{cB}	25.54 ^{cC}	0.32 ^{cA}	0.29 ^{cAB}	0.23 ^{cB}
$PPFD^{100}$ rfr^{5}	44.34 ^{bA}	36.73 ^{bB}	32.83 ^{bC}	0.37 ^{cA}	0.29 ^{cA}	0.31 ^{cA}
$PPFD^{100}$ $rfr^{1.5}$	52.01 ^{aA}	48.73 ^{aAB}	46.63 ^{aB}	0.37 ^{cA}	0.41 ^{cA}	0.33 ^{cA}
Second Experiment						
$PPFD^{160}$ rfr^{5}	45.15 ^{aA}	36.01 ^{aB}	33.35 ^{bB}	0.50 ^{bB}	0.61 ^{aA}	0.49 ^{bB}
$PPFD^{160}$ $rfr^{1.5}$	45.47 ^{aA}	44.61 ^{aA}	44.22 ^{abA}	0.77 ^{aA}	0.52 ^{aB}	0.59 ^{bB}
$PPFD^{160}$ $rfr^{0.6}$	40.16 ^{aB}	42.03 ^{aB}	44.26 ^{bA}	0.72 ^{abA}	0.70 ^{aA}	0.87 ^{aA}

3.1. Internodes

The length of the third internode was influenced significantly by PPFD and R:FR with the maximum length reached by the combination of low PPFD and low R:FR, but with the strongest effect of decreasing PPFD (Figure 3a). Comparing high PPFD with low PPFD, the internode length of, for instance, cv. Merlin increased substantially from 1.48 to 7.02 cm, which corresponds to 373%, whereas a reduction in R:FR increased length to 3.68 cm at high PPFD and 14.47 cm at low PPFD, which corresponds to an increase by 148% and 106%, respectively (Figure 3a). The cv. Lissabon responded lesser to low R:FR than the other two cultivars with a 63% increased length at high PPFD and a 53% increase at low PPFD in the first experiment and no significant response in the second experiment. The response of cv. Sultana was stronger to a decrease in R:FR at high PPFD than the other two cultivars with an increased length by 192%. Except from cv. Lissabon, the tendency of the responses to reduced R:FR in the second experiment were similar to the first experiment and showed an additional elongation under R:FR of 0.6 compared to 1.5 (Figure 3b).

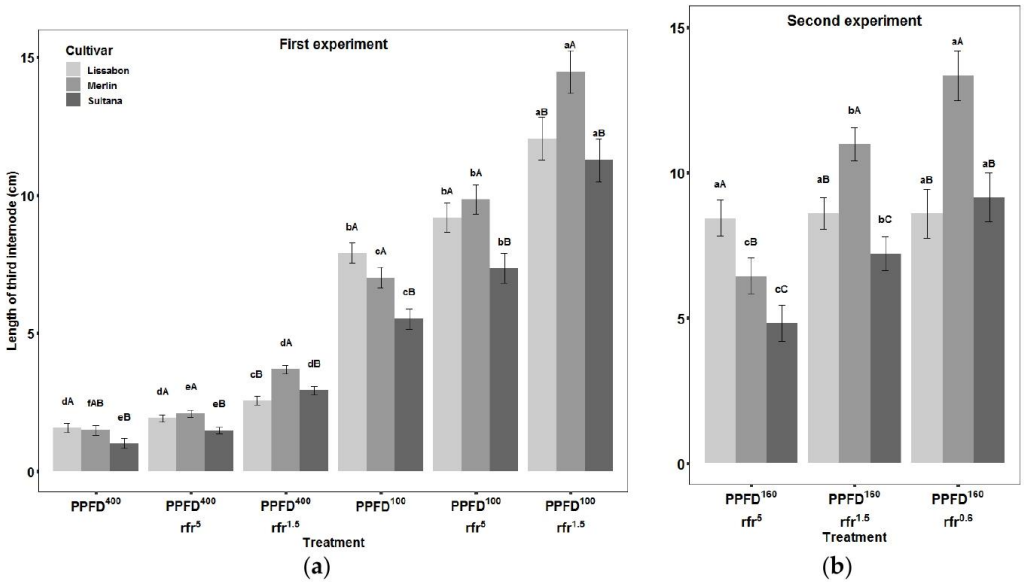

Figure 3. The least square means of third internode length for the three cultivars in first (**a**) and second (**b**) experiment. Error bars indicate standard error of the LS-mean. For each experiment, lower case letters indicate significant differences between treatments for each cultivar, and upper case letters indicate significant differences between cultivars for each treatment ($p < 0.05$).

The diameter of the third internode was mainly influenced by low PPFD with a reduction of 37% to 42% across cultivars (Table 4). On the contrary, the internode diameter tended to increase under low R:FR. For cv. Merlin, there was a significant increase by 23% under low R:FR at a low PPFD and 34% to 38% at an R:FR of 0.6 in the second experiment for the cvs. Lissabon and Sultana (Table 4). Still, internode length to the diameter ratio increased under both low PPFD and low R:FR.

Both internode length, diameter, and their ratio showed, for the same R:FR ratios in the second experiment, an intermediate response between high and low PPFD of the first experiment (Figure 3, Table 4).

Table 4. The least square means of internode diameter for the three cultivars in the first (top) and second (bottom) experiment. For each experiment, lower case letters indicate significant differences between treatments for each cultivar, and upper case letters indicate significant differences between cultivars for each treatment ($p < 0.05$).

Treatment	Third Internode Diameter (mm)			Third Internode Length:Diameter		
	Lissabon	Merlin	Sultana	Lissabon	Merlin	Sultana
First Experiment						
$PPFD^{400}$	2.47 ^{abB}	2.88 ^{aA}	2.73 ^{aAB}	6.48 ^{cA}	5.33 ^{dAB}	4.06 ^{eB}
$PPFD^{400}$ rfr^{5}	2.41 ^{bB}	2.95 ^{aA}	2.90 ^{aA}	8.10 ^{cA}	7.12 ^{dA}	5.08 ^{eB}
$PPFD^{400}$ $rfr^{1.5}$	2.86 ^{aA}	2.79 ^{aA}	3.03 ^{aA}	8.72 ^{cB}	12.93 ^{cA}	9.44 ^{dB}
$PPFD^{100}$	1.47 ^{cA}	1.66 ^{cA}	1.72 ^{bA}	47.99 ^{bA}	42.98 ^{bAB}	31.66 ^{cB}
$PPFD^{100}$ rfr^{5}	1.65 ^{cA}	1.73 ^{bcA}	1.59 ^{bA}	58.91 ^{bA}	57.10 ^{aA}	49.58 ^{bA}
$PPFD^{100}$ $rfr^{1.5}$	1.65 ^{cB}	2.05 ^{bA}	1.68 ^{bB}	76.33 ^{aA}	73.55 ^{aA}	68.67 ^{aA}
Second Experiment						
$PPFD^{160}$ rfr^{5}	1.84 ^{bB}	2.25 ^{aA}	2.19 ^{bA}	27.71 ^{bA}	27.66 ^{cA}	28.14 ^{bA}
$PPFD^{160}$ $rfr^{1.5}$	2.40 ^{aA}	2.15 ^{aA}	2.33 ^{bA}	44.84 ^{aA}	37.38 ^{bA}	35.62 ^{bA}
$PPFD^{160}$ $rfr^{0.6}$	2.47 ^{aB}	2.29 ^{aB}	3.03 ^{aA}	47.81 ^{aA}	50.04 ^{aA}	48.09 ^{aA}

3.2. Petioles

Contrary to internode length, the length of the third petiole increased less under low PPFD and showed the strongest increase under low R:FR (Figure 4a). In cv. Merlin, the response to low PPFD was an increased length from 2.05 to 3.07 cm corresponding to 50% and the response to low R:FR was an increased length to from 2.05 to 6.33 cm at high PPFD and an increase from 3.07 to 6.14 cm at low PPFD, which corresponds to 209% and 100%, respectively. In cv. Merlin, this led to no difference in petiole length between high and low PPFD at low R:FR and in cv. Lissabon to significantly longer petioles under low R:FR at high PPFD than at low PPFD. In the second experiment, the elongation responses to R:FR were further increased in the treatment with an R:FR of 0.6 compared to 1.5 (Figure 4b). For instance, the length of the third petiole of cv. Merlin increased from 6.14 cm to 8.49 cm under a R:FR of 1.5 and to 11.73 cm under a R:FR of 0.6, which corresponds to 38% and 91%, respectively. The cv. Lissabon had the strongest response to a R:FR of 0.6 with an increase of 147% when compared to a R:FR of 5. This led to the petioles of the cv. Lissabon no longer being significantly different from the other cultivars under a R:FR of 0.6, even though they were significantly shorter than the other cultivars under an R:FR of 5.

Similar tendencies of a strong response to low R:FR were present for the lengths of the third center rachis. Only rachis length of the cv. Sultana responded significantly at low PPFD, but all cultivars responded significantly under low R:FR at high PPFD (Table 5). Comparing PPFD levels of the two experiments, both petiole and rachis had a tendency of increased length in the second experiment compared to both high and low PPFD in the first experiment (Figure 4, Table 5).

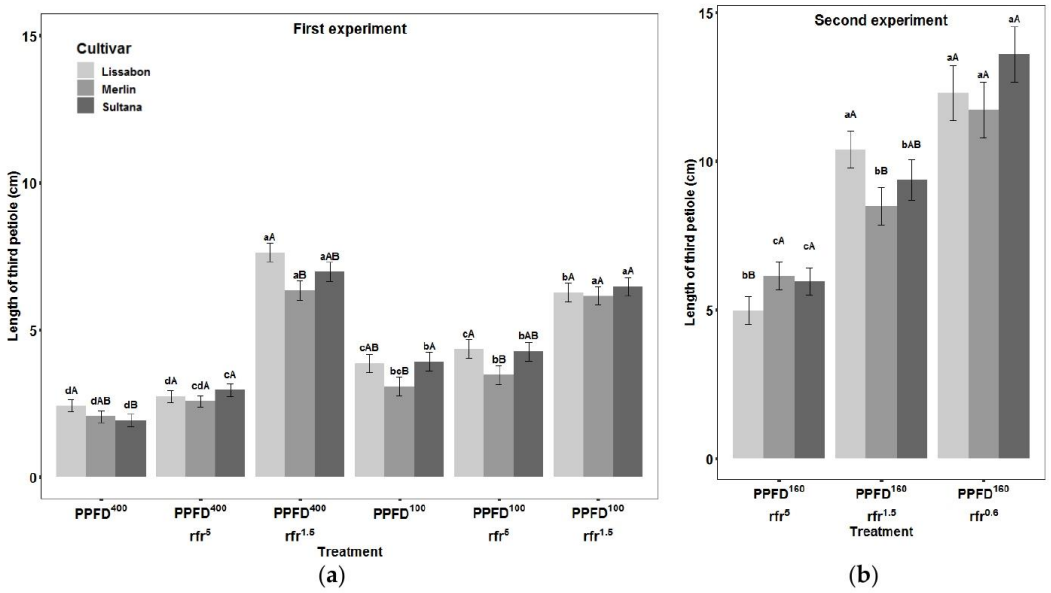

Figure 4. The least square means of third petiole length for the three cultivars in first (**a**) and second (**b**) experiment. Error bars indicate standard error of the LS-mean. For each experiment, lower case letters indicate significant differences between treatments for each cultivar, and upper case letters indicate significant differences between cultivars for each treatment ($p < 0.05$).

Table 5. The least square means of rachis length for the three cultivars in the first (top) and second (bottom) experiment. For each experiment, lower case letters indicate significant differences between treatments for each cultivar, and upper case letters indicate significant differences between cultivars for each treatment ($p < 0.05$).

Treatment	Third Center Rachis Length (cm)		
	Lissabon	Merlin	Sultana
First Experiment			
$PPFD^{400}$	0.92 ^{bA}	0.80 ^{cAB}	0.72 ^{dB}
$PPFD^{400}$ rfr^{5}	1.07 ^{bA}	0.98 ^{bAB}	0.87 ^{cdB}
$PPFD^{400}$ $rfr^{1.5}$	1.62 ^{aA}	1.67 ^{aA}	1.30 ^{aA}
$PPFD^{100}$	0.95 ^{bA}	0.85 ^{bcA}	0.98 ^{bcA}
$PPFD^{100}$ rfr^{5}	0.97 ^{bA}	0.83 ^{bcA}	0.88 ^{cdA}
$PPFD^{100}$ $rfr^{1.5}$	1.13 ^{bA}	1.03 ^{bcA}	1.18 ^{abA}
Second Experiment			
$PPFD^{160}$ rfr^{5}	0.96 ^{bA}	1.06 ^{bA}	1.03 ^{bA}
$PPFD^{160}$ $rfr^{1.5}$	1.38 ^{aA}	1.24 ^{bA}	1.42 ^{aA}
$PPFD^{160}$ $rfr^{0.6}$	1.61 ^{aA}	1.78 ^{aA}	1.65 ^{aA}

3.3. Leaves

Leaf length was generally less influenced by PPFD and R:FR compared to internodes and petioles. Low PPFD had no significant influence on leaf length of the cv. Merlin, but increased the leaf length of the cvs. Lissabon and Sultana with 11% to 13% (Figure 5). R:FR did not influence the leaf length at low PPFD or in the second experiment, but at high PPFD, low R:FR increased leaf length with 18% to 26% across cultivars.

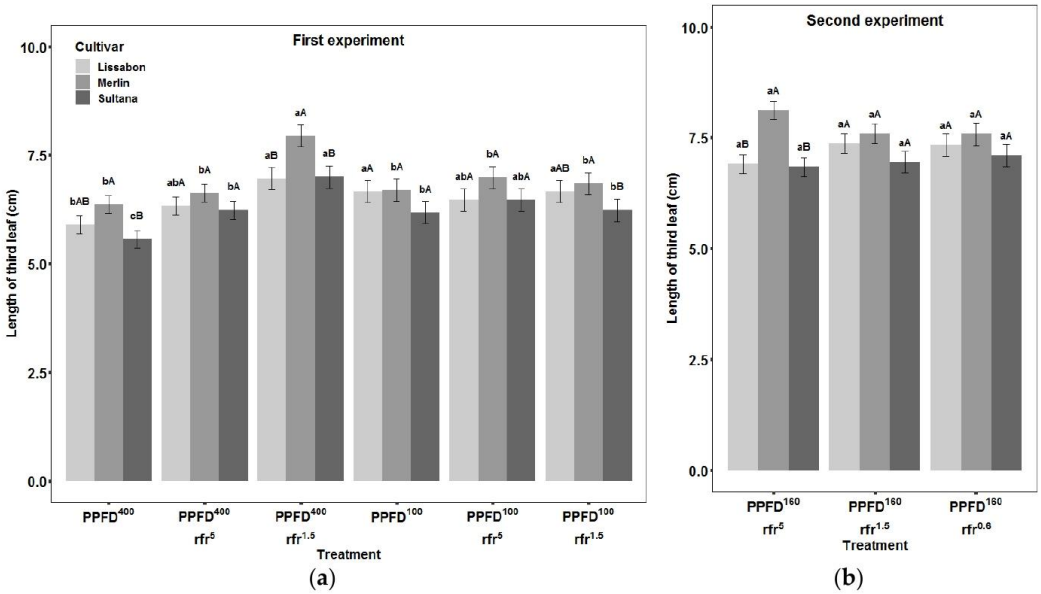

Figure 5. The least square means of leaf length of the third leaf for the three cultivars in the first (**a**) and second (**b**) experiment. Error bars indicate standard error of the LS-mean. For each experiment, lower case letters indicate significant differences between treatments for each cultivar, and upper case letters indicate significant differences between cultivars for each treatment ($p < 0.05$).

The SLA and LAR responded mainly to low PPFD with an increase of 178% to 200% and 142% to 181%, respectively (Table 6). In the first experiment, R:FR had an additive influence on SLA with a maximum increase in cv. Lissabon at low PPFD of 23%, while R:FR decreased LAR with a maximum decrease in cv. Sultana of 18%. In the second experiment, leaf length, SLA, and LAR were not influenced significantly by R:FR. This was in accordance with the first experiment at either low or high PPFD, where they were also not influenced significantly by R:FR, which compared an R:FR of 5 and 1.5. Similar to internodes, SLA and LAR were intermediate in the second experiment compared to low and high PPFD. Under low PPFD, LMR significantly decreased by 9% to 14% in cvs. Merlin and Lissabon and, under low R:FR LMR, decreased by 10% to 24%. In the second experiment, LMR decreased by 15% to 23% from R:FR of 5 to 0.6. Comparing the cultivars, cv. Sultana maintained the highest LMR at low PPFD and low R:FR.

Table 6. The least square means of specific leaf area, the leaf area ratio, and the leaf mass ratio for the three cultivars in the first (top) and second (bottom) experiment. For each experiment, lower case letters indicate significant differences between treatments for each cultivar, and upper case letters indicate significant differences between cultivars for each treatment ($p < 0.05$).

Treatment	Specific Leaf Area ($cm^2\ g^{-1}$)			Leaf Area Ratio			Leaf Mass Ratio		
	Lissabon	Merlin	Sultana	Lissabon	Merlin	Sultana	Lissabon	Merlin	Sultana
First experiment									
$PPFD^{400}$	247.31 ^{cdB}	242.19 ^{cB}	280.22 ^{cA}	170.72 ^{bB}	170.86 ^{cB}	209.30 ^{dA}	0.69 ^{aB}	0.71 ^{aB}	0.75 ^{abA}
$PPFD^{400}$ rfr^{5}	245.21 ^{dB}	243.60 ^{cB}	326.17 ^{bA}	168.32 ^{bB}	167.59 ^{cB}	248.35 ^{cA}	0.69 ^{aB}	0.69 ^{aB}	0.76 ^{aA}
$PPFD^{400}$ $rfr^{1.5}$	278.16 ^{cB}	277.83 ^{bB}	319.13 ^{bA}	172.66 ^{bB}	169.71 ^{cB}	209.63 ^{dA}	0.62 ^{bB}	0.61 ^{bcB}	0.66 ^{cA}
$PPFD^{100}$	687.99 ^{bB}	726.19 ^{aAB}	816.74 ^{aA}	412.36 ^{aB}	466.52 ^{abB}	588.27 ^{aA}	0.59 ^{bcC}	0.65 ^{bB}	0.72 ^{bA}
$PPFD^{100}$ rfr^{5}	695.94 ^{bB}	817.27 ^{aA}	791.52 ^{aA}	395.18 ^{aB}	485.04 ^{aA}	526.43 ^{bA}	0.57 ^{cB}	0.60 ^{cB}	0.67 ^{cA}
$PPFD^{100}$ $rfr^{1.5}$	843.77 ^{aA}	833.10 ^{aA}	850.56 ^{aA}	405.19 ^{aB}	409.10 ^{bB}	481.52 ^{bA}	0.49 ^{dB}	0.49 ^{dB}	0.57 ^{dA}
Second Experiment									
$PPFD^{160}$ rfr^{5}	592.98 ^{aB}	614.07 ^{aAB}	701.66 ^{abA}	330.74 ^{aB}	357.98 ^{aB}	457.75 ^{aA}	0.55 ^{aC}	0.59 ^{aB}	0.65 ^{aA}
$PPFD^{160}$ $rfr^{1.5}$	599.19 ^{aB}	703.47 ^{aA}	793.77 ^{aA}	298.79 ^{aB}	365.25 ^{aA}	416.26 ^{aA}	0.50 ^{bA}	0.51 ^{bA}	0.53 ^{bA}
$PPFD^{160}$ $rfr^{0.6}$	658.65 ^{aA}	672.45 ^{aA}	604.34 ^{bA}	306.23 ^{aA}	309.16 ^{aA}	299.78 ^{bA}	0.47 ^{bB}	0.47 ^{cAB}	0.50 ^{bA}

4. Discussion

4.1. Response to PPFD and R:FR

The results showed that the response of soybean to low PPFD and low R:FR can be characterized as an interactive response with differences between organs. Internodes elongated the most in response to low PPFD with an additive effect from the addition of low R:FR. Yet, the increase of petiole elongation was more stimulated by R:FR than PPFD. The main elongation response of petioles to low R:FR and of internodes to low PPFD are consistent with a study by Pauch et al. [20]. However, in their study, the internode length was not influenced or even reduced under low R:FR. On the contrary, Yang et al. [14] showed that the increase in seedling height of soybean intercropped with maize correlated more with R:FR than with PPFD. This might be explained by a greater effect of R:FR on the hypocotyl and epicotyl than the following internodes [4], which would not have been fully captured in our study, because the light treatments were applied after the development of the epicotyl had already started. The internode diameter responded mainly to decreased PPFD with a tendency toward an increased diameter under low R:FR. Only a few studies have examined the internode diameter response to low R:FR under high PPFD. Hussain et al. [21] also found the internode diameter of soybean to decrease mainly as a response to decreased PPFD, but with a tendency toward a decreased diameter under low R:FR and similar results were found for the sunflower [30]. However, as expected, an increase of the length to the diameter ratio under low R:FR was present and the tendency of increased diameter might be a necessary response to stabilize the plant due to the more extreme elongation of the internodes, than in the study of Hussain et al. [21].

The results indicated that, in addition to the expected elongation response to low PPFD, an increased PPFD might increase the elongation response to R:FR. The response to low PPFD is considered a response to decreased blue light mediated by cryptochrome, whereas a response to increased PPFD could be a result of increased availability of assimilates. This effect could be observed in petiole length under low R:FR, since the length was not increased under low PPFD compared to high PPFD and a tendency of an increased response at 160 µmol m^{-2} s^{-1} compared to the low PPFD treatments at 100 µmol m^{-2} s^{-1}. These results should be examined further with more levels of PPFD between 100 and 400 µmol m^{-2} s^{-1} and measurements of photosynthesis for a better understanding. Earlier studies on soybean found changes in the photosynthetic system [17] and stem carbohydrate concentration as well as composition under low PPFD [21], and changes in carbon export from tomato leaves depending on PPFD and light quality [31].

In general, the response of the leaf length was minor when compared to internodes and petioles, but length increased under low PPFD and low R:FR at high PPFD. Soybean shaded by maize in an intercropping system (low R:FR at low PPFD) had a decreased leaf area [19]. Pauch et al. [20] found an increase in leaf area with decreased R:FR in the greenhouse, but smaller leaf area under climate chamber conditions, which had a lower average light intensity. This indicated a response of leaf area similar to petioles, which results in opposite responses to R:FR depending on the PPFD level.

The response of leaves was mainly a considerable increased LAR and SLA, i.e., decreased thickness of the leaf under low PPFD, and no effect of R:FR on SLA. An increase in SLA has also been observed in an earlier study on the PPFD level [22], in intercropped soybean [19], and is generally consistent with observations from other species [11]. In *Arabidopsis thaliana* (L.) Heynh, it was shown that leaf thickness is regulated mainly by light intensity through redox-signaling or sugar signaling and not through photoreceptors [12,32]. In accordance with earlier studies in soybean [16,20], elongation responses in this study resulted in a decreased LMR.

The second experiment with a lower R:FR treatment, which is comparable to field conditions, underlined the results from the first experiment and showed that the internode diameter, the elongation of the internode, and petiole were further increased under an R:FR of 0.6. A comparable study with sunflower also showed that the elongation response of internodes to decreasing R:FR were similar when comparing unnaturally high to high R:FR or high to low R:FR [30]. Regarding field conditions,

the strong response of petioles to low R:FR in this study, indicated that petiole elongation would be the main response in soybeans in response to the threat of shade recognized by a decreased R:FR due to reflected FR from neighboring vegetation [3], e.g., emerging weeds. While the response to true shade, for instance, by taller neighboring plants in intercropping decreases both PPFD and R:FR, the response would lead to an elongation of both internodes and petioles.

4.2. Cultivar Differences and Aspects for Crop Management

Assuming that the data sheet information given on the three cultivars are recorded in a mono-cropping system, it is the most relevant to compare these data with the treatments under high PPFD including R:FR. The cultivar Merlin was, as expected, the tallest cultivar, whereas cv. Sultana, not in line with the cultivar description, was shorter than cv. Lissabon. This is likely to be due to the early termination of growth or problems with comparing information on relative height from different companies. Assuming the ratio of the internode length to diameter as an expression for the lodging tendency, cv. Merlin had the highest ratio as expected from the cultivar description.

Relevant for mono-cropping systems is the response to R:FR, since this determines the response to the thread of shade at high light intensity, which can affect the yield negatively [4,25]. In this context, cultivars differed in their response to R:FR under high PPFD with a preferable low internode elongation of the cv. Lissabon and low petiole elongation of cv. Merlin. The response of petioles to a change in R:FR indicated that petiole elongation could be one reason for the weed induced upregulation of PIF-like genes in soybean [25]. In the context of intercropping, knowledge on gene regulation under low R:FR should be accompanied by further knowledge on gene regulations under low PPFD, which influences e.g., internode length, which was not influenced in the study of Horvath et al. [25]. A shade tolerant plant is expected to have a high SLA, LAR, and LMR, according to the hypothesis of maximizing net carbon gain [18]. Considering the shade tolerance of the three cultivars, cv. Sultana had a higher LMR and LAR and smaller decrease in these by decreased PPFD or R:FR than the other cultivars, which indicates potential cultivar differences in the carbon investment in the SAR. Intercropping of the soybean can be further divided depending on the duration of the overlapping growth period. If the overlap with e.g., maize is only during the early soybean growth, a stable crop is still important to avoid lodging, but shade tolerant traits e.g., a high LAR might be of less importance when shade is no longer present. In this context, it would be interesting to further disentangle the effect and underlying mechanisms of internode elongation regulated by photoreceptors and leaf morphology, which is regulated by other mechanisms [12,30]. In addition, interactions between morphological and photosynthetic adaptations to shade [17] could be interesting for further studies and cultivar improvements. For instance, it would be intriguing to determine whether an increased photosynthetic shade adaptation results in a stronger elongation response due to an increase in assimilate availability. The effect of fluctuating light occurring diurnally or for certain time periods during the co-growing period should also be taken into account in future studies for better understanding the influence of acclimation to different levels of PPFD and R:FR on carbon assimilation and translocation.

The interactions between the cultivar and the light environment and the different morphological responses e.g., between internodes and petioles, substantiate the need for a genetic selection within intercropping trials [23,24]. Based on this, a selection for the optimal response in e.g., internode elongation, length to diameter ratio, and allocation of assimilates between organs e.g., for an optimal LAR would be possible.

5. Conclusions

The shade avoidance response of the soybean to low PPFD and R:FR differed between organs. This supported a differentiated response to the threat of shade (low R:FR) with strong petiole elongation and to the true shade (low R:FR and PPFD) with considerable elongation of both internodes and petioles. Regarding petiole elongation, the results indicated an additional interaction with the availability of assimilates. For a deeper understanding, this interaction should be further studied together with a

disentanglement of the responses of leaf morphology, which is dependent on photoreceptors and those dependent on e.g., sugar signaling.

The different responses of organs to the light environment typical for different crop practices and the interactions between the cultivar and the light environment showed interesting possibilities for future breeding. Consideration of these differentiations and interactions could help in understanding molecular responses of soybean to shade and those important for developing cultivars with an optimized shade avoidance response for specific crop management (e.g., mono-cropping and intercropping). Further studies should examine the effect of PPFD and R:FR on carbon assimilation and translocation, include a larger and more diverse genetic panel, and align experiments under controlled and field conditions to transfer knowledge into practice.

Author Contributions: Conceptualization, T.H. and S.M. Data curation, T.H. Formal analysis, T.H. and J.H. Funding acquisition, S.G.-H. and S.M. Investigation, T.H. Methodology, T.H., J.H., and S.M. Project administration, S.M. Supervision, S.G.-H. Visualization, T.H. Writing—original draft, T.H. and J.H. Writing—review & editing, S.G.-H. and S.M.

Funding: The German Federal Ministry for Economic Affairs and Energy according to a decision of the German Federal Parliament within the Central Innovation Program for SMEs (ZF4279901CR6) and the German Research Foundation (DFG-321566826) funded this research.

Acknowledgments: We acknowledge the proofreader Cameron Anderson.

Conflicts of Interest: The authors declare no conflict of interest.

References

1. Pierik, R.; de Wit, M. Shade avoidance: Phytochrome signalling and other aboveground neighbour detection cues. *J. Exp. Bot.* **2014**, *65*, 2815–2824. [CrossRef] [PubMed]
2. Franklin, K.A. Shade avoidance. *New Phytol.* **2008**, *179*, 930–944. [CrossRef] [PubMed]
3. Ballare, C.L.; Scopel, A.L.; Sanchez, R.A. Far-Red Radiation Reflected from Adjacent Leaves: An Early Signal of Competition in Plant Canopies. *Science* **1990**, *247*, 329–332. [CrossRef] [PubMed]
4. Green-Tracewicz, E.; Page, E.R.; Swanton, C.J. Shade Avoidance in Soybean Reduces Branching and Increases Plant-to-Plant Variability in Biomass and Yield Per Plant. *Weed Sci.* **2011**, *59*, 43–49. [CrossRef]
5. Fraser, D.P.; Hayes, S.; Franklin, K.A. Photoreceptor crosstalk in shade avoidance. *Curr. Opin. Plant. Biol.* **2016**, *33*, 1–7. [CrossRef]
6. Li, J.; Li, G.; Wang, H.; Wang Deng, X. Phytochrome signaling mechanisms. *Arabidopsis Book* **2011**, *9*, e0148. [CrossRef] [PubMed]
7. Yu, X.; Liu, H.; Klejnot, J.; Lin, C. The Cryptochrome Blue Light Receptors. *Arabidopsis Book* **2010**, *8*, e0135. [CrossRef]
8. De Wit, M.; Keuskamp, D.H.; Bongers, F.J.; Hornitschek, P.; Gommers, C.M.M.; Reinen, E.; Martínez-Cerón, C.; Fankhauser, C.; Pierik, R. Integration of Phytochrome and Cryptochrome Signals Determines Plant Growth during Competition for Light. *Curr. Biol.* **2016**, *26*, 3320–3326. [CrossRef]
9. Keller, M.M.; Jaillais, Y.; Pedmale, U.V.; Moreno, J.E.; Chory, J.; Ballaré, C.L. Cryptochrome 1 and phytochrome B control shade-avoidance responses in Arabidopsis via partially independent hormonal cascades. *Plant. J.* **2011**, *67*, 195–207. [CrossRef]
10. Pedmale, U.V.; Huang, S.C.; Zander, M.; Cole, B.J.; Hetzel, J.; Ljung, K.; Reis, P.A.B.; Sridevi, P.; Nito, K.; Nery, J.R.; et al. Cryptochromes Interact Directly with PIFs to Control Plant Growth in Limiting Blue Light. *Cell* **2016**, *164*, 233–245. [CrossRef]
11. Park, Y.; Runkle, E.S. Far-red radiation and photosynthetic photon flux density independently regulate seedling growth but interactively regulate flowering. *Environ. Exp. Bot.* **2018**, *155*, 206–216. [CrossRef]
12. Weston, E.; Thorogood, K.; Vinti, G.; López-Juez, E. Light quantity controls leaf-cell and chloroplast development in Arabidopsis thaliana wild type and blue-light-perception mutants. *Planta* **2000**, *211*, 807–815. [CrossRef] [PubMed]
13. Liu, W.; Zou, J.; Zhang, J.; Yang, F.; Wan, Y.; Yang, W. Evaluation of Soybean (*Glycine max*) Stem Vining in Maize-Soybean Relay Strip Intercropping System. *Plant Prod. Sci.* **2015**, *18*, 69–75. [CrossRef]

14. Yang, F.; Huang, S.; Gao, R.; Liu, W.; Yong, T.; Wang, X.; Wu, X.; Yang, W. Growth of soybean seedlings in relay strip intercropping systems in relation to light quantity and red:far-red ratio. *Field Crop. Res.* **2014**, *155*, 245–253. [CrossRef]
15. Su, B.Y.; Song, Y.X.; Song, C.; Cui, L.; Yong, T.W.; Yang, W.Y. Growth and photosynthetic responses of soybean seedlings to maize shading in relay intercropping system in Southwest China. *Photosynthetica* **2014**, *52*, 332–340. [CrossRef]
16. Gong, W.Z.; Jiang, C.D.; Wu, Y.S.; Chen, H.H.; Liu, W.Y.; Yang, W.Y. Tolerance vs. avoidance: Two strategies of soybean (Glycine max) seedlings in response to shade in intercropping. *Photosynthetica* **2015**, *53*, 259–268. [CrossRef]
17. Yao, X.; Li, C.; Li, S.; Zhu, Q.; Zhang, H.; Wang, H.; Yu, C.; Martin, S.K.S.; Xie, F. Effect of shade on leaf photosynthetic capacity, light-intercepting, electron transfer and energy distribution of soybeans. *Plant. Growth Regul.* **2017**, *83*, 409–416. [CrossRef]
18. Valladares, F.; Niinemets, Ü. Shade Tolerance, a Key Plant Feature of Complex Nature and Consequences. *Annu. Rev. Ecol. Evol. Syst.* **2008**, *39*, 237–257. [CrossRef]
19. Gong, W.; Qi, P.; Du, J.; Sun, X.; Wu, X.; Song, C.; Liu, W.; Wu, Y.; Yu, X.; Yong, T.; et al. Transcriptome Analysis of Shade-Induced Inhibition on Leaf Size in Relay Intercropped Soybean. *PLoS ONE* **2014**, *9*, e98465. [CrossRef]
20. Pauch, R.C.; Britz, S.J.; Mulchi, C.L. Growth and photosynthesis of soybean (Glycine max (L.) Merr.) in simulated vegetation shade: Influence of the ratio of red to far-red radiation *. *Plant Cell Environ.* **1991**, *14*, 647–656. [CrossRef]
21. Hussain, S.; Iqbal, N.; Rahman, T.; Liu, T.; Brestic, M.; Safdar, M.E.; Asghar, M.A.; Farooq, M.U.; Shafiq, I.; Ali, A.; et al. Shade effect on carbohydrates dynamics and stem strength of soybean genotypes. *Environ. Exp. Bot.* **2019**, *162*, 374–382. [CrossRef]
22. Feng, L.; Raza, M.A.; Li, Z.; Chen, Y.; Khalid, M.H.B.; Du, J.; Liu, W.; Wu, X.; Song, C.; Yu, L.; et al. The Influence of Light Intensity and Leaf Movement on Photosynthesis Characteristics and Carbon Balance of Soybean. *Front. Plant Sci.* **2019**, *9*, 1952. [CrossRef] [PubMed]
23. Munz, S.; Feike, T.; Chen, Q.; Claupein, W.; Graeff-Hönninger, S. Understanding interactions between cropping pattern, maize cultivar and the local environment in strip-intercropping systems. *Agric. For. Meteorol.* **2014**, *195–196*, 152–164. [CrossRef]
24. Brooker, R.W.; Bennett, A.E.; Cong, W.-F.; Daniell, T.J.; George, T.S.; Hallett, P.D.; Hawes, C.; Iannetta, P.P.M.; Jones, H.G.; Karley, A.J.; et al. Improving intercropping: A synthesis of research in agronomy, plant physiology and ecology. *New Phytol.* **2015**, *206*, 107–117. [CrossRef]
25. Horvath, D.P.; Hansen, S.A.; Moriles-Miller, J.P.; Pierik, R.; Yan, C.; Clay, D.E.; Scheffler, B.; Clay, S.A. RNAseq reveals weed-induced PIF3-like as a candidate target to manipulate weed stress response in soybean. *New Phytol.* **2015**, *207*, 196–210. [CrossRef]
26. Hiebsch, C.K.; Tetio-Kagho, F.; Chirembo, A.M.; Gardner, F.P. Plant Density and Soybean Maturity in a Soybean-Maize Intercrop. *Agron. J.* **1995**, *87*, 965. [CrossRef]
27. Stroup, W.W. Power analysis based on spatial effects mixed models: A tool for comparing design and analysis strategies in the presence of spatial variability. *J. Agric. Biol. Environ. Stat.* **2002**, *7*, 491–511. [CrossRef]
28. Wolfinger, R. Covariance structure selection in general mixed models. *Commun. Stat.-Simul. Comput.* **1993**, *22*, 1079–1106. [CrossRef]
29. Piepho, H.P. An Algorithm for a Letter-Based Representation of All-Pairwise Comparisons. *J. Comput. Graph. Stat.* **2004**, *13*, 456–466. [CrossRef]
30. Kurepin, L.V.; Emery, R.J.N.; Pharis, R.P.; Reid, D.M. Uncoupling light quality from light irradiance effects in Helianthus annuus shoots: Putative roles for plant hormones in leaf and internode growth. *J. Exp. Bot.* **2007**, *58*, 2145–2157. [CrossRef]
31. Lanoue, J.; Leonardos, E.D.; Grodzinski, B. Effects of Light Quality and Intensity on Diurnal Patterns and Rates of Photo-Assimilate Translocation and Transpiration in Tomato Leaves. *Front. Plant. Sci.* **2018**, *9*, 756. [CrossRef]
32. Kim, G.-T.; Yano, S.; Kozuka, T.; Tsukaya, H. Photomorphogenesis of leaves: Shade-avoidance and differentiation of sun and shade leaves. *Photochem. Photobiol. Sci.* **2005**, *4*, 770. [CrossRef]

7. General discussion

The primary objectives of this thesis were to explore the effect of spectral light composition on soybean morphology and to develop an FSP model of soybean with an integrated response to spectrum within a virtual LED chamber. In **Chapter I**, the chamber model was developed and light simulations were evaluated in multiple locations relevant for FSP modelling and optimization of chamber design. In **Chapter II,** the static FSP model of soybean was integrated with the reconstruction of an experimental setup. This chapter applied the chamber model combined with the static FSP model for evaluation and optimization of experimental setups. In **Chapter III,** the dynamic FSP model of soybean was integrated and a response curve of internode elongation to BPFD was derived from simulation with the calibrated model. After the response curve was integrated in the model, it was applied for spectral light optimization in an alternative chamber design. Additionally, this chapter covered the morphological influence of BPFD levels under stable PPFD. **Chapter IV** covered the influence of R:FR and PPFD to disentangle their influence on SAR.

The results of the individual publications were already discussed within each chapter and will not be discussed here individually. Instead, the general discussion will discuss the response of soybean to the spectrum from UV to FR, by combining the results from Chapter III and IV and additional results from preliminary UV experiments. The second part of the discussion will discuss the perspectives of FSP modelling for optimization of crop production in indoor farming. Finally, the optimization of spectra in indoor farming will be discussed in the context of applying knowledge of spectral effects on plant morphology, biomass and quality and the advantages of FSP modelling.

7.1 Soybean response to light spectrum

Low BPFD, R:FR and PPFD are signals of shade arising due to the absorption and reflection of light in the surrounding vegetation. In a natural environment, it is difficult to distinguish the effect of these factors individually. Decreased R:FR appears alone associated with the threat of shade, whereas low PPFD, low R:FR and low BPFD appears simultaneous under true shade. This thesis utilized the advantages of a flexible spectrum in LED chambers to explore the influence of fluctuations in one shade factor independent from the others. Chapter III explored the influence of BPFD under a constant PPFD and Chapter IV aimed towards the disentanglement of low R:FR and PPFD. Table 7.1 summarizes the influence of the three shade factors low BPFD, low R:FR and low PPFD on morphology and biomass.

Low R:FR and low BPFD are the two factors strictly related to spectral distribution. The influence of these two factors was the same for the majority of plant measurements. This is supported by previous studies stating that phytochrome and cryptochrome interact to fine tune the response to e.g. the tread of shade or true shade (de Wit et al., 2016; Fraser et al., 2016; Keller et al., 2011; Pedmale et al., 2016). Only one of the two spectral shade factors had an influence on internode diameter, leaf biomass and LAR. This indicated that cryptochrome is the main regulator of leaf biomass through BPFD perception, while phytochrome is the main regulator of internode diameter through R:FR perception. The results of previous studies are conflicting and showed both increased and decreased leaf biomass of soybean under low R:FR (Green-Tracewicz et al., 2011; Pauch et al., 1991). Regarding low BPFD, an earlier study found only a small increase of leaf biomass of soybean, but this could be due to the lower ratio of B under the maximum BPFD (Dougher and Bugbee, 2001). The response of leaf biomass to R:FR

and BPFD should be clarified in further studies, which could also explore the tendency of an antagonistic influence from by BPFD and R:FR on SLA (Table 7.1).
Only internode length, internode length:diameter and LMR clearly responded in a common way to all three factors of shade, whereas the other plant measurements were inconsistent in the response. Petiole length showed only a minor discrepancy with no response to low PPFD under low R:FR, otherwise petiole length also increased under all three shade factors. The influence of PPFD on biomass, LAR, SLA and internode diameter worked antagonistically to the influence of BPFD and/or low R:FR (Table 7.1).

Table 7.1. The increasing (+), decreasing (-) or no (0) influence of the three shade factors blue photon flux density (BPFD), red:far-red ratio (R:FR), and photosynthetic photon flux density (PPFD) on plant morphology and biomass.

Measurement	Low BPFD	Low R:FR	Low PPFD
Internode length	+	+	+
Petiole length	+	+	0 / +
Leaf length	0	0 / +	0
Internode diameter	0	0 / +	-
Internode length:diameter	+	+	+
Total biomass	+	+	-
Leaf biomass	+	0	-
Stem biomass	+	+	-
SLA	0 / -	0 / +	+
LAR	0	0 / -	+
LMR	-	-	-

Low BPFD is perceived by cryptochrome, which does also perceive UVA. At the beginning of the project, it was hypothesized that UV-A could amplify the reduction in height that was achieved under high BPFD. This hypothesis was tested in preliminary experiments, but was not further pursued in context of the speed breeding system. Still, the preliminary results are interesting in the context of increasing the understanding of soybean response to spectra, especially as earlier literature on the influence of UVA compared to the influence of B is limited (Verdaguer et al., 2017).

The UVA experiments were performed in the chambers from COMPLED Solutions GmbH as described in Chapter I-III. In both experiments the cv. Amphor, ESSenator, Josefine and Merlin grew under a twelve-hour photoperiod. The project partner from the State Plant Breeding Institute performed an experiment with two treatments. Both treatments consisted of a broad spectrum including B, G and R with a PPFD of 557 µmol m^{-2} s^{-1} and one treatment additionally consisted of 25 µmol m^{-2} s^{-1} of UVA. The presented results are from one replicate, as the experiment was not repeated. The other UVA experiment consisted of four treatments and was performed with two replicates. In this experiment, UVA was not added to the spectrum, but instead included in the BPFD level of the treatments. This approach resulted in varying PPFD of the treatments from 170-200 µmol m^{-2} s^{-1}, but it was chosen to explore if UVA reduced height more effective than B. Additionally, the experiment tested the response under two R-ratios (0.6 and 0.4).
The results of the first experiment showed that the plants were shorter under the additional UVA (BGRUV), but did not proof an additional effect of UVA compared to an increased BPFD (fig.

7.1). The results of the experiment with UVA included in BPFD showed no reduction of height under UVA (R120BUV80 and R80BUV120) (fig. 7.2). On the contrary, a slight tendency of increased height under UVA was present, but this could be due to other factors e.g. the lower PPFD of the UVA treatments.

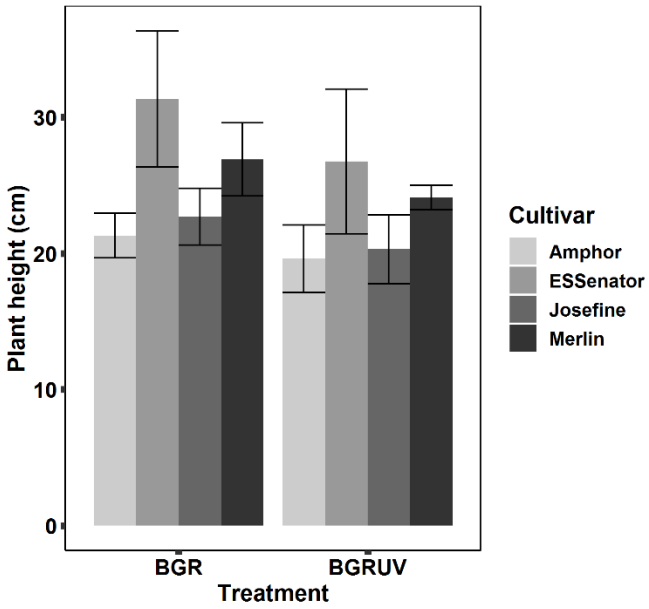

Fig. 7.1. Plant height under a broad spectrum (PPFD: 557 µmol m^{-2} s^{-1}) with (BGRUV) and without (BGR) additional UVA.

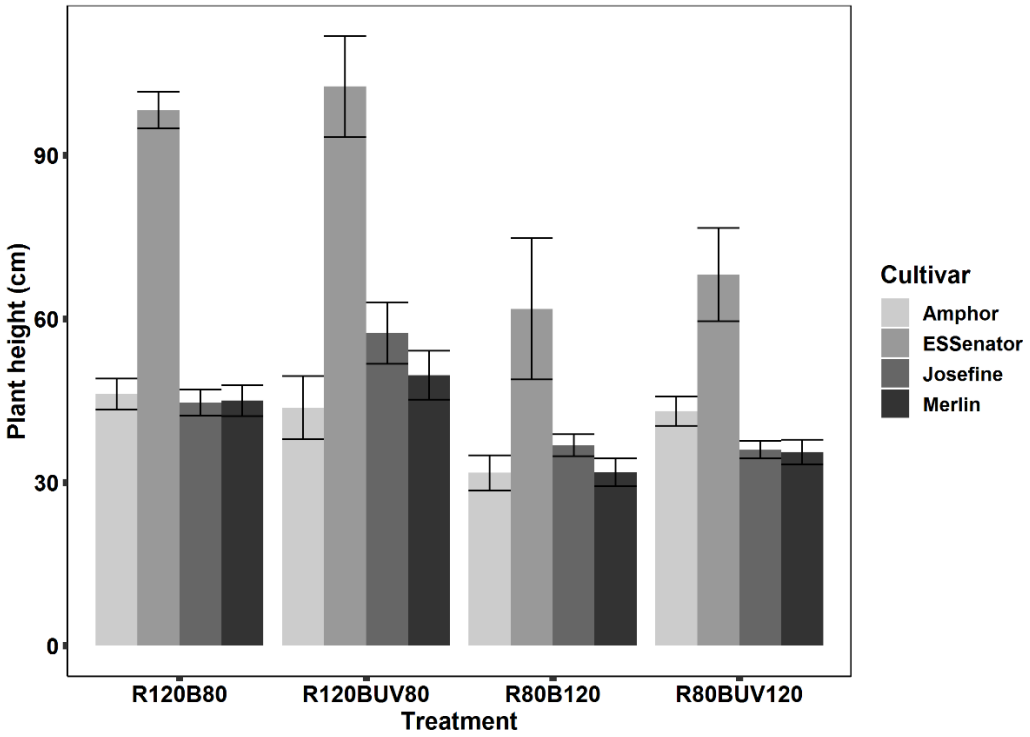

Fig. 7.2. Plant height under a narrowed peak spectrum (PPFD+UVA: 200 µmol m^{-2} s^{-1}) with (R120BUV80; R80BUV120) and without (R120B80; R80B120) UVA included in BPFD under different R to B ratios.

It was concluded from the experiments, that UVA was not advantageous compared to B to achieve a short soybean plant. This was mainly based on the results of no additional reduction of height in the second experiment, including UVA in BPFD. Further studies are needed to

determine, if UVA is less effective than B as indicated in the second experiment (Fig. 7.2). Studies on UVA are relatively few and especially studies of the distinct effect of UVA compared to B, are lacking (Verdaguer2017).
Plant height can also be reduced with UVB (Neugart and Schreiner, 2018) perceived by the photoreceptor UVR-8 instead of cryptochrome. The different perception would, at least to some extent, result in UV-B working through different mechanisms than B. Whether the magnitude of the response to UVB differs from the response to increased B is unknown (Robson et al., 2019).

Future studies should explore the influences and mechanisms of the single factors of shade, including treatments representing all three factors low BPFD, R:FR and PPFD within the same study. These studies could help in understanding the fundamental responses of plants to fluctuations in the perceived light environment associated with SAR. Especially in the context of indoor farming, studies of specific wavelengths are interesting. For instance, the importance of a spectrum corresponding to the absorption spectra of photoreceptors or photosynthetic pigments and synergetic effects between wavelengths. Also, the distinct influence of UVA and B and the influence of UVB are interesting aspects of further studies of spectral influences on plants. These studies should include physiological measurements of e.g. photosynthesis and hormone and sugar production for a deeper understanding of interactions and underlying mechanisms.

7.2 Perspectives of FSP modelling in indoor farming

The many complex interactions of light on plant morphology and physiology need substantial studies for a better understanding. LED chambers represent a possibility to study the influence of very specific wavelengths by designing narrow-peaked spectra. An obstacle in LED chamber studies is, that light within a climate chamber can be very heterogeneous (Delepoulle et al., 2009), but also that the experimental setup in published literature varies substantially regarding e.g. light sources, chamber dimensions and plant density. This heterogeneity constrains the comparison of studies and the transfer of knowledge to crop production in e.g. indoor farming. The simulation of the perceived light with FSP modelling could be a valuable method to overcome these constraints. Chapter IV is an example of how FSP modelling could be applied to both increase the knowledge gained from the experiment and facilitate the transfer of knowledge. The study was performed in a chamber constructed for scientific purposes and determined relative differences and effects of the factors PPFD and R:FR. It is difficult from this study alone to determine absolute values necessary to trigger a response in a production facility or in the field. By combining the experiment with an FSP model it would be possible to estimate absolute values for individual organs of the plant and these results could easily be transferred to FSP models of soybean in a production environment.
Another valuable outcome of FSP models in the context of exploring plant responses is an increased insight in underlying plant mechanisms (e.g. Bongers et al., 2018; Yoshinaka et al., 2018). Gautier et al. (2000) described the impact of self-shading on the response to R:FR on different phytomer levels of clover. The increased self-shading at later phytomers was used to explain the longer internodes of these. Whereas decreased R:FR is a proportional change in spectra, BPFD is an absolute change. Based on simulations with the FSP model of soybean, this thesis found that the perceived BPFD in a similar way was influenced from increased self-shading at the third internode compared to the second.

Furthermore, FSP modelling is applied for the optimization of crop production systems. The developed FSP model within an LED chamber was already applied in the context of optimizing

spectral composition in a speed breeding system. Several earlier FSP models were developed for optimization of greenhouse production, which use artificial lighting as an addition to natural sunlight. Buck-Sorlin et al. (2011) constructed a greenhouse environment for cut rose. The model aimed towards integrating the influence of changed canopy structure through pruning, cutting or bending to assist in determining the optimal plant arrangement. Chen et al. (2014) applied a cucumber model to study the light interception and photosynthesis in different layers of the canopy. Visser et al. (2014) explored different locations of LED lights combined with different leaf angles of tomato and Sarlikioti et al. (2011) found that a changed morphology of tomato plants could improve light interception and suggested an ideotype with a more open canopy for better light penetration. Dieleman et al. (2019) parameterized a static FSP model of tomato with data from greenhouse experiments under additional B, G, amber, R, white or R/B LEDs. The model was applied to optimize carbon assimilation by simulating combinations of morphologies induced from one spectrum with light simulations of another spectrum. The maximum assimilation was simulated in a plant under R that was initially grown under G (Dieleman et al., 2019).

No earlier FSP models aimed at optimizing an indoor farming production only using artificial light sources within a controlled chamber environment. The FSP model of soybean was developed with this purpose by integrating the spectral influence on morphology. From the insight into BPFD perception of different phytomers gained in Chapter III, it was suggested to change the spectrum during growth if the bottom reflected a high proportion of light. Another possible adaptation of the light regime to the insight of BPFD perception on phytomer level could be inter-lighting. For instance, blue LEDs could be placed between the rows pointing towards the plants, while BPFD of the LEDs above the plants could be reduced. Assuming that this would increase internode perception of BPFD and have the potential to further decrease the total BPFD of the LED lighting. It is important to consider possible morphological adaptations of the plant to a change in light regime. For instance, is phototropism controlled by phototropins, which also perceive B (Christie, 2007). This response could change leaf orientation and result in a similar shade of the internode using inter-lighting as with light from above only. The FSP model can consider these feed-back mechanisms between light regime and plant morphology as e.g. leaf angle. Simulations of various LED placements and leaf angles can test the theory of inter-lighting and test which adaptations of plant morphology makes the approach disadvantageous – or advantageous. Subsequently, selected experiments could be performed to reveal whether the morphological adaptations are acceptable making inter-lighting advantageous.

The FSP model of soybean can be expanded for other purposes of indoor farming than speed breeding e.g. production of secondary plant compounds or biomass. Applying the model for optimization of the content of secondary plant compounds, the integration of production and translocation of secondary compounds would be important. Buck-Sorlin et al. (2008) integrated gibberellic acid in an FSP model of barley and Merklein et al. (2018) integrated xylem and phloem flux in an apple branch.

Simulating photosynthetic rate and biomass accumulation and translocation would be important for expanding the presented model for biomass optimization. Based on the total PPFD this is already a common integration in FSP models e.g. based on the photosynthetic models of Farquhar et al. (1980) and Ball et al. (1987). These models consider e.g. temperature and humidity, but not the influence of different wavelengths, which is an important factor in an LED chamber environment with an unnatural spectrum. In the FSP model of Dieleman et al. (2019) photosynthesis was adjusted according to the McCree curve. This curve aimed towards determining the action spectrum, absorbance and spectral quantum yield of CO_2 uptake in crop plants (McCree, 1972). The McCree curve is several decades old and it has been suggested that

new studies are required under higher light intensity and with a consistent wavelength increment (Wu et al., 2019). This is e.g. supported by the observation of the same photosynthesis rate under G, as under other light treatments (Lanoue et al., 2018) and the same photosynthetic rate at all BPFD levels in Chapter III, which is not expected according to the McCree curve. Terashima et al. (2009), found that under high light intensity G drove photosynthesis more effective than R, which was probably due to a deeper penetration in the leaf. Another important aspect for correct simulation of photosynthesis from a variety of spectra is the integration of enhancing effects of some wavelengths on other wavelengths. For instance, the Emerson effect of increased photosynthesis under FR under simultaneous R (Emerson et al., 1957) and the immediately increased photosynthesis from shorter wavelengths by addition of FR (Zhen and van Iersel, 2017).

Chapter IV showed an example of how cultivars can interact with the spectra, which could be relevant for indoor farming. Breeding could e.g. aim towards optimizing plant stability or light interception under a spectrum optimized for the production of secondary compounds. In this context integration of genetic information into the FSP model can turn it into a potential tool for both breeding and investigation of new cultivars (Qi et al., 2010; Struik, 2016; Xu et al., 2011). A recent study demonstrated the combination of genome-wide information with an FSP model of apple (Migault et al., 2017) and Xu et al. (2011) integrated QTL information in an FSP model of rice.
The developed FSP model of soybean is a step towards exploring this variety of open questions regarding optimization of indoor farming with FSP modelling. The model can be extended as knowledge of the spectral effect on plants increases and simultaneously assists in achieving this knowledge. General progress in FSP modelling, e.g. integration of genetic information, can be combined with the present model, which hereby represents an important foundation for future FSP models adapted to a specific aim of scientific work or crop production.

7.3 Spectral optimization in indoor farming

Chapter III explored high BPFD levels for the specific use in speed breeding and found a BPFD of 260 µmol m^{-2} s^{-1} optimal to achieve short soybean plants within the used chamber. This was a relative high BPFD compared to what is necessary to achieve normal plant growth (e.g. 7 % in cucumber (Hogewoning et al., 2010)). Earlier studies of BPFD in soybean focused on a lower BPFD (Cope and Bugbee, 2013; Dougher and Bugbee, 2001; Wheeler et al., 1991) and two earlier studies found a saturation at a considerable lower level of BPFD than this thesis (30-50 µmol m^{-2} s^{-1}) (Cope and Bugbee, 2013; Wheeler et al., 1991). This deviation is an example of the difficulties in transferring knowledge from a study to a specific application due to e.g. variation in other parts of the spectrum and experimental setup as discussed in 6.2.
Spectral optimization in Chapter III aimed towards a reduced energy consumption, which was achieved with a high reflective bottom and changing BPFD during growth. A possibility to further decrease the energy consumption would be to decrease PPFD, but maintain the positive effects of high BPFD. In this context, Park and Runkle (2018) performed an interesting experiment in the three species geranium, petunia, and coleus. They hypothesized that under a stable BPFD, the PPFD levels would not influence the R:FR response. This was found true for plant height of two species and PPFD only had a minor influence on plant height of the third species. Assuming this is also true for soybean, PPFD could be reduced to below the 400 µmol m^{-2} s^{-1} used in Chapter III, without inducing an increased plant height. For instance, the BPFD of 260 µmol m^{-2} s^{-1} could be combined with 40 µmol m^{-2} s^{-1} of R to reduce the total PPFD to 300 µmol m^{-2} s^{-1}. Further studies should derive a response curve to PPFD independent from BPFD and clarify the interactions and distinct effects of PPFD and BPFD to test this alternative

spectrum. By integrating the results of additional experiments in the FSP model of soybean, optimization regarding both factors could be performed. Furthermore, the extended model could assist in evaluating the risk of a thinner stem under low PPFD to avoid a low stability of the plant.
The UVA was not found more effective than B to achieve short plants and is therefore not recommended for a speed breeding system. For a complete exclusion of UV light further studies also considering UVB should be performed. Even if advantages of UV light are identified, at least three other factors should be considered. First, UV light is not photosynthetic active as B, secondly, the price of UV-LEDs compared to B-LEDs and third, UV light and especially UVB is harmful for human skin (Ichihashi et al., 2003). This means, that unless a production facility is completely atomized with robots, UV light should be turned off during working hours.

In the context of indoor farming in general, an important factor for optimization is increased biomass. For an efficient use of the light source a high biomass per µmol m^{-2} s^{-1} emitted light is a requirement for the spectrum (Pennisi et al., 2019). In this context, the lower biomass under high BPFD found in Chapter III is a negative influence and a BPFD lower than the 260 µmol m^{-2} s^{-1} would be preferable. From Chapter III the optimal BPFD levels for biomass production cannot be determined as it might continue to increase with a BPFD below the 60 µmol m^{-2} s^{-1} applied in the lowest BPFD treatment. Soybean is normally not used for biomass production, but studies in other species also found decreased biomass under high B e.g. in basil (Pennisi et al., 2019) and ice plant (He et al., 2017). Although biomass decreases under high BPFD, an intermediate BPFD is preferable compared to very low BPFD. For instance, the maximum biomass was found around 9 % B in several crops relevant for indoor production (Naznin et al., 2019).

The R:FR also influenced plant height, but as FR increased height and was found unimportant for flowering, it was not recommended for a speed breeding system. In the context of biomass production, the increase in biomass under increased R:FR in Chapter IV makes the inclusion of FR interesting. In lettuce, increased biomass was also found under a spectrum including FR (Lee et al., 2016; Meng et al., 2019) and in tomato FR increased fruit yield (Kalaitzoglou et al., 2019). Only biomass of the stem and not of the leaves was influenced in soybean, which implies that organ specific measurements of biomass are important for an optimization. In e.g. basil the advantage of FR might be small, if only stem weight is increased without influencing the leaf biomass. Optimized biomass of specific organs, could also be explored with FSP modelling by incorporating translocation of assimilates. Simultaneous, modelling could assist in optimizing the stability of the crop by considering the risk of increased length:diameter ratio of the internode under low R:FR.

The developed chamber model was applied to evaluate heterogeneity of light in scenarios with alternative placements of the LED modules (Chapter I) increasing plant density (Chapter II) and alternative optical properties of the bottom material (Chapter III) in the context of experimental setup or speed breeding (Fig. 7.3).

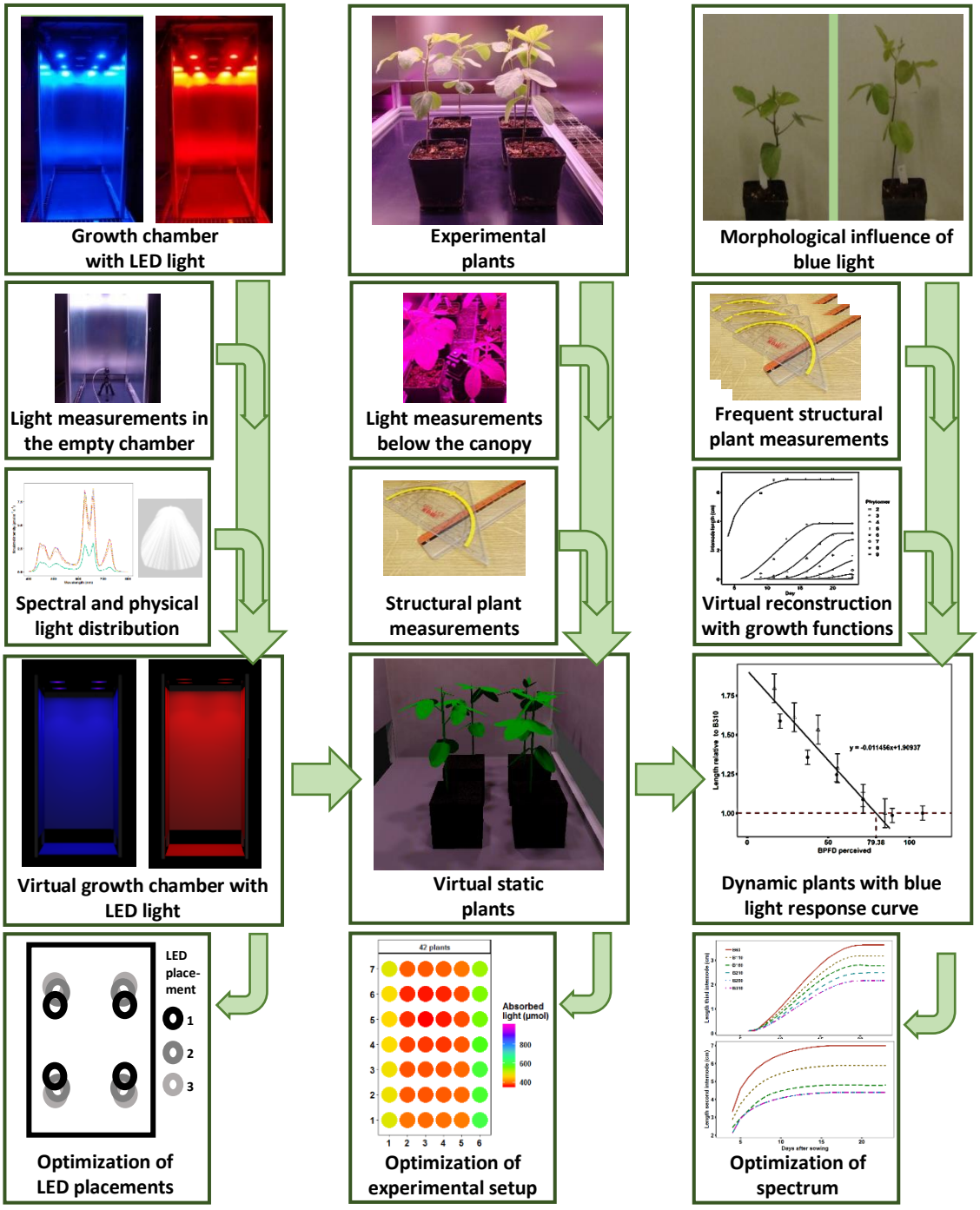

Fig. 7.3. Work flow to develop the FSP model of soybean in a virtual LED chamber and the application of the model at different stages.

The same approaches as in Fig. 7.3 can be transferred for light optimization in indoor farming in general. If the light from individual LED types is not mixed to a homogenous spectrum across the crop, but i.e. have a B gradient, it can be presumed that the biomass of the crop will exhibit the same gradient. Similar, the increased heterogeneity of light with increased plant density found in Chapter II, would also apply for a production facility. In both examples, the light gradients across the crop can result in a more heterogeneous crop. Spectral light simulations with the chamber model can be applied to evaluate the effects of e.g. LED placements and crop density in scenarios representing crop production facilities to optimize them with a similar approach as used for spectral optimization in a speed breeding system (Fig. 7.3).

The complexity of the plant's response to the light spectrum still requires considerable experimentation to be finally able to optimize the spectral light composition for different indoor farming purposes. Additional, the light environment interacts with other environmental factors also influencing the crop production e.g. temperature and supply of nutrients and water.
The FSP model of soybean with its possible expansions discussed in 6.2 is an essential tool to use FSP modelling at all stages of spectral optimization in indoor farming, from the understanding of plant responses to light environment to optimization of a specific production. Traditional agriculture producing field crops can also profit from an FSP model in an LED chamber. As described in the introduction crop management can result in a fluctuating light environment perceived by the crop. Experiments in LED chambers can increase the understanding of how these fluctuation influence the crop similar to the experiments performed in Chapter IV. The FSP modelling of the perceived light can facilitate the transfer of knowledge into practice using FSP models in a field environment e.g. to optimize the management of weeds and intercropping.

Summary

The development of soybean cultivars for the climatic conditions in Europe is an urgent need in order to increase the European production and to decrease the dependence of imported soybean. A speed breeding system can accelerate the process of developing new cultivars by growing more generations per season in climate chambers. The project MoLED-Plant aimed towards the development of a speed breeding system for soybean under LED lighting. One advantage of LED light is the possibility to design a specific spectrum, but it also require many experiments to optimize it for crop production. Simulations of multiple scenarios with functional-structural plant (FSP) modelling is an essential tool to test possible spectral combinations. It was important for the speed breeding system to define a spectrum that did not delay flowering in order to permit the collection of at least one soybean seed in a short time. Moreover, the spectrum should promote short plants to create room for more layers of soybean plants. The shade avoidance response (SAR) is a major regulator of plant height and is i.a. triggered by spectral changes. Spectral changes under shade are a decreased red to far-red ratio (R:FR) and a decreased photosynthetic photon flux density (PPFD), which is associated with decreased blue photon flux density (BPFD).
The major objectives of this thesis were to: (i) construct a three dimensional model of an LED chamber to simulate micro-light climate, (ii) develop a FSP model of soybean and derive a BPFD response curve from simulations, (iii) apply the FSP model with the integrated response curve for spectral optimization, (iv) explore the influence of BPFD under constant PPFD, and (v) disentangle the influence of R:FR and PPFD on SAR. The objectives were fulfilled with a combination of FSP modelling in the Growth Grammar-related Interactive Modelling Platform (GroIMP) and plant experiments under multiple spectra in LED chambers.

The presented LED chamber model was the first three dimensional environment, which was developed for spectral optimizations in indoor farming using FSP modeling. The final chamber model represented the experimental LED chambers, but for simulation of alternative chamber designs a possibility for an easy adjustment of the model was incorporated. Measurements performed with a spectrometer in multiple heights and orientations were compared to simulations recorded with a virtual sensor at the same locations. The accuracy of the simulations compared to measurements were high with R^2 between 0.901 and 0.965 with data from different heights and R^2 between 0.959 and 0.997 with data from different orientations of the sensor. The mean absolute percentage errors between measured and simulated light intensity in different orientations were 12.7%, 2.8%, 8.9% and 30.6% for blue, green, red and far-red light, respectively. The model was evaluated as a tool for assessment of spectral light heterogeneity under an alternative placement of the LED modules. Applying the model can assist in choosing the best chamber design and placements of LEDs to assure homogeneous light conditions.
Subsequently, static soybean plants were incorporated into the chamber model. Detailed structural plant measurements were performed during an experiment in order to make an exact virtual reconstruction of the plants. Comparison of light simulations and measurements from below the soybean canopy in four reconstructed scenarios assured a good simulation of micro-light climate. The accuracy of the simulations was an R^2 between 0.798 and 0.956 and a mean absolute percentage error between 5.85 and 35.14 %. The model was applied to simulate the effect of an increased plant density in an experiment in the chamber. The simulations of light homogeneity in the experimental setup can assist in choosing the optimal design.
The developed dynamic FSP model of soybean within the chamber model represents the first FSP model with an integrated response to BPFD. The soybean model was calibrated with data

from BPFD experiments. From simulations, a common response curve of internode elongation to the perceived BPFD was derived for the second and third internode. The response curve was integrated in the model and was applied for spectral optimization in a chamber scenario with an alternative high reflective bottom material. The aim was to achieve a short soybean plant under minimum BPFD to reduce energy consumption, which according to simulations could be achieved with a reduced BPFD until the initiation of the third internode.

The soybean response to BPFD under constant PPFD and the influence of R:FR and PPFD on SAR was explored by designing specific spectra from LEDs. Soybean experiments were performed under six levels of BPFD (60-310 µmol m^{-2} s^{-1}) and constant PPFD (400 µmol m^{-2} s^{-1}). Plant height and biomass decreased, leaf mass ratio increased and the ratio of stem biomass (internode plus petiole) translocated to the internode decreased under high BPFD.
Three soybean cultivars were grown under nine light treatments to disentangle the effect of R:FR and PPFD. Internode elongation responded mainly to low PPFD with an additive effect from low R:FR, whereas petiole elongation was influenced to a great extent by low R:FR. In the context of SAR, petiole elongation can be seen as the main response to the threat of shade (high PPFD and low R:FR) and both petiole and internode elongation as the response to true shade (low PPFD and low R:FR). Additionally, interactions were found between light environment and cultivar, indicating the possibility to develop cultivars for different cropping systems.

This thesis showed how PPFD, BPFD and R:FR work both independently, antagonistically and synergistically on the physiology and morphology of soybean. The increased insight in these responses can e.g. support crop breeding and spectral optimization in indoor farming. Furthermore, interesting and important objectives for future research were identified. For instance, studies to disentangle shade factors should include all shade factors (PPFD, BPFD and R:FR) and test them independently from each other. For a further reduction of energy consumption in speed breeding a response curve to PPFD independent from BPFD should be derived. Also, knowledge of the interactions between PPFD and BPFD is necessary. These experiments should include physiological measurements for a deeper understanding of interactions and underlying mechanisms.
Spectral optimization of indoor farming depends on the purpose of the production. For instance, a high BPFD of 260 µmol m^{-2} s^{-1} was optimal for speed breeding, whereas an intermediate BPFD would be preferable to increase biomass. Comprehensive investigation of spectral influence on plant physiology and morphology is necessary to fully utilize the spectral flexibility of LED lighting. The developed FSP model of soybean in a virtual LED chamber represents an important step towards utilizing the advantages of FSP modelling by simulation of a wide variety of scenarios.
The model can be adjusted or extended depending on the purpose of the model. It can be calibrated for other crop species and the setting of the chamber dimensions can be changed. With a similar procedure as for BPFD the model can be extended with a response to other wavelength ranges and PPFD. Furthermore, physiological mechanisms e.g. photosynthesis and the production and translocation of assimilates or secondary compounds can be incorporated. The developed model with its possibility for extension is an essential tool to apply FSP modelling for understanding of plant responses to light and spectral optimization. By simulating the perceived light during experiments, the model can assist in the transfer of spectral knowledge to practice in agriculture and indoor farming.

Zusammenfassung

Die Züchtung von Sojabohnensorten für europäische Klimabedingungen ist eine dringende Notwendigkeit, um die europäische Produktion zu steigern und die Abhängigkeit von importierter Sojabohne zu reduzieren. Speed-züchtung kann den Prozess der Entwicklung neuer Sorten beschleunigen, indem mehr Generationen pro Saison in Klimakammern wachsen. Das Projekt MoLED-Plant zielte auf die Entwicklung eines Speed-Züchtungssystems für Sojabohne unter LED-Beleuchtung ab. Ein Vorteil von LED-Licht ist die Möglichkeit, ein spezifisches Spektrum zu gestalten, aber die vielen möglichen Spektren erfordern auch einen hohen Aufwand an Versuchen, um es für den Pflanzenanbau zu optimieren. Die Simulation mehrerer Szenarien mit funktional-strukturellen Pflanzen (FSP) Modellen ist ein essentielles Instrument, um alle Spektralkombinationen zu testen. Wichtig für das Speed-Züchtungssystem war es, ein Spektrum zu definieren, dass die Blüte nicht verzögert, um die Ernte von mindestens einem Sojabohnensamen in kurzer Zeit zu ermöglichen. Außerdem sollte das Spektrum niedrige Pflanzen fördern, um Platz für mehr übereinanderstehende Pflanzen zu schaffen. Die Schattenvermeidungsreaktion (SAR) ist ein wichtiger Regulator der Pflanzenhöhe und wird u.a. durch spektrale Veränderungen induziert. Die SAR wird unter anderem durch spektrale Veränderungen im Zusammenhang mit Schatten ausgelöst. Spektrale Veränderungen durch Beschattung sind ein geringeres Rot-Fernrot-Verhältnis (R:FR) und eine geringere photosynthetische Photonen-Flussdichte (PPFD), die mit einer verminderten blauen Photonen-Flussdichte (BPFD) verbunden ist.
Die Hauptziele dieser Arbeit waren: (i) ein dreidimensionales Modell einer LED-Kammer zur Simulation des Mikrolichtklimas zu konstruieren, (ii) ein FSP-Modell von Sojabohne zu entwickeln und eine BPFD-Reaktionskurve aus Simulationen abzuleiten, (iii) das FSP-Modell mit der integrierten Reaktionskurve zur spektralen Optimierung anzuwenden, (iv) den Einfluss von BPFD unter konstanter PPFD zu untersuchen und (v) den Einfluss von R:FR und PPFD auf SAR zu trennen. Die Ziele wurden mit einer Kombination aus FSP-Modellierung in der Growth Grammar-related Interactive Modelling Platform (GroIMP) und Pflanzenversuchen unter mehreren Spektren in LED-Kammern erreicht.

Das vorgestellte LED-Kammermodell war die erste dreidimensionale Umgebung, die für spektrale Optimierungen des Indoor-Farmings mittels FSP-Modellierung entwickelt wurde. Das konstruierte Kammermodell **s**tellte die experimentellen LED-Kammern dar, aber zur Simulation alternativer Kammerdesigns wurde eine Möglichkeit zur einfachen Anpassung des Modells integriert. Messungen wurden mit einem Spektrometer in mehreren Höhen und Orientierungen durchgeführt und mit Simulationen verglichen, die mit einem virtuellen Sensor an den gleichen Stellen aufgezeichnet wurden. Die Genauigkeit der Simulationen im Vergleich zu den Messungen war hoch mit R^2 zwischen 0,901 und 0,965 mit Daten aus verschiedenen Höhen und R^2 zwischen 0,959 und 0,997 mit Daten aus verschiedenen Orientierungen des Sensors. Der mittlere absolute prozentuale Fehler zwischen gemessener und simulierter Lichtintensität in verschiedenen Orientierungen betrugen 12,7%, 2,8%, 8,9% und 30,6% für blaues, grünes, rotes und fernrotes Licht. Das Modell wurde als Instrument zur Beurteilung der spektralen Lichtheterogenität mit einer alternativen Platzierung der LED-Module bewertet. Die Anwendung des Modells kann bei der Auswahl des besten Kammerdesigns und der besten LED-Platzierung helfen, um homogene Lichtverhältnisse zu gewährleisten.
Anschließend wurden statische Pflanzen in das Kammermodell integriert. Detaillierte strukturelle Pflanzenmessungen wurden während eines Experiments zur exakten virtuellen Rekonstruktion der Pflanzen durchgeführt. Der Vergleich von Lichtsimulationen und

Messungen unterhalb der Sojablätter in vier rekonstruierten Szenarien stellte eine gute Simulation des Mikrolichtklimas sicher. Die Genauigkeit der Simulationen lag bei einem R^2 zwischen 0,798 und 0,956 und einem mittleren absoluten prozentualen Fehler zwischen 5,85 und 35,14 %. Das Modell wurde angewendet, um den Effekt einer erhöhten Pflanzendichte auf die Lichthomogenität in der Kammer zu simulieren. Die Simulationen können bei der Auswahl des optimalen Versuchsaufbaus helfen.
Das entwickelte dynamische FSP-Modell mit der Sojabohne innerhalb der Kammer stellt das erste FSP-Modell mit einer integrierten Reaktion auf die BPFD dar. Das Sojabohnenmodell wurde mit Daten aus BPFD-Versuchen kalibriert. Aus Simulationen wurden für das zweite und dritte Internodium eine gemeinsame Reaktionskurve der Internodienstreckung auf die wahrgenommene BPFD abgeleitet. Die Reaktionskurve wurde in das Modell integriert und zur spektralen Optimierung in einem Kammerszenario mit einem alternativen hochreflektierenden Bodenmaterial eingesetzt. Ziel war es, eine niedrige Sojapflanze unter minimaler BPFD zu erreichen, um den Energieverbrauch zu reduzieren, was anhand der Simulationen mit einer reduzierten BPFD bis zur Initiierung des dritten Internodiums erreicht werden konnte.

Die Reaktion der Sojabohne auf BPFD bei konstanter PPFD und der Einfluss von R:FR und PPFD auf SAR wurde durch die Gestaltung spezifischer Spektren von LEDs untersucht. Es wurden Versuche mit Sojabohnen unter sechs Stufen von BPFD (60-310 µmol m^{-2} s^{-1}) und konstanter PPFD (400 µmol m^{-2} s^{-1}) durchgeführt. Pflanzenhöhe und Biomasse wurden verringert, das Blattmassenverhältnis wurde erhöht und der Anteil der Stängelbiomasse (Internodium plus Blattstiel), die in die Internodien verlagert wurde, nahm unter hoher BPFD ab.
Drei Sojabohnensorten wurden unter neun Lichtbehandlungen angebaut, um den Einfluss von R:FR und PPFD zu trennen. Die Internodienstreckung reagierte hauptsächlich auf niedrige PPFD mit einem additiven Effekt von niedrigem R:FR, während die Blattstielstreckung weitestgehend durch niedriges R:FR beeinflusst wurde. Im Zusammenhang mit SAR kann die Internodienstreckung als die wichtigste Reaktion auf die Bedrohung durch Beschattung (hohe PPFD und niedrige R:FR) und die Blattstielstreckung und Internodienstreckung als Reaktion auf tatsächliche Beschattung (niedrige PPFD und niedrige R:FR) angesehen werden. Außerdem wurden Wechselwirkungen zwischen Lichtumgebung und Sorte gefunden, die auf die Möglichkeit hinweisen, Sorten für verschiedene landwirtschaftliche Anbausysteme zu entwickeln.

Diese Arbeit zeigte, wie PPFD, BPFD und R:FR sowohl unabhängig als auch antagonistisch und synergistisch die Physiologie und Morphologie der Sojabohne beeinflussen. Der erhöhte Einblick in diese Reaktionen kann z.B. die Pflanzenzüchtung und die spektrale Optimierung im Indoor-Farming unterstützen. Außerdem wurden interessante und wichtige Ziele für die zukünftige Forschung identifiziert. So sollten beispielsweise Studien zur Trennung von Schattenfaktoren alle Faktoren (PPFD, BPFD und R:FR) berücksichtigen und unabhängig voneinander getestet werden. Für eine weitere Reduzierung des Energieverbrauchs bei der Speed-züchtung sollte eine von der BPFD unabhängige Reaktionskurve auf PPFD abgeleitet werden. Außerdem ist die Kenntnis der Wechselwirkungen zwischen PPFD und BPFD erforderlich. Diese Versuche sollten physiologische Messungen zum tieferen Verständnis von Wechselwirkungen und zugrundeliegenden Mechanismen beinhalten.
Die spektrale Optimierung im Indoor-Farming hängt vom Zweck der Produktion ab. So war beispielsweise eine hohe BPFD von 260 µmol m^{-2} s^{-1} optimal für die Speed-züchtung, während eine intermediäre BPFD zur Erhöhung der Biomasse vorzuziehen wäre. Eine umfassende Untersuchung des spektralen Einflusses auf die Pflanzenphysiologie und -morphologie ist notwendig, um die Vorteile der LED-Beleuchtung durch spektrale Optimierung voll

auszunutzen. Das entwickelte FSP-Modell der Sojabohne in einer virtuellen LED-Kammer stellt einen wichtigen Schritt dar, um die Vorteile der FSP-Modellierung durch Simulation verschiedener Szenarien zu nutzen.

Das Modell kann je nach Ziel angepasst oder erweitert werden. Es kann für andere Kulturpflanzen kalibriert und die Einstellung der Kammermaße geändert werden. Mit einem ähnlichen Verfahren wie bei BPFD kann das Modell um eine Reaktion auf andere Wellenlängenbereiche und PPFD erweitert werden. Außerdem können physiologische Mechanismen, wie z.B. die Photosynthese und die Produktion und Translokation von Assimilaten oder sekundäre Pflanzenstoffe einbezogen werden. Das entwickelte Modell mit seinen Erweiterungsmöglichkeiten ist ein wesentliches Instrument zur Anwendung der FSP-Modellierung zum Verständnis der Pflanzenreaktionen auf Licht und spektrale Optimierung. Durch die Simulation des wahrgenommenen Lichts während der Versuche kann das Modell zur Übertragung von spektralem Wissen in die Praxis der Landwirtschaft und des Indoor-Farmings beitragen.

References

Ahlman, L., Bånkestad, D., Wik, T., 2017. Using chlorophyll a fluorescence gains to optimize LED light spectrum for short term photosynthesis. Comput. Electron. Agric. 142, 224–234. https://doi.org/10.1016/J.COMPAG.2017.07.023

Ahmad, M., Grancher, N., Heil, M., Black, R.C., Giovani, B., Galland, P., Lardemer, D., 2002. Action Spectrum for Cryptochrome-Dependent Hypocotyl Growth Inhibition in Arabidopsis. PLANT Physiol. 129, 774–785. https://doi.org/10.1104/pp.010969

Bakhshandeh, E., Kamkar, B., Tsialtas, J.T., 2011. Application of linear models for estimation of leaf area in soybean [Glycine max (L.) Merr]. Photosynthetica 49, 405–416. https://doi.org/10.1007/s11099-011-0048-5

Ball, J.T., Woodrow, I.E., Berry, J.A., 1987. A Model Predicting Stomatal Conductance and its Contribution to the Control of Photosynthesis under Different Environmental Conditions, in: Progress in Photosynthesis Research. Springer Netherlands, Dordrecht, pp. 221–224. https://doi.org/10.1007/978-94-017-0519-6_48

Ballare, C.L., Scopel, A.L., Sanchez, R.A., 1990. Far-Red Radiation Reflected from Adjacent Leaves: An Early Signal of Competition in Plant Canopies. Science (80-.). 247, 329–332. https://doi.org/10.1126/science.247.4940.329

Banerjee, R., Schleicher, E., Meier, S., Viana, R.M., Pokorny, R., Ahmad, M., Bittl, R., Batschauer, A., 2007. The Signaling State of *Arabidopsis* Cryptochrome 2 Contains Flavin Semiquinone. J. Biol. Chem. 282, 14916–14922. https://doi.org/10.1074/jbc.M700616200

Bantis, F., Smirnakou, S., Ouzounis, T., Koukounaras, A., Ntagkas, N., Radoglou, K., 2018. Current status and recent achievements in the field of horticulture with the use of light-emitting diodes (LEDs). Sci. Hortic. (Amsterdam). 235, 437–451. https://doi.org/10.1016/j.scienta.2018.02.058

Berkovich, Y.A., Konovalova, I.O., Smolyanina, S.O., Erokhin, A.N., Avercheva, O.V., Bassarskaya, E.M., Kochetova, G.V., Zhigalova, T.V., Yakovleva, O.S., Tarakanov, I.G., 2017a. LED crop illumination inside space greenhouses. Reach - Rev. Hum. Sp. Explor. 6, 11–24. https://doi.org/10.1016/J.REACH.2017.06.001

Bongers, F.J., Pierik, R., Anten, N.P.R., Evers, J.B., 2018. Subtle variation in shade avoidance responses may have profound consequences for plant competitiveness. Ann. Bot. 121, 863–873. https://doi.org/10.1093/aob/mcx151

Boonen, C., Samson, R., Janssens, K., Pien, H., Lemeur, R., Berckmans, D., 2002. Scaling the spatial distribution of photosynthesis from leaf to canopy in a plant growth chamber. Ecol. Modell. 156, 201–212. https://doi.org/10.1016/S0304-3800(02)00171-0

Borthwick, H.A., Hendricks, S.B., Parker, M.W., Toole, E.H., Toole, V.K., 1952. A Reversible Photoreaction Controlling Seed Germination. Proc. Natl. Acad. Sci. U. S. A. 38, 662–6. https://doi.org/10.1073/pnas.38.8.662

Buck-Sorlin, G., de Visser, P.H., Henke, M., Sarlikioti, V., van der Heijden, G.W., Marcelis, L.F., Vos, J., 2011. Towards a functional–structural plant model of cut-rose: simulation of light environment, light absorption, photosynthesis and interference with the plant structure. Ann. Bot. -LONDON- OUP THEN Acad. Press THEN OXFORD Univ. Press. 108, 1121–1134.

Buck-Sorlin, G., Hemmerling, R., Kniemeyer, O., Burema, B., Kurth, W., 2008. A rule-based model of barley morphogenesis, with special respect to shading and gibberellic acid signal transduction. Ann. Bot. 101, 1109–23. https://doi.org/10.1093/aob/mcm172

Bula, R.J., Morrow, R.C., Tibbitts, T.W., Barta, D.J., Ignatius, R.W., Martin, T.S., 1991. Light-emitting diodes as a radiation source for plants. HortScience 26, 203–5.

Burgess, A.J., Retkute, R., Pound, M.P., Mayes, S., Murchie, E.H., 2017. Image-based 3D canopy reconstruction to determine potential productivity in complex multi-species crop systems. Ann. Bot. 119, 517–532. https://doi.org/10.1093/aob/mcw242

Carabelli, M., Possenti, M., Sessa, G., Ciolfi, A., Sassi, M., Morelli, G., Ruberti, I., 2007. Canopy shade causes a rapid and transient arrest in leaf development through auxin-induced cytokinin oxidase activity. Genes & Dev. 21, 1863–1868. https://doi.org/10.1101/gad.432607

Casal, J.J., 2012. Shade avoidance. Arab. B. 10, e0157. https://doi.org/10.1199/tab.0157

Chelle, M., Evers, J.B., Combes, D., Varlet-Grancher, C., Vos, J., Andrieu, B., 2007a. Simulation of the three-dimensional distribution of the red:far-red ratio within crop canopies. New Phytol. 176, 223–234. https://doi.org/10.1111/j.1469-8137.2007.02161.x

Chelle, M., Renaud, C., Delepoulle, S., Combes, D., 2007b. Modeling light phylloclimate within growth chambers. Napier, NZ.

Chen, T.-W., Henke, M., de Visser, P.H.B., Buck-Sorlin, G., Wiechers, D., Kahlen, K., Stützel, H., 2014. What is the most prominent factor limiting photosynthesis in different layers of a greenhouse cucumber canopy? Ann. Bot. 114, 677–688. https://doi.org/10.1093/aob/mcu100

Christie, J.M., 2007. Phototropin Blue-Light Receptors. Annu. Rev. Plant Biol. 58, 21–45. https://doi.org/10.1146/annurev.arplant.58.032806.103951

Christie, J.M., Blackwood, L., Petersen, J., Sullivan, S., 2015. Plant Flavoprotein Photoreceptors. Plant Cell Physiol. 56, 401–413. https://doi.org/10.1093/pcp/pcu196

Ciolkosz, D.E., Both, A.J., Albright, L.D., 2001. Selection and Placement of Greenhouse Luminaires for Uniformity. Appl. Eng. Agric.

Collini, E., 2019. Carotenoids in Photosynthesis: The Revenge of the “Accessory” Pigments. Chem 5, 494–495. https://doi.org/10.1016/j.chempr.2019.02.013

Cope, K.R., Bugbee, B., 2013. Spectral Effects of Three Types of White Light-emitting Diodes on Plant Growth and Development: Absolute versus Relative Amounts of Blue Light. HortScience 48, 504–509.

Corré, W.J., 1983. Growth and morphogenesis of sun and shade plants II. The influence of light quality. Acta Bot. Neerl. 32, 185–202. https://doi.org/10.1111/j.1438-8677.1983.tb01700.x

de Myttenaere, A., Golden, B., Le Grand, B., Rossi, F., 2016. Mean Absolute Percentage Error for regression models. Neurocomputing, Advances in artificial neural networks, machine learning and computational intelligence 192, 38–48. https://doi.org/10.1016/j.neucom.2015.12.114

de Wit, M., Keuskamp, D.H., Bongers, F.J., Hornitschek, P., Gommers, C.M.M., Reinen, E., Martínez-Cerón, C., Fankhauser, C., Pierik, R., 2016. Integration of Phytochrome and Cryptochrome Signals Determines Plant Growth during Competition for Light. Curr. Biol. 26, 3320–3326. https://doi.org/10.1016/j.cub.2016.10.031

Delepoulle, S., Renaud, C., Chelle, M., 2009. Improving Light Position in a Growth Chamber through the Use of a Genetic Algorithm, in: Artificial Intelligence Techniques for Computer Graphics, Studies in Computational Intelligence. Springer, Berlin, Heidelberg, pp. 67–82.

Dieleman, J.A., De Visser, P.H.B., Meinen, E., Grit, J.G., Dueck, T.A., 2019. Integrating Morphological and Physiological Responses of Tomato Plants to Light Quality to the Crop Level by 3D Modeling. Front. Plant Sci. 10, 839. https://doi.org/10.3389/fpls.2019.00839

Dougher, T.A., Bugbee, B., 2001. Differences in the response of wheat, soybean and lettuce to reduced blue radiation. Photochem. Photobiol. 73, 199–207.

Emerson, R., Chalmers, R., Cederstrand, C., 1957. Some factors influencing the long-wave limit of photosynthesis. Proc. Natl. Acad. Sci. U. S. A. 43, 133–43. https://doi.org/10.1073/pnas.43.1.133

European commission, 2018. Report from the commission to the council and the european parliament on the development of plant proteins in the European Union.

Evers, J.B., 2016. Simulating Crop Growth and Development Using Functional-Structural Plant Modeling. Springer, Dordrecht, pp. 219–236. https://doi.org/10.1007/978-94-017-7291-4_8

Evers, J.B., Bastiaans, L., 2016. Quantifying the effect of crop spatial arrangement on weed

suppression using functional-structural plant modelling. J. Plant Res. 129, 339–351. https://doi.org/10.1007/s10265-016-0807-2

Evers, J.B., Moeller, C., Hanan, J., 2015. Potential role of 3D modelling of canopy architecture to explore G x E x M interactions in wheat - UQ eSpace. Australian Society of Agronomy, Hobart, Australia.

Evers, J.B., Vos, J., Chelle, M., Andrieu, B., Fournier, C., Struik, P.C., 2007a. Simulating the effects of localized red:far-red ratio on tillering in spring wheat (Triticum aestivum) using a three-dimensional virtual plant model. New Phytol. 176, 325–336. https://doi.org/10.1111/j.1469-8137.2007.02168.x

Farquhar, G.D., von Caemmerer, S., Berry, J.A., 1980. A biochemical model of photosynthetic CO2 assimilation in leaves of C3 species. Planta 149, 78–90. https://doi.org/10.1007/BF00386231

Feng, L., Raza, M.A., Li, Z., Chen, Y., Khalid, M.H. Bin, Du, J., Liu, W., Wu, X., Song, C., Yu, L., Zhang, Z., Yuan, S., Yang, W., Yang, F., 2019. The Influence of Light Intensity and Leaf Movement on Photosynthesis Characteristics and Carbon Balance of Soybean. Front. Plant Sci. 9, 1952. https://doi.org/10.3389/fpls.2018.01952

Franklin, K.A., 2008. Shade avoidance. New Phytol. 179, 930–944. https://doi.org/10.1111/j.1469-8137.2008.02507.x

Franklin, K.A., Quail, P.H., 2010. Phytochrome functions in Arabidopsis development. J. Exp. Bot. 61, 11–24. https://doi.org/10.1093/jxb/erp304

Fraser, D.P., Hayes, S., Franklin, K.A., 2016. Photoreceptor crosstalk in shade avoidance. Curr. Opin. Plant Biol. 33, 1–7. https://doi.org/10.1016/j.pbi.2016.03.008

Garner, W.W., Allard, H.A., 1920. Effect of the relative length of the day and night and other factors of the environment on growth and reproduction in plants1. Mon. Weather Rev. 48, 415–415. https://doi.org/10.1175/1520-0493(1920)48<415b:EOTRLO>2.0.CO;2

Gautier, H, Měch, R., Prusinkiewicz, P., Varlet-Grancher, C., 2000. 3D Architectural Modelling of Aerial Photomorphogenesis in White Clover (Trifolium repens L.) using L-systems. Ann. Bot. 85, 359–370. https://doi.org/10.1006/anbo.1999.1069

Gitz, D.C., Liu-Gitz, L., Britz, S.J., Sullivan, J.H., 2005. Ultraviolet-B effects on stomatal density, water-use efficiency, and stable carbon isotope discrimination in four glasshouse-grown soybean (Glyicine max) cultivars. Environ. Exp. Bot. 53, 343–355. https://doi.org/10.1016/j.envexpbot.2004.04.005

Gong, W.Z., Jiang, C.D., Wu, Y.S., Chen, H.H., Liu, W.Y., Yang, W.Y., 2015. Tolerance vs. avoidance: two strategies of soybean (Glycine max) seedlings in response to shade in intercropping. Photosynthetica 53, 259–268. https://doi.org/10.1007/s11099-015-0103-8

Green-Tracewicz, E., Page, E.R., Swanton, C.J., 2011. Shade Avoidance in Soybean Reduces Branching and Increases Plant-to-Plant Variability in Biomass and Yield Per Plant. Weed Sci. 59, 43–49. https://doi.org/10.1614/WS-D-10-00081.1

He, J., Qin, L., Chong, E.L.C., Choong, T.-W., Lee, S.K., 2017. Plant Growth and Photosynthetic Characteristics of Mesembryanthemum crystallinum Grown Aeroponically under Different Blue- and Red-LEDs. Front. Plant Sci. 8, 361. https://doi.org/10.3389/fpls.2017.00361

Hemmerling, R., Kniemeyer, O., Lanwert, D., Kurth, W., Buck-Sorlin, G., 2008. The rule-based language XL and the modelling environment GroIMP illustrated with simulated tree competition. Funct. Plant Biol. 35, 739. https://doi.org/10.1071/FP08052

Henke, M., Buck-Sorlin, G.H., 2018. Using a Full Spectral Raytracer for Calculating Light Microclimate in Functional-Structural Plant Modelling. Comput. INFORMATICS 36, 1492–1522.

Henke, M., Kurth, W., Buck-Sorlin, G.H., 2016. FSPM-P: towards a general functional-structural plant model for robust and comprehensive model development. Front. Comput. Sci. 10, 1103–1117. https://doi.org/10.1007/s11704-015-4472-8

Hernández, R., Kubota, C., 2016. Physiological responses of cucumber seedlings under different blue and red photon flux ratios using LEDs. Environ. Exp. Bot. 121, 66–74. https://doi.org/10.1016/J.ENVEXPBOT.2015.04.001

Hitz, T., Hartung, J., Graeff-Hönninger, S., Munz, S., 2019a. Morphological Response of Soybean (Glycine max (L.) Merr.) Cultivars to Light Intensity and Red to Far-Red Ratio. Agronomy 9, 428. https://doi.org/10.3390/agronomy9080428

Hitz, T., Henke, M., Graeff-Honninger, S., Munz, S., 2018. Simulating light spectrum within a soybean canopy in an LED growth chamber, in: 2018 6th International Symposium on Plant Growth Modeling, Simulation, Visualization and Applications (PMA). IEEE, pp. 120–125. https://doi.org/10.1109/PMA.2018.8611598

Hitz, T., Henke, M., Graeff-Hönninger, S., Munz, S., 2019b. Three-dimensional simulation of light spectrum and intensity within an LED growth chamber. Comput. Electron. Agric. 156, 540–548. https://doi.org/10.1016/J.COMPAG.2018.11.043

Hogewoning, S.W., Trouwborst, G., Maljaars, H., Poorter, H., van Ieperen, W., Harbinson, J., 2010. Blue light dose-responses of leaf photosynthesis, morphology, and chemical composition of Cucumis sativus grown under different combinations of red and blue light. J. Exp. Bot. 61, 3107–3117. https://doi.org/10.1093/jxb/erq132

Hogewoning, S.W., Wientjes, E., Douwstra, P., Trouwborst, G., van Ieperen, W., Croce, R., Harbinson, J., 2012. Photosynthetic quantum yield dynamics: from photosystems to leaves. Plant Cell 24, 1921–35. https://doi.org/10.1105/tpc.112.097972

Ichihashi, M., Ueda, M., Budiyanto, A., Bito, T., Oka, M., Fukunaga, M., Tsuru, K., Horikawa, T., 2003. UV-induced skin damage. Toxicology 189, 21–39. https://doi.org/10.1016/S0300-483X(03)00150-1

Jacquemoud, S., Baret, F., Hanocq, J.F., 1992. Modeling spectral and bidirectional soil reflectance. Remote Sens. Environ. 41, 123–132. https://doi.org/10.1016/0034-4257(92)90072-R

Jähne, F., Balko, C., Hahn, V., Würschum, T., Leiser, W.L., 2019. Cold stress tolerance of soybeans during flowering: QTL mapping and efficient selection strategies under controlled conditions. Plant Breed. pbr.12734. https://doi.org/10.1111/pbr.12734

Kahlen, K., Chen, T.-W., 2015. Predicting Plant Performance Under Simultaneously Changing Environmental Conditions—The Interplay Between Temperature, Light, and Internode Growth. Front. Plant Sci. 6, 1130. https://doi.org/10.3389/fpls.2015.01130

Kahlen, K., Stützel, H., 2011. Modelling photo-modulated internode elongation in growing glasshouse cucumber canopies. New Phytol. 190, 697–708. https://doi.org/10.1111/j.1469-8137.2010.03617.x

Kalaitzoglou, P., van Ieperen, W., Harbinson, J., van der Meer, M., Martinakos, S., Weerheim, K., Nicole, C.C.S., Marcelis, L.F.M., 2019. Effects of Continuous or End-of-Day Far-Red Light on Tomato Plant Growth, Morphology, Light Absorption, and Fruit Production. Front. Plant Sci. 10, 322. https://doi.org/10.3389/fpls.2019.00322

Kalantari, F., Tahir, O.M., Joni, R.A., Fatemi, E., 2018. Opportunities and Challenges in Sustainability of Vertical Farming: A Review. J. Landsc. Ecol. 11, 35–60. https://doi.org/10.1515/jlecol-2017-0016

Kang, B., Grancher, N., Koyffmann, V., Lardemer, D., Burney, S., Ahmad, M., 2008. Multiple interactions between cryptochrome and phototropin blue-light signalling pathways in Arabidopsis thaliana. Planta 227, 1091–1099. https://doi.org/10.1007/s00425-007-0683-z

Kang, W.H., Park, J.S., Park, K.S., Son, J.E., 2016. Leaf photosynthetic rate, growth, and morphology of lettuce under different fractions of red, blue, and green light from light-emitting diodes (LEDs). Hortic. Environ. Biotechnol. 57, 573–579. https://doi.org/10.1007/s13580-016-0093-x

Kasperbauer, M.J., 1987. Far-Red Light Reflection from Green Leaves and Effects on Phytochrome-Mediated Assimilate Partitioning under Field Conditions. Plant Physiol. 85, 350–4. https://doi.org/10.1104/PP.85.2.350

Keating, B.A., Carberry, P.S., 1993. Resource capture and use in intercropping: solar radiation. F. Crop. Res. 34, 273–301. https://doi.org/10.1016/0378-4290(93)90118-7

Keller, M.M., Jaillais, Y., Pedmale, U. V., Moreno, J.E., Chory, J., Ballaré, C.L., 2011. Cryptochrome 1 and phytochrome B control shade-avoidance responses in Arabidopsis via partially independent hormonal cascades. Plant J. 67, 195–207. https://doi.org/10.1111/j.1365-313X.2011.04598.x

Kim, G.-T., Yano, S., Kozuka, T., Tsukaya, H., 2005. Photomorphogenesis of leaves: shade-avoidance and differentiation of sun and shade leaves. Photochem. Photobiol. Sci. 4, 770. https://doi.org/10.1039/b418440h

Kniemeyer, O., Buck-Sorlin, G., Kurth, W., 2007. GroIMP as a platform for functional-structural modelling of plants, in: Functional–Structural Plant Modelling in Crop Production. Dordrecht, the Netherlands: Springer, pp. 43–52.

Lanoue, J., Leonardos, E.D., Grodzinski, B., 2018. Effects of Light Quality and Intensity on Diurnal Patterns and Rates of Photo-Assimilate Translocation and Transpiration in Tomato Leaves. Front. Plant Sci. 9, 756. https://doi.org/10.3389/fpls.2018.00756

Lee, M.-J., Son, K.-H., Oh, M.-M., 2016. Increase in biomass and bioactive compounds in lettuce under various ratios of red to far-red LED light supplemented with blue LED light. Hortic. Environ. Biotechnol. 57, 139–147. https://doi.org/10.1007/s13580-016-0133-6

Li, J., Li, G., Wang, H., Wang Deng, X., 2011. Phytochrome signaling mechanisms. Arab. B. 9, e0148. https://doi.org/10.1199/tab.0148

Lin, C., Yang, H., Guo, H., Mockler, T., Chen, J., Cashmore, A.R., 1998. Enhancement of blue-light sensitivity of Arabidopsis seedlings by a blue light receptor cryptochrome 2. Proc. Natl. Acad. Sci. U. S. A. 95, 2686–90. https://doi.org/10.1073/pnas.95.5.2686

Lindenmayer, A., 1968a. Mathematical models for cellular interactions in development II. Simple and branching filaments with two-sided inputs. J. Theor. Biol. 18, 300–315. https://doi.org/10.1016/0022-5193(68)90080-5

Lindenmayer, A., 1968b. Mathematical models for cellular interactions in development I. Filaments with one-sided inputs. J. Theor. Biol. 18, 280–299. https://doi.org/10.1016/0022-5193(68)90079-9

Liu, W., Zou, J., Zhang, J., Yang, F., Wan, Y., Yang, W., 2015. Evaluation of Soybean (*Glycine max*) Stem Vining in Maize-Soybean Relay Strip Intercropping System. Plant Prod. Sci. 18, 69–75. https://doi.org/10.1626/pps.18.69

Más, P., Devlin, P.F., Panda, S., Kay, S.A., 2000. Functional interaction of phytochrome B and cryptochrome 2. Nature 408, 207–211. https://doi.org/10.1038/35041583

Massa, G.D., Kim, H.-H., Wheeler, R.M., Mitchell, C.A., 2008. Plant Productivity in Response to LED Lighting. HortScience 43, 1951–1956. https://doi.org/10.21273/HORTSCI.43.7.1951

McCree, K.J., 1972. The action spectrum, absorptance and quantum yield of photosynthesis in crop plants. Agric. Meteorol. 9, 191–216. https://doi.org/10.1016/0002-1571(71)90022-7

Measures, M., Weinberger, P., Baer, H., 1973. Variability of Plant Growth Within Controlled-Environment Chambers as Related to Temperature and Light Distribution. Can. J. Plant Sci. 53, 215–220. https://doi.org/10.4141/cjps73-038

Meng, Q., Kelly, N., Runkle, E.S., 2019. Substituting green or far-red radiation for blue radiation induces shade avoidance and promotes growth in lettuce and kale. Environ. Exp. Bot. 162, 383–391. https://doi.org/10.1016/j.envexpbot.2019.03.016

Merklein, J., Poirier-Pocovi, M., Buck-Sorlin, G.H., Kurth, W., Long, Q., 2018. A dynamic model of xylem and phloem flux in an apple branch, in: 2018 6th International Symposium on Plant Growth Modeling, Simulation, Visualization and Applications (PMA). IEEE, pp. 50–55. https://doi.org/10.1109/PMA.2018.8611561

Migault, V., Pallas, B., Costes, E., 2017. Combining Genome-Wide Information with a Functional Structural Plant Model to Simulate 1-Year-Old Apple Tree Architecture. Front. Plant Sci. 7, 2065. https://doi.org/10.3389/fpls.2016.02065

Morrow, R.C., 2008. LED Lighting in Horticulture. HortScience 43, 1947–1950.

Nagatani, A., Chory, J., Furuya, M., 1991. Phytochrome B Is Not Detectable in the hy3 Mutant of Arabidopsis, Which Is Deficient in Responding to End-of-Day Far-Red Light Treatments. Plant Cell Physiol. 32, 1119–1122. https://doi.org/10.1093/oxfordjournals.pcp.a078177

Naznin, M., Lefsrud, M., Gravel, V., Azad, M., 2019. Blue Light added with Red LEDs Enhance Growth Characteristics, Pigments Content, and Antioxidant Capacity in Lettuce, Spinach, Kale, Basil, and Sweet Pepper in a Controlled Environment. Plants 8, 93. https://doi.org/10.3390/plants8040093

Neugart, S., Schreiner, M., 2018. UVB and UVA as eustressors in horticultural and agricultural crops. Sci. Hortic. (Amsterdam). 234, 370–381. https://doi.org/10.1016/J.SCIENTA.2018.02.021

Olle, M., Viršile, A., 2013. The effects of light-emitting diode lighting on greenhouse plant growth and quality. Agric. Food Sci. 22, 223–234.

Park, Y., Runkle, E.S., 2018. Far-red radiation and photosynthetic photon flux density independently regulate seedling growth but interactively regulate flowering. Environ. Exp. Bot. 155, 206–216. https://doi.org/10.1016/J.ENVEXPBOT.2018.06.033

Parks, B.M., Folta, K.M., Spalding, E.P., 2001. Photocontrol of stem growth. Curr. Opin. Plant Biol. 4, 436–440. https://doi.org/10.1016/S1369-5266(00)00197-7

Pauch, R.C., Britz, S.J., Mulchi, C.L., 1991. Growth and photosynthesis of soybean (Glycine max (L.) Merr.) in simulated vegetation shade: influence of the ratio of red to far-red radiation*. Plant, Cell Environ. 14, 647–656. https://doi.org/10.1111/j.1365-3040.1991.tb01537.x

Pedmale, U.V., Huang, S.C., Zander, M., Cole, B.J., Hetzel, J., Ljung, K., Reis, P.A.B., Sridevi, P., Nito, K., Nery, J.R., Ecker, J.R., Chory, J., 2016. Cryptochromes Interact Directly with PIFs to Control Plant Growth in Limiting Blue Light. Cell 164, 233–245. https://doi.org/10.1016/J.CELL.2015.12.018

Pennisi, G., Blasioli, S., Cellini, A., Maia, L., Crepaldi, A., Braschi, I., Spinelli, F., Nicola, S., Fernandez, J.A., Stanghellini, C., Marcelis, L.F.M., Orsini, F., Gianquinto, G., 2019. Unraveling the Role of Red:Blue LED Lights on Resource Use Efficiency and Nutritional Properties of Indoor Grown Sweet Basil. Front. Plant Sci. 10, 305. https://doi.org/10.3389/fpls.2019.00305

Phong, B.T., 1975. Illumination for Computer Generated Pictures. Commun. ACM 18, 311–317. https://doi.org/10.1145/360825.360839

Piepho, H.-P., 2004. An Algorithm for a Letter-Based Representation of All-Pairwise Comparisons. J. Comput. Graph. Stat. 13, 456–466. https://doi.org/10.1198/1061860043515

Pierik, R., de Wit, M., 2014. Shade avoidance: phytochrome signalling and other aboveground neighbour detection cues. J. Exp. Bot. 65, 2815–2824. https://doi.org/10.1093/jxb/ert389

Prusinkiewicz, P., 2007. Modelling architecture of crop plants using L-systems. Frontis 27–42.

Qi, R., Ma, Y., Hu, B., de Reffye, P., Cournède, P.-H., 2010. Optimization of source–sink dynamics in plant growth for ideotype breeding: A case study on maize. Comput. Electron. Agric. 71, 96–105. https://doi.org/10.1016/J.COMPAG.2009.12.008

R Core Team, 2018. R: A Language and Environment for Statistical Computing. R Found. Stat. Comput. Vienna, Austria.

Robson, T.M., Aphalo, P.J., Banaś, A.K., Barnes, P.W., Brelsford, C.C., Jenkins, G.I., Kotilainen, T.K., Łabuz, J., Martínez-Abaigar, J., Morales, L.O., Neugart, S., Pieristè, M., Rai, N., Vandenbussche, F., Jansen, M.A.K., 2019. A perspective on ecologically relevant plant-UV research and its practical application. Photochem. Photobiol. Sci. 18, 970–988. https://doi.org/10.1039/C8PP00526E

Sarlikioti, V., de Visser, P.H.B., Buck-Sorlin, G.H., Marcelis, L.F.M., 2011. How plant architecture affects light absorption and photosynthesis in tomato: towards an ideotype for plant architecture using a functional–structural plant model. Ann. Bot. 108, 1065–1073. https://doi.org/10.1093/aob/mcr221

Schmitt, J., 1997. Is photomorphogenic shade avoidance adaptive? Perspectives from population biology. Plant, Cell Environ. 20, 826–830. https://doi.org/10.1046/j.1365-3040.1997.d01-96.x

Schulze, P.S.C., Barreira, L.A., Pereira, H.G.C., Perales, J.A., Varela, J.C.S., 2014. Light emitting diodes (LEDs) applied to microalgal production. Trends Biotechnol. 32, 422–430. https://doi.org/10.1016/J.TIBTECH.2014.06.001

Sellaro, R., Crepy, M., Trupkin, S.A., Karayekov, E., Buchovsky, A.S., Rossi, C., Casal, J.J., 2010. Cryptochrome as a Sensor of the Blue/Green Ratio of Natural Radiation in Arabidopsis. Plant Physiol. 154, 401–409. https://doi.org/10.1104/pp.110.160820

Singh, D., Basu, C., Meinhardt-Wollweber, M., Roth, B., 2015. LEDs for energy efficient greenhouse lighting. Renew. Sustain. Energy Rev. 49, 139–147. https://doi.org/10.1016/J.RSER.2015.04.117

Smith, H., 1982. Light Quality, Photoperception, and Plant Strategy. Annu. Rev. Plant Physiol. 33, 481–518. https://doi.org/10.1146/annurev.pp.33.060182.002405

Somers, D.E., Sharrock, R.A., Tepperman, J.M., Quail, P.H., 1991. The hy3 Long Hypocotyl Mutant of Arabidopsis Is Deficient in Phytochrome B. Plant Cell 3, 1263–1274. https://doi.org/10.1105/tpc.3.12.1263

Stoner, E.R., Baumgardner, M.F., 1981. Characteristic Variations in Reflectance of Surface Soils1. Soil Sci. Soc. Am. J. 45, 1161. https://doi.org/10.2136/sssaj1981.03615995004500060031x

Struik, P.C., 2016. Bridging the genotype–phenotype gap in 3D. J. Exp. Bot. 67, 4427–4430. https://doi.org/10.1093/jxb/erw264

Taulavuori, K., Julkunen-Tiitto, R., Hyöky, V., Taulavuori, E., 2013. Blue Mood for Superfood. Nat. Prod. Commun. 8, 1934578X1300800. https://doi.org/10.1177/1934578X1300800627

Terashima, I., Fujita, T., Inoue, T., Chow, W.S., Oguchi, R., 2009. Green Light Drives Leaf Photosynthesis More Efficiently than Red Light in Strong White Light: Revisiting the Enigmatic Question of Why Leaves are Green. Plant Cell Physiol. 50, 684–697. https://doi.org/10.1093/pcp/pcp034

Tian, T., Wu, L., Henke, M., Ali, B., Zhou, W., Buck-Sorlin, G., 2017. Modeling Allometric Relationships in Leaves of Young Rapeseed (Brassica napus L.) Grown at Different Temperature Treatments. Front. Plant Sci. 8, 313. https://doi.org/10.3389/fpls.2017.00313

Tilbrook, K., Arongaus, A.B., Binkert, M., Heijde, M., Yin, R., Ulm, R., 2013. The UVR8 UV-B Photoreceptor: Perception, Signaling and Response. Arabidopsis Book 11. https://doi.org/10.1199/TAB.0164

Valladares, F., Niinemets, Ü., 2008. Shade Tolerance, a Key Plant Feature of Complex Nature and Consequences. Annu. Rev. Ecol. Evol. Syst. 39, 237–257. https://doi.org/10.1146/annurev.ecolsys.39.110707.173506

Van Antwerpen, D G., 2011. Unbiased physically based rendering on the GPU. (Dissertation for the Master Degree). Delft University of Technology.

Verdaguer, D., Jansen, M.A.K., Llorens, L., Morales, L.O., Neugart, S., 2017. UV-A radiation effects on higher plants: Exploring the known unknown. Plant Sci. 255, 72–81. https://doi.org/10.1016/J.PLANTSCI.2016.11.014

Visser, D., Bram, P.H., van der Heijden, G., Buck-Sorlin, G., 2014. Optimizing illumination in the greenhouse using a 3D model of tomato and a ray tracer. Front. Plant Sci. 5. https://doi.org/10.3389/fpls.2014.00048

Vos, J., Evers, J.B., Buck-Sorlin, G.H., Andrieu, B., Chelle, M., de Visser, P.H.B., 2010. Functional–structural plant modelling: a new versatile tool in crop science. J. Exp. Bot. 61, 2101–2115. https://doi.org/10.1093/jxb/erp345

Wang, Q., Liu, Q., Wang, X., Zuo, Z., Oka, Y., Lin, C., 2018. New insights into the mechanisms

of phytochrome-cryptochrome coaction. New Phytol. 217, 547–551. https://doi.org/10.1111/nph.14886

Watson, A., Ghosh, S., Williams, M.J., Cuddy, W.S., Simmonds, J., Rey, M.-D., Asyraf Md Hatta, M., Hinchliffe, A., Steed, A., Reynolds, D., Adamski, N.M., Breakspear, A., Korolev, A., Rayner, T., Dixon, L.E., Riaz, A., Martin, W., Ryan, M., Edwards, D., Batley, J., Raman, H., Carter, J., Rogers, C., Domoney, C., Moore, G., Harwood, W., Nicholson, P., Dieters, M.J., DeLacy, I.H., Zhou, J., Uauy, C., Boden, S.A., Park, R.F., Wulff, B.B.H., Hickey, L.T., 2018. Speed breeding is a powerful tool to accelerate crop research and breeding. Nat. Plants 4, 23–29. https://doi.org/10.1038/s41477-017-0083-8

Weston, E., Thorogood, K., Vinti, G., López-Juez, E., 2000. Light quantity controls leaf-cell and chloroplast development in Arabidopsis thaliana wild type and blue-light-perception mutants. Planta 211, 807–815. https://doi.org/10.1007/s004250000392

Wheeler, R.M., Mackowiak, C.L., Sager, J.C., 1991. Soybean stem growth under high-pressure sodium with supplemental blue lighting. Agron. J. 83, 903–6.

Wu, B.-S., Rufyikiri, A.-S., Orsat, V., Lefsrud, M.G., 2019. Re-interpreting the photosynthetically action radiation (PAR) curve in plants. Plant Sci. 110272. https://doi.org/10.1016/J.PLANTSCI.2019.110272

Xu, L., Henke, M., Zhu, J., Kurth, W., Buck-Sorlin, G., 2011. A functional–structural model of rice linking quantitative genetic information with morphological development and physiological processes. Ann. Bot. 107, 817–828. https://doi.org/10.1093/aob/mcq264

Yan, H.-P., Kang, M.Z., de Reffye, P., Dingkuhn, M., 2004. A dynamic, architectural plant model simulating resource-dependent growth. Ann. Bot. 93, 591–602. https://doi.org/10.1093/aob/mch078

Yang, F., Feng, L., Liu, Q., Wu, X., Fan, Y., Raza, M.A., Cheng, Y., Chen, J., Wang, X., Yong, T., Liu, W., Liu, J., Du, J., Shu, K., Yang, W., 2018. Effect of interactions between light intensity and red-to- far-red ratio on the photosynthesis of soybean leaves under shade condition. Environ. Exp. Bot. 150, 79–87. https://doi.org/10.1016/J.ENVEXPBOT.2018.03.008

Yang, F., Huang, S., Gao, R., Liu, W., Yong, T., Wang, X., Wu, X., Yang, W., 2014. Growth of soybean seedlings in relay strip intercropping systems in relation to light quantity and red:far-red ratio. F. Crop. Res. 155, 245–253. https://doi.org/10.1016/j.fcr.2013.08.011

Yeh, N., Chung, J.-P., 2009. High-brightness LEDs—Energy efficient lighting sources and their potential in indoor plant cultivation. Renew. Sustain. Energy Rev. 13, 2175–2180. https://doi.org/10.1016/J.RSER.2009.01.027

Yin, X., Goudriaan, J., Lantinga, E.A., Vos, J., Spiertz, H.J., 2003. A Flexible Sigmoid Function of Determinate Growth. Ann. Bot. 91, 361–371. https://doi.org/10.1093/aob/mcg029

Yoshinaka, K., Nagashima, H., Yanagita, Y., Hikosaka, K., 2018. The role of biomass allocation between lamina and petioles in a game of light competition in a dense stand of an annual plant. Ann. Bot. 121, 1055–1064. https://doi.org/10.1093/aob/mcy001

Yu, X., Liu, H., Klejnot, J., Lin, C., 2010. The Cryptochrome Blue Light Receptors. Arab. B. 8, e0135. https://doi.org/10.1199/tab.0135

Zhen, S., van Iersel, M.W., 2017. Far-red light is needed for efficient photochemistry and photosynthesis. J. Plant Physiol. 209, 115–122. https://doi.org/10.1016/J.JPLPH.2016.12.004

Zoltowski, B.D., Imaizumi, T., 2014. Structure and function of the ZTL/FKF1/LKP2 group proteins in Arabidopsis. Enzym. 35, 213. https://doi.org/10.1016/B978-0-12-801922-1.00009-9

Acknowledgements

I would like to thank my supervisor, Prof. Dr. agr. Simone Graeff-Hönninger from the Institute of Crop Science, for her guidance through the process of this dissertation. From the same institute I would like to thank Dr. sc. agr. Sebastian Munz for scientific discussion, guidance and feedback on my work. I would also like to thank my research partner Felix Jähne from the State Plant Breeding Institute, for good cooperation on the project.

For funding of this research, I would like to thank the German Federal Ministry for Economic Affairs and Energy according to a decision of the German Federal Parliament within the Central Innovation Program for SMEs (ZF4279901CR6).

My family, especially my husband Daniel Hitz, I would like to thank for the unceasing support to complete this dissertation.